Effects of Microbial Community Stress Response and Emerging Contaminants on Wastewater Treatment Plants

Jacob William Metch

Dissertation submitted to the faculty of the Virginia Polytechnic Institute and State University in partial fulfillment of the requirements for the degree of

Doctor of Philosophy
In
Civil Engineering

Amy J. Pruden, Chair
Peter J. Vikesland
Marc A. Edwards
John T. Novak
Brian D. Badgley

March 20, 2017
Blacksburg, VA

Keywords: Wastewater treatment, engineered nanoparticles, nitrifying microorganisms, antibiotic resistance, disinfection by-products

Effects of Microbial Community Stress Response and Emerging Contaminants on Wastewater Treatment Plants

Jacob William Metch

ABSTRACT

As the population in water stressed areas increases, it is critical that wastewater treatment plants (WWTPs) continue to replenish depleted water supplies, and serve as an alternative water source. WWTPs depend on microorganisms in activated sludge to remove pollutants from wastewater and therefore an understanding of how these microorganisms are affected by various conditions and pollutants is needed. Also, as consumer products and industrial processes evolve, so do the pollutants they discharge to wastewater. The research herein assesses microbial community dynamics of the response of nitrifying microorganisms in activated sludge to variation in ammonia concentration and evaluates the impact of engineered nanoparticles on activated sludge microbial communities and other emerging pollutants, such as antibiotic resistance genes and disinfection by-products.

In order to assess microbial community dynamics of the response of nitrifying microorganisms to removal of ammonia in the feed, nitrifying activated sludge reactors were operated at various relevant temperatures and the nitrifying microbial community was characterized using activity assays and bio-molecular techniques. We found that *Nitrospira* spp. were the dominant nitrifying microorganisms, exhibiting stable relative abundance across multiple trials and over a range of temperatures. These results indicate the possibility of comammox bacteria in the system and highlight the complexity of nitrifying microbial communities in activated sludge relative to past understanding.

Both microbial and chemical impacts of engineered nanoparticles on WWTP processes were also investigated. Metagenomic analysis of DNA extracted from activated sludge sequencing batch reactors dosed with gold nanoparticles with varied surface coating and morphology indicated that nanoparticle morphology impacted the microbial

community and antibiotic resistance gene content more than surface coating. However, nanoparticle fate was controlled by surface coating more than morphology. Disinfection by-product formation in the presence of nanoparticles during WWTP disinfection was assessed using silver, titanium dioxide, ceria, and zero valent iron nanoparticles. Silver nanoparticles were found to enhance trihalomethane formation, which was attributed to the citrate coating of the nanoparticles. These studies both raise concern over the relationship between engineered nanoparticles and other emerging concerns in WWTPs, and take a step towards informing nanoparticle design in a manner that limits their associated environmental impact.

Effects of Microbial Community Stress Response and Emerging Contaminants on Wastewater Treatment Plants

Jacob William Metch

GENERAL AUDIENCE ABSTRACT

Wastewater treatment plants (WWTPs) are crucial to protect human and environmental health by removing pathogens and pollutants in sewage before they are released into aquatic environments used for recreation and drinking water. As populations living in water stressed areas continues to rise, the continued recovery of clean water from WWTPs is essential to both replenish water supplies and serve as an alternative water source. WWTPs depend on a complex mixture of microorganisms called activated sludge to remove pollutants from water. In order for WWTPs to continue discharging acceptable water in the future, a greater understanding of how these important microorganisms respond to environmental changes such as temperature and sewage content is needed. Sewage flowing into WWTPs is also evolving as advances in technology and chemicals used in consumer products and industrial settings discharge new pollutants into waste streams. Therefore, an understanding for how these new pollutants affect WWTP processes is also needed. In this dissertation, two challenges facing WWTPs were evaluated: 1) how bacteria responsible for nitrogen removal in WWTPs respond to the stress of starvation, and 2) how engineered nanoparticles in sewage impact the microorganisms in activated sludge and disinfection in WWTPs.

Nitrogen removal is important because it can cause algal blooms when treated wastewater is discharged and because some forms, like ammonia, are toxic. The first step of nitrogen removal in WWTPs involves forming nitrate from ammonia, performed by nitrifying bacteria and archaea. This nitrate is then transformed into nitrogen gas by other microorganisms and therefore removed from the wastewater. How nitrifying microorganisms responded to decreased ammonia concentrations in the feed was determined using nucleic acid based techniques. Traditionally it is thought that in

wastewater treatment, ammonia is oxidized to nitrite by one group of microorganisms, and nitrite is then oxidized to nitrate by separate microorganisms. However, in this study only microorganisms from the latter group were detected, which demonstrates the possibility of microorganisms capable of both ammonia and nitrite oxidation present in our system (as has been found in other environments).

Also, the increased use of engineered nanoparticles in consumer products and industrial processes has led to their increased presence in wastewater. Nanoparticle are particles that are 1-100 nm in one dimension and have unique properties compared to larger forms of the material they are made of. These particles are sometimes utilized for their antimicrobial activity and therefore may impact the microorganisms used in WWTPs. Using activated sludge bioreactors dosed with gold nanoparticles with various morphologies and surface coatings, implications of these nanoparticle properties on activated sludge microorganisms was assessed. We found that nanoparticle morphology was more important than surface coating in affecting the activated sludge microbial communities. However, gold nanoparticle fate in the bioreactors was determined more by surface coating than morphology. These results and further research on how nanoparticle properties affect WWTPs and the environment may inform nanoparticle design that can be tailored to decrease environmental impact.

The impact of nanoparticles on WWTP disinfection processes was also evaluated. WWTPs often use chlorine and/or ultraviolet (UV) disinfection in order to inactivate pathogens in wastewater. Chemical reactions between organics in the wastewater and chlorine produce disinfection by-products which can be toxic. Nanoparticles are used to enhance desired chemical reactions in industry, and therefore may enhance the undesired reactions of disinfection by-product formation in WWTPs. Here several types of nanoparticle (silver, titanium dioxide, ceria, and zero valent iron) were dosed to WWTP effluents and then subjected to chlorine and/or UV disinfection, then this was analyzed for trihalomethanes (a common type of disinfection by-product). It was found that the citrate coating on silver nanoparticles led to increased trihalomethane formation. More research is needed to determine the mechanisms involved with this phenomenon, and to determine other nanoparticle-coating combinations that may have similar effect

ACKNOWLEDGEMENTS

So many people have given me support and guidance on the path that has taken me from a small town in upstate New York to getting a PhD at Virginia Tech. Without these people in my life, there would be no chance of me succeeding in my PhD.

First, I would like to thank my advisors Dr. Amy Pruden and Dr. Peter Vikesland. You both set an amazing example of how to approach your work with dedication and enthusiasm. Thank you so much for all of the guidance in how to be successful in research and communicating results. I cannot thank you enough for the experiences you both have given me in my time at Virginia Tech. You have shown me that good research can and should cross borders, cultures, and disciplines. My time in China, India, Philippines, and Hong Kong has changed my view of the world and I will continue to draw on these experiences to guide me going forward.

Thank you to committee members Dr. Marc Edwards, Dr. John Novak, and Dr. Brian Badgely. I have valued the interest you show in my work, as well as the input that you have given.

During my time here, I have had the great privilege of working with some of the smartest people I know. I cannot describe how much I appreciate the help, support, distractions, food, and friendship that has been shown to me by the Pruden, Vikesland, and Edwards research groups. You are all great people and researchers and I am excited to follow your careers to see the great things you all accomplish.

And last, but in no way least, thank you to my friends and family. Grad school would not have been the same without all of the fun I have had with friends here. I look forward to continued hiking, golfing, game nights, and the occasional bar night with you all. Thank you to my family that has been so supportive of every decision I have made (mostly) that led me to this point. Thank you to Tucker and Sadie for all of the tail wags and comforting. And most of all, thank you to my wife, Mary Kate. Your support, patience, and love has gotten me through hard times and your company during the good times is irreplaceable.

ATTRIBUTIONS

The research presented here is a product of collaborative efforts across fields and institutions. The contributions of each coauthor is described herein:

Dr. Amy Pruden (Civil and Environmental Engineering, Virginia Tech). Ph.D. advisor, committee chair and project PI. Co-author of Chapters 2, 3, and 4. Contributed guidance on experimental design and data interpretation as well as assistance in manuscript preparation and review.

Dr. Peter Vikesland (Civil and Environmental Engineering, Virginia Tech). Ph.D. committee member and project co-PI. Co-author of Chapters 2, 3 and 4. Contributed guidance on experimental design and data interpretation as well as assistance in manuscript preparation and review.

Dr. Jennifer Miller (Civil and Environmental Engineering, Virginia Tech) **and Dr. Charles Bott** (Civil and Environmental Engineering, Virginia Tech) **Dr. Matt Higgins** (Civil and Environmental Engineering, Bucknell University) **Dr. Sudhir Murthy** (DC Water) **Dr. Hong Wang** (Environmental Science, Tongji University). Co-authors of Chapter 2. Involved in experimental design and execution, as well as sample collection and processing.

Dr. Nathan D. Burrows and Dr. Catherine J. Murphy (Chemistry, University of Illinois). Co-authors of Chapter 3. Performed synthesis and characterization of gold nanoparticles as well as assistance in manuscript review.

Dr. Yanjun Ma (Civil and Environmental Engineering, University of Illinois). Co-author of Chapter 4. Assisted in experimental design and manuscript review.

TABLE OF CONTENTS

LIST OF FIGURES

LIST OF TABLES

CHAPTER 1: INTRODUCTION

Wastewater treatment represents a key component of the engineered systems society has developed to protect public health and the environment. Wastewater treatment plants (WWTPs) are charged with the purification of polluted water to protect receiving waters from pathogens, nutrients, and oxygen-demanding pollutants, as well as the replenishment of water supplies for downstream uses. As population growth and the need for sustainable development continues to increase,[1,2] research on wastewater treatment must keep pace with new challenges associated with purifying this valuable resource into the future.

New challenges and concerns with respect to wastewater treatment make continued research necessary to address removal of both traditional and emerging contaminates for sustained protection of protect public health and receiving environments. Increasing pressure for WWTPs to remove more nutrients from water as receiving waters struggle with eutrophication around the world[3] has led to innovative approaches to biological nutrient removal, such as the use of nitrification, denitrification, anammox and biological phosphorous removal.[4] Increasing efficiency concerns have led to the development of processes to decrease energy demand, such as shortcut nitrification-denitrification,[5] as well as technologies to recover energy from sewage, like biogas production and microbial fuel cells.[6] While the above processes have been studied for decades in some cases, our understanding of them is often based on empirical observations and a "black box" model with respect to actual microbiological processes occurring. For future advances in these important WWTP processes a better understanding of the microbiology behind them is needed.

In addition to nutrient removal and efficiency goals, increased awareness and emergence of new pollutants has led to more challenges for WWTPs. Advances in pharmaceuticals, cosmetics, and other consumer products and industrial systems, coupled with improvements in analytical techniques needed to detect pollutants has led to increased concern about the fate of micropollutants in WWTPs and the environment.[7,8] Antibiotics, antibiotic resistant pathogens, engineered nanomaterials, and disinfection by-products have all become concerns in WWTPs.

In this dissertation, modern molecular and analytical tools were applied to gain insight into two current challenges faced by WWTPs: 1) understanding the effects of system stress on the dynamics and activity of microbial communities depended upon to nitrify and remove ammonia from wastewater; and 2) determining the fate of engineered nanoparticles in activated sludge systems, and their potential to disrupt microbial communities depended upon for biological treatment and to enhance health concerns in the finished water.

1.1 MICROBIAL ECOLOGY OF WASTEWATER

After primary treatment, most WWTPs depend on a complex microbial community called activated sludge for the removal of pollutants in sewage. Pollutants are removed through microbial growth and respiration (used as substrate and subsequent mineralization), and through adsorption to activated sludge. Microbial communities in activated sludge have long been studied using culture dependent and molecular techniques.[9] Recently, the application of high-throughput DNA sequencing has allowed investigations into activated sludge microbial ecology to better understand genomic and functional composition and diversity,[10–14] as well as impacts of environmental factors.[15,16] These studies have found extreme diversity in activated sludge with *Proteobacteria* being the dominant phylum with several other abundant phyla such as *Firmicutes*, *Bacteroidetes*, and *Actinobacteria*, the abundance of which vary with location and seasonality.[11,17] These investigations include either the amplification and sequencing of 16S rRNA genes for taxonomic characterization,[18] or metagenomic analysis in which microbial community DNA libraries are constructed, sequenced and screened for taxonomic and functional gene composition.[19]

Although nitrifying microorganisms are crucial to nitrification and therefore nitrogen removal in WWTPs, relatively little is known about them in activated sludge and nitrification design parameters are oversimplified as a result.[20] Nitrification traditionally involves a two-step process in which ammonia is oxidized to nitrite by ammonia oxidizing microorganisms (AOM) and subsequently nitrite is oxidized to nitrate by nitrite oxidizing bacteria (NOB). This model has been challenged recently with the discovery of bacteria capable of complete ammonia oxidation to nitrate.[21] Within activated sludge, the

main nitrifiers are thought to be *Nitrosomonas* and *Nitrosospira* for AOM, and *Nitrobacter* and *Nitrospira* for NOB.[22,23]

Nitrifying bacteria in natural and engineered environments are routinely exposed to dramatic fluctuations in temperature, dissolved oxygen, and electron donor concentrations which has led to several adaptations including physiological, enzymatic, and molecular mechanisms that allow them to survive in extreme environmental conditions.[24–29] While several stress response studies have been carried out using pure or enriched culture, in the more complex mixed culture environment of activated sludge, other variables such as predation,[30] competition with heterotrophs for nutrients[24] and other microbial community dynamics are likely to factor into microbial stress responses. This research seeks improve understanding of how microbial community dynamics impact nitrifying microorganism stress response using high-throughput sequencing techniques.

1.2 EMERGING CONCERNS IN WASTEWATER TREATMENT

In order to meet wastewater treatment needs in the future, understanding emerging concerns will be critical in designing processes that continue to protect public health and environmental quality. In order to accomplish this the fate and impact of new pollutants need to be closely monitored in WWTPs. This research focusses on the assessment of engineered nanoparticles, antibiotic resistance genes, and disinfection by-products in wastewater treatment, and characterizes relationships among these emerging concerns.

1.2.1 Engineered Nanoparticles

Engineered nanoparticles are rapidly being applied in industrial processes and consumer products for their antimicrobial, photocatalytic, and optical properties along with other features[31]. Nanoparticles in consumer products are released to sewers through product washing as in the case of textiles containing silver nanoparticles[32] and through product use such as nanoparticles in foods, lotions, and sunscreens.[33] Although it is difficult to measure nanoparticles in wastewater streams directly, there has been an effort to predict nanoparticle disposal via modeling, which has identified WWTPs as a major

discharge pathway[34] with a large portion (47,300 metric tons per year) of nanoparticles will be disposed of via WWTPs.[35]

It is key to understand nanoparticle-microbial interactions since many nanoparticles have been found to be toxic in pure culture studies,[36,37] and are known to accumulate in activated sludge flocs in WWTPs.[38] Concerns have now been raised over the potential for nanoparticles to inhibit activated sludge microbial communities which may impact nutrient and pollutant removal in WWTPs.[39,40] Assessment of the impacts of nanomaterial discharges on microbial communities is challenging since nanoparticle interactions with bacterial proteins, membranes, cells, DNA and organelles are complex and influenced by nanoparticle properties.[41–44] Recent studies have shown that activated sludge microbial communities exhibit changes in response to silver nanoparticle exposures that are distinct from the effects of ionic silver.[45–47] These observations indicates that silver nanoparticles impart a selective pressure on the microbial community distinct from the selective pressure of silver ions. Microbial community shifts in response to nanoparticle exposure highlight the need to better understand the precise effects of nanoparticles within WWTPs. This research aims to characterize effects of varying nanoparticle properties on activated sludge microbial communities and therefore inform design of nanoparticles to limit impact in WWTPs.

1.2.2 Antibiotic Resistance and Nanoparticles

Shifts in activated sludge microbial community composition can not only potentially affect the removal of pollutants from wastewater[48] but also increase selection of some antibiotic resistance genes (ARGs) can occur in conjunction with, and as a result of microbial community dynamics.[46,49] Antibiotic resistance is an urgent public health threat, with at least two million people contracting antibiotic resistant infections and over 23,000 deaths as a result of resistant pathogens each year in the U.S. alone.[50] Natural environments are an important reservoir for ARGs and WWTPs are known to contribute to that reservoir.[51–54] Bacterial stress response mechanisms are closely related to antibiotic resistance and ARGs due to the activation of common mechanisms such as oxidative stress response, efflux systems, envelope stress response, and SOS responses.[55–57] Such responses may lead to ARG proliferation through co-selection in which bacteria

containing ARGs outcompete non-resistant bacteria in the presence of the environmental stressor,[58] as well as horizontal gene transfer where mobile genetic elements such as plasmids, transposons, and integrons containing ARGs are transferred among bacteria.[59] Metals in particular have been found to impart a selective pressure that increases both ARGs and metal resistance genes (MRGs)[58,60,61] and also influence horizontal gene transfer.[62] WWTPs have a combination of influent pathogens and resistant bacteria with stressors such as antibiotics, metals, nanoparticles and others. Therefore, activated sludge processes may be critical in the environmental dissemination of ARGs, MRGs, and the plasmids that potentially house these genes.[59,63] A better understanding of the selective pressures that lead to the proliferation of these genes is critically needed. This research attempts to characterize selective pressures imparted by various nanoparticle properties.

1.2.3 Disinfection By-Products

In addition to potential negative microbial effects of nanoparticles in activated sludge, nanoparticles may catalyze undesirable chemical reactions in other WWTP processes. Chlorine disinfection is often used to inactivate pathogens in WWTP effluents, however, toxic disinfection by-products are produced in this process.[64,65] UV disinfection is sometimes used instead of, or in conjunction with chlorine disinfection and could increase the potential for disinfection by-product production due to photo-rearrangement of organic matter.[66] These toxins may not only impact natural aquatic ecosystems, but also public health through indirect and direct reuse of WWTP effluents.[67,68] The concern of disinfection by-product formation in WWTPs is enhanced by the presence of nanoparticles in wastewater influents. Several nanomaterials are used for their catalytic abilities in industry[69] and some have been shown to catalyze undesired reactions in waste incineration.[70] The ability for nanoparticles to catalyze undesired reactions in WWTP disinfection needs further investigation to better understand how the emerging concerns of nanoparticles and disinfection by-products relate to each other and influence effluent quality. This knowledge gap is investigated herein.

1.3 RESEARCH OBJECTIVES

This research aims to assess microbial community dynamics in activated sludge exposed to various stressors, and examine the effects nanoparticles have on WWTP effluent quality in order to inform robust design of wastewater treatment processes to protect public health and the environment. In pursuing this general objective, the following specific objectives were addressed:

1) Assess microbial community dynamics of nitrifying microorganisms in activated sludge subject to decreased ammonia concentration (i.e., no external ammonia or carbon addition) in order to better understand stress response.

2) Determine the influence of engineered nanoparticle design on nanoparticle fate in WWTPs and their effects on activated sludge microbial communities.

3) Evaluate the potential for nanoparticles to affect WWTP effluent disinfection and enhance disinfection by-products formation.

1.4 ANNOTATED DISSERTATION OUTLINE

Chapter 1: Introduction.

Chapter 2: Insight into Nitrifying Microbial Community Starvation Response using Illumina 16S rRNA Amplicon Sequencing. This manuscript sought to address the first specific objective and characterize nitrifying microbial communities throughout starvation. A combination of metabolic activity assays, quantitative polymerase chain reaction (qPCR), and 16S rRNA amplicon sequencing was used to assess nitrifying microorganisms at various relevant temperatures in reactors seeded with activated sludge from the DC Water Blue Plains Advanced WWTP nitrification basin. Observations made in this study contribute to understanding dynamics of nitrifying microbial communities in activated sludge. This manuscript is in preparation for submission to *Water Research*.

Chapter 3: Metagenomic Analysis of Microbial Communities Yields Insight into Impacts of Nanoparticle Design. This manuscript addresses the second specific objective through a comparison of the metagenomes of activated sludge sequencing batch reactors dosed with gold nanoparticles of varying morphology and surface coating. This metagenomic characterization of microbial communities as well as ARG, MRG, and plasmid content revealed nanoparticle morphology influenced microbial community stress response more

than surface coating. Fate of gold nanoparticles was assessed using inductively coupled plasma mass spectrometry and found to be driven by the surface coating of the particles. This manuscript is currently under peer-review at *Nature Nanotechnology*.

Chapter 4: Enhanced Disinfection By-Product Formation Due to Nanoparticles in Wastewater Treatment Plant Effluents. This manuscript addressed the third specific objective and assessed the potential for silver, titanium dioxide, ceria, and zero valent iron nanoparticles to impact the formation of disinfection by-products in two wastewater treatment plant effluents. Trihalomethane formation was measured in three disinfection scenarios executed on effluents containing varying concentrations of nanoparticles. This study discusses the potential for nanoparticles to enhance undesired reactions in WWTP disinfection. This manuscript has been accepted for publication:

Metch JW, Ma Y, Pruden A, Vikesland PJ. Enhanced disinfection by-product formation due to nanoparticles in wastewater treatment plant effluents. *Environmental Science: Water Research & Technology*. **2015**,1 (6), 823-831.

Chapter 5: Conclusion. This chapter summarizes the contribution of this research in understanding emerging challenges in wastewater treatment and recommends future research based on the observations made herein.

REFERENCES

1. Steffen, W. *et al.* Planetary boundaries: Guiding human development on a changing planet. *Science* **347,** 1259855 (2015).
2. Hoekstra, A. Y. & Wiedmann, T. O. Humanity's unsustainable environmental footprint. *Science (80-.).* **344,** 1114–1117 (2014).
3. Lewis, W. M., Wurtsbaugh, W. A. & Paerl, H. W. Rationale for control of anthropogenic nitrogen and phosphorus to reduce eutrophication of inland waters. *Environ. Sci. Technol.* **45,** 10300–10305 (2011).
4. Metcalf and Eddy Inc. *Wastewater Engineerin: Treatment and Reuse*. (McGraw Hill, 2003).
5. Gao, D., Peng, Y., Li, B. & Liang, H. Shortcut nitrification-denitrification by real-time control strategies. *Bioresour. Technol.* **100,** 2298–2300 (2009).

6. McCarty, P. L., Bae, J. & Kim, J. Domestic wastewater treatment as a net energy producer - can this be achieved? *Environ. Sci. Technol.* **45,** 7100–6 (2011).
7. Luo, Y. *et al.* A review on the occurrence of micropollutants in the aquatic environment and their fate and removal during wastewater treatment. *Sci. Total Environ.* **473–474,** 619–641 (2014).
8. Rivera-Utrilla, J., Sánchez-Polo, M., Ferro-García, M. Á., Prados-Joya, G. & Ocampo-Pérez, R. Pharmaceuticals as emerging contaminants and their removal from water. A review. *Chemosphere* **93,** 1268–1287 (2013).
9. Wagner, M., Amann, R. & Lemmer, H. Probing activated sludge with oligonucleotides specific for proteobacteria--- inadequacy of culture-dependent methods for describing microbial community structure..pdf. **59,** 1520–1525 (1993).
10. Sanapareddy, N. *et al.* Molecular diversity of a North Carolina wastewater treatment plant as revealed by pyrosequencing. *Appl. Environ. Microbiol.* **75,** 1688–96 (2009).
11. Zhang, T., Shao, M.-F. & Ye, L. 454 Pyrosequencing Reveals Bacterial Diversity of Activated Sludge From 14 Sewage Treatment Plants. *ISME J.* **6,** 1137–47 (2012).
12. Yang, C. *et al.* Phylogenetic diversity and metabolic potential of activated sludge microbial communities in full-scale wastewater treatment plants. *Environ. Sci. Technol.* **45,** 7408–15 (2011).
13. Ye, L., Zhang, T., Wang, T. & Fang, Z. Microbial Structures, Functions, and Metabolic Pathways in Wastewater Treatment Bioreactors Revealed Using High-Throughput Sequencing. (2012).
14. Saunders, A. M., Albertsen, M., Vollesen, J. & Nielsen, P. H. The activated sludge ecosystem contains a core community of abundant organisms. *ISME J.* **10,** 11–20 (2016).
15. Gao, P. *et al.* Correlating microbial community compositions with environmental factors in activated sludge from four full-scale municipal wastewater treatment plants in Shanghai, China. *Appl. Microbiol. Biotechnol.* **100,** 4663–4673 (2016).
16. Yadav, T. C., Khardenavis, A. a & Kapley, A. Shifts in microbial community in response to dissolved oxygen levels in activated sludge. *Bioresour. Technol.* **165,** 257–64 (2014).

17. Ju, F., Guo, F., Ye, L., Xia, Y. & Zhang, T. Metagenomic analysis on seasonal microbial variations of activated sludge from a full-scale wastewater treatment plant over 4 years. *Environ. Microbiol. Rep.* **6,** 80–89 (2014).
18. Caporaso, J. G. *et al.* Global patterns of 16S rRNA diversity at a depth of millions of sequences per sample. (2010). doi:10.1073/pnas.1000080107/-/DCSupplemental.www.pnas.org/cgi/doi/10.1073/pnas.1000080107
19. Simon, C. & Daniel, R. Metagenomic analyses: Past and future trends. *Appl. Environ. Microbiol.* **77,** 1153–1161 (2011).
20. Graham, D. W. *et al.* Experimental demonstration of chaotic instability in biological nitrification. *ISME J.* **1,** 385–393 (2007).
21. Nunes-alves, C. Do it yourself nitrification. *Nat. Publ. Gr.* **16461,** 16461 (2015).
22. Dytczak, M. a., Londry, K. L. & Oleszkiewicz, J. a. Activated sludge operational regime has significant impact on the type of nitrifying community and its nitrification rates. *Water Res.* **42,** 2320–2328 (2008).
23. Kim, Y. M., Cho, H. U., Lee, D. S., Park, D. & Park, J. M. Influence of operational parameters on nitrogen removal efficiency and microbial communities in a full-scale activated sludge process. *Water Res.* **45,** 5785–5795 (2011).
24. Geets, J., Boon, N. & Verstraete, W. Strategies of aerobic ammonia-oxidizing bacteria for coping with nutrient and oxygen fluctuations. *FEMS Microbiol. Ecol.* **58,** 1–13 (2006).
25. Schmidt, I., Look, C., Bock, E. & Jetten, M. S. M. Ammonium and hydroxylamine uptake and accumulation in Nitrosomonas. *Microbiology* **150,** 1405–1412 (2004).
26. Tappe, W. *et al.* Maintenance energy demand and starvation recovery dynamics of Nitrosomonas europaea and Nitrobacter winogradskyi cultivated in a retentostat with complete biomass retention. *Appl. Environ. Microbiol.* **65,** 2471–7 (1999).
27. Tappe, W., Tomaschewski, C., Rittershaus, S. & Groeneweg, J. Cultivation of nitrifying bacteria in the retentostat, a simple fermenter with internal biomass retention. *FEMS Microbiol. Ecol.* **19,** 47–52 (1996).

28. Johnstone, B. & Jones, R. Physiological effects of long-term energy-source deprivation on the survival of a marine chemolithotrophic ammonium-oxidizing bacterium. *Mar. Ecol. Prog. Ser.* **49,** 295–303 (1988).
29. Stein, L. Y., Sayavedra-Soto, L. a., Hommes, N. G. & Arp, D. J. Differential regulation of amoA and amoB gene copies in Nitrosomonas europaea. *FEMS Microbiol. Lett.* **192,** 163–168 (2000).
30. Lee, Y. & Oleszkiewicz, J. a. Effects of predation and ORP conditions on the performance of nitrifiers in activated sludge systems. *Water Res.* **37,** 4202–10 (2003).
31. Vance, M. E. *et al.* Nanotechnology in the real world: Redeveloping the nanomaterial consumer products inventory. *Beilstein J. Nanotechnol.* **6,** 1769–1780 (2015).
32. Benn, T. M. & Westerhoff, P. Nanoparticle Silver Released into Water from Commercially Available Sock Fabrics. *Environ. Sci. Technol.* **42,** 4133–4139 (2008).
33. Weir, A., Westerhoff, P., Fabricius, L., Hristovski, K. & von Goetz, N. Titanium dioxide nanoparticles in food and personal care products. *Environ. Sci. Technol.* **46,** 2242–50 (2012).
34. Gottschalk, F., Sonderer, T., Scholz, R. W. & Nowack, B. Modeled environmental concentrations of engineered nanomaterials (TiO2, ZnO, Ag, CNT, fullerenes) for different regions. *Environ. Sci. Technol.* **43,** 9216–9222 (2009).
35. Keller, A. a. & Lazareva, A. Predicted Releases of Engineered Nanomaterials: From Global to Regional to Local. *Environ. Sci. Technol. Lett.* **1,** 65–70 (2014).
36. Diao, M. & Yao, M. Use of zero-valent iron nanoparticles in inactivating microbes. *Water Res.* **43,** 5243–51 (2009).
37. Li, M., Zhu, L. & Lin, D. Toxicity of ZnO Nanoparticles to Escherichia coli : Mechanism and the Influence of Medium Components. 1977–1983 (2011).
38. Kiser, M. a, Ryu, H., Jang, H., Hristovski, K. & Westerhoff, P. Biosorption of nanoparticles to heterotrophic wastewater biomass. *Water Res.* **44,** 4105–14 (2010).
39. Eduok, S. *et al.* Evaluation of engineered nanoparticle toxic effect on wastewater microorganisms: current status and challenges. *Ecotoxicol. Environ. Saf.* **95,** 1–9 (2013).

40. Brar, S. K., Verma, M., Tyagi, R. D. & Surampalli, R. Y. Engineered nanoparticles in wastewater and wastewater sludge--evidence and impacts. *Waste Manag.* **30,** 504–20 (2010).
41. Nel, A. E. *et al.* Understanding biophysicochemical interactions at the nano-bio interface. *Nat. Mater.* **8,** 543–557 (2009).
42. Klaine, S. J. *et al.* Nanomaterials in the Environment: Behavior, Fate, Bioavailability, and Effects. *Environ. Toxicol. Chem.* **27,** 1825–1851 (2008).
43. Neal, A. L. What can be inferred from bacterium-nanoparticle interactions about the potential consequences of environmental exposure to nanoparticles? *Ecotoxicology* **17,** 362–371 (2008).
44. Wigginton, N. S. *et al.* Binding of silver nanoparticles to bacterial proteins depends on surface modifications and inhibits enzymatic activity. *Environ. Sci. Technol.* **44,** 2163–2168 (2010).
45. Yang, Y. *et al.* Pyrosequencing reveals higher impact of silver nanoparticles than Ag+ on the microbial community structure of activated sludge. *Water Res.* **48,** 317–25 (2014).
46. Ma, Y., Metch, J. W., Yang, Y., Pruden, A. & Zhang, T. Shift in antibiotic resistance gene profiles associated with nanosilver during wastewater treatment. 1–8 (2016). doi:10.1093/femsec/fiw022
47. Ma, Y. *et al.* Microbial community response of nitrifying sequencing batch reactors to silver, zero-valent iron, titanium dioxide and cerium dioxide nanomaterials. *Water Res.* **68,** 87–97 (2015).
48. Yuan, Z. & Blackall, L. L. Sludge population optimisation: a new dimension for the control of biological wastewater treatment systems. *Water Res.* **36,** 482–90 (2002).
49. Aminov, R. I. & Mackie, R. I. Evolution and ecology of antibiotic resistance genes. *FEMS Microbiol. Lett.* **271,** 147–161 (2007).
50. Frieden, T. Antibiotic resistance threats. *Cdc* 22–50 (2013). doi:CS239559-B
51. Martínez, J. L. Antibiotics and antibiotic resistance genes in natural environments. *Science* **321,** 365–7 (2008).

52. Pruden, A., Pei, R., Storteboom, H. & Carlson, K. H. Antibiotic resistance genes as emerging contaminants: Studies in northern Colorado. *Environ. Sci. Technol.* **40,** 7445–7450 (2006).

53. Muñoz-Aguayo, J., Lang, K. S., LaPara, T. M., González, G. & Singer, R. S. Evaluating the effects of chlortetracycline on the proliferation of antibiotic-resistant bacteria in a simulated river water ecosystem. *Appl. Environ. Microbiol.* **73,** 5421–5 (2007).

54. Pruden, A., Larsson, D. G. J., Amézquita, A., Collignon, P. & Brandt, K. K. EHP – Management Options for Reducing the Release of Antibiotics and Antibiotic Resistance Genes to the Environment. **878,** 878–886 (2013).

55. Laubacher, M. E. & Ades, S. E. The Rcs phosphorelay is a cell envelope stress response activated by peptidoglycan stress and contributes to intrinsic antibiotic resistance. *J. Bacteriol.* **190,** 2065–2074 (2008).

56. Poole, K. Stress responses as determinants of antimicrobial resistance in Gram-negative bacteria. *Trends Microbiol.* **20,** 227–234 (2012).

57. Mah, T. F. C. & O'Toole, G. A. Mechanisms of biofilm resistance to antimicrobial agents. *Trends Microbiol.* **9,** 34–39 (2001).

58. Baker-Austin, C., Wright, M. S., Stepanauskas, R. & McArthur, J. V. Co-selection of antibiotic and metal resistance. *Trends Microbiol.* **14,** 176–182 (2006).

59. Zhang, T., Zhang, X.-X. & Ye, L. Plasmid metagenome reveals high levels of antibiotic resistance genes and mobile genetic elements in activated sludge. *PLoS One* **6,** e26041 (2011).

60. Li, L.-G., Xia, Y. & Zhang, T. Co-occurrence of antibiotic and metal resistance genes revealed in complete genome collection. *ISME J.* **11,** 651–662 (2016).

61. Li, A.-D., Li, L.-G. & Zhang, T. Exploring antibiotic resistance genes and metal resistance genes in plasmid metagenomes from wastewater treatment plants. *Front. Microbiol.* **6,** (2015).

62. Klümper, U. *et al.* Different metal stressors consistently modulate bacterial conjugal plasmid uptake potential in a phylogenetically conserved manner. *ISME J.* **Accepted,** 1–14 (2016).

63. Ma, L., Li, B. & Zhang, T. Abundant rifampin resistance genes and significant correlations of antibiotic resistance genes and plasmids in various environments revealed by metagenomic analysis. *Appl. Microbiol. Biotechnol.* **98,** 5195–5204 (2014).

64. Krasner, S. W., Westerhoff, P., Chen, B., Rittmann, B. E. & Amy, G. Occurrence of disinfection byproducts in United States wastewater treatment plant effluents. *Environ. Sci. Technol.* **43,** 8320–5 (2009).

65. Du, Y. *et al.* Increase of cytotoxicity during wastewater chlorination: Impact factors and surrogates. *J. Hazard. Mater.* **324,** 681–690 (2017).

66. Magnuson, M. L. *et al.* Effect of UV Irradiation on Organic Matter Extracted from Treated Ohio River Water Studied through the Use of Electrospray Mass Spectrometry. *Environ. Sci. Technol.* **36,** 5252–5260 (2002).

67. Rice, J., Wutich, A. & Westerho, P. Assessment of De Facto Wastewater Reuse across the U.S.: Trends between 1980 and 2008. (2013).

68. Wang, C.-C., Niu, Z.-G. & Zhang, Y. Health risk assessment of inhalation exposure of irrigation workers and the public to trihalomethanes from reclaimed water in landscape irrigation in Tianjin, North China. *J. Hazard. Mater.* **262,** 179–88 (2013).

69. Hemalatha, K. *et al.* Function of Nanocatalyst in Chemistry of Organic Compounds Revolution: An Overview. *J. Nanomater.* **2013,** 1–23 (2013).

70. Vejerano, E. P., Leon, E. C., Holder, A. L. & Marr, L. C. Characterization of particle emissions and fate of nanomaterials during incineration. *Environ. Sci. Nano* **1,** 133–143 (2014).

CHAPTER 2: CHARACTERIZATION OF NITRIFYING MICROBIAL COMMUNITY RESPONSE TO STARVATION VIA 16S RRNA AMPLICON SEQUENCING

Jacob W. Metch, Jennifer H. Miller, Hong Wang, Peter Vikesland, Charles Bott, Matt Higgins, Sudhir Murthy, Amy Pruden

2.1 ABSTRACT:

The design of wastewater treatment plants (WWTPs) often relies on a "black box" process; however, with recent advances in biomolecular tools, a fundamental understanding of the microorganisms responsible for pollutant removal in wastewater treatment is possible. For example, although nitrification is crucial for nitrogen removal in WWTPs, knowledge of who the microorganisms are that actually carry out the process is lacking. Nitrifying bacteria and archaea are known to be sensitive to environmental stresses, such as non-ideal temperatures and variations in substrate concentration (ammonia). However, little is known about how nitrifying microbial communities respond and change as a result of such stress. Increased understanding of the stress response process may lead to optimized management of WWTP parameters like aeration, food to microorganism ratios, and wasting rates to select for an ideal and resilient microbial community, therefore resulting in decreased reactor upsets and faster recovery for the nitrification process. In order to utilize such strategies, first an understanding of how a resilient nitrifying microbial community is structured is needed. Here we used Illumina 16S rRNA amplicon sequencing to characterize microbial communities in reactors filled with activated sludge collected from the nitrification basin of DC Water Blue Plains Advanced WWTP and subject to ammonia starvation conditions in several trials over a range of temperatures typical to wastewater treatment (14 °C, 20 °C, 27 °C and 30 °C). The microbial community composition was characterized with time via amplicon sequencing of genomic (DNA) and transcriptomic (cDNA) 16S rRNA genes. *Nitrospira* and *Nitrosomonas* were the only known nitrifying genera detected in the dataset and *Nitrosomonas* was only detected in 4 of the 84 samples sequenced. Relative abundances of *Nitrospira* DNA and cDNA remained relatively consistent throughout

starvation conditions and did not vary based on temperature, indicating the possibility of metabolic diversity in *Nitrospira* species, which would allow them to compete with heterotrophic organisms in activated sludge. This study demonstrates the stability of *Nitrospira* throughout the experiments and contributes to understanding shifts in activated sludge community composition as a function of starvation stress and temperature.

2.2 INTRODUCTION:

In order to develop activated sludge process design beyond the traditional "black box" approach, biomolecular tools can be utilized to better understand the microorganisms responsible for specific functions and therefore inform design.[71,72] For example, nitrification is a critical process for nitrogen removal in wastewater treatment, and although widely studied, recent discoveries are changing our understanding of the microorganisms responsible. It has traditionally been assumed that nitrification exclusively involves a two-step process in which ammonia is oxidized to nitrite by ammonia oxidizing bacteria (AOB) and subsequently nitrite is oxidized to nitrate by nitrite oxidizing bacteria (NOB). More recently, ammonia oxidizing archaea (AOA) have been described and appear to sometimes be the dominant ammonia oxidizing microorganisms (AOM) driving nitrification in activated sludge[73]. Further, anaerobic ammonia oxidizing (anammox) bacteria, which use nitrite as an electron acceptor and ammonia as an electron donor,[74] and the discovery of *Nitrospira* spp., which are capable of completely oxidizing ammonia to nitrate,[21] have recently been discovered and increasingly are being implemented in wastewater treatment.

Reactor upsets due to influent variations and environmental conditions are a common and often expensive nuisance in WWTP management.[75] In particular, nitrification is known to be very sensitive to several types of stress including variations in dissolved oxygen concentration,[76] salinity,[77] temperature,[78] and substrate concentration.[79] Nitrifying bacteria cope with these stresses using various mechanisms. For example, stress responses involved in low substrate concentration include increased intracellular ammonia concentrations,[25] dormant or resting states,[26,27] maintaining high ribosomal content,[28] and even maintaining multiple copies of the gene encoding the enzyme

responsible for ammonia oxidation, ammonia monooxygenase (amo) with varying ammonia activity.[29] Variations in stress response mechanisms within the nitrification microbial community may lead to selective advantages for some nitrifying microorganisms over others and thus influence key process parameters, such as activity and decay rates. Indeed, environmental factors such as dissolved oxygen, pH, ammonia and nitrite concentrations have been used to select for ideal nitrifying microbial communities that limit nitrite oxidation (short-cut nitrification) or are better suited for high or low ammonia concentrations.[22,80] Varying operational parameters has been shown to impact nitrifying communities, with *Nitrosomonas* and *Nitrobacter* thriving in an alternating aerobic/anaerobic reactor and *Nitrosospira* and *Nitrospira* dominating in strictly aerobic reactors.[22] Seasonality also impacts nitrifying microbial community structure and performance, with *Nitrospira* being better suited for high temperatures and *Nitrobacter* dominating at low temperatures.[76] With further understanding of the impacts of stresses to nitrifying microbial communities, it may be possible to inform WWTP design to minimize nitrification reactor upsets and improve recovery after reactor upset or dormancy by selecting for nitrifying microorganisms best suited to handle stresses in a given wastewater.

Recent developments in high throughput DNA sequencing allow for deep profiling of microbial community composition. Specifically, 16S rRNA regions are amplified by polymerase chain reaction and subject to Illumina DNA sequencing (i.e., Illumina 16S rRNA gene amplicon sequencing), which allows for identification and estimation of relative abundance of taxa within the sample.[18] In the current study, nitrifying microbial communities were characterized using Illumina 16S rRNA amplicon sequencing, throughout a period of starvation, with no ammonia or organic carbon provided in the feed. Trials were run at various temperatures representing seasonal variations in WWTPs. Variations in genomic- and transcriptomic-based microbial community compositions were observed throughout each experimental trial allowing the characterization of both the microorganisms present in the reactor, and the microorganisms active in the reactor. This high-throughput sequencing data was compared to other nitrifying microorganisms characterization techniques such as nitrate

production rate (NPR), NO_x production rate (NO_xPR) and qPCR of nitrifying bacterial marker genes.

2.3 MATERIALS AND METHODS:

2.3.1 Experimental Set-Up

Activated sludge samples were collected from the effluent of a DC Water Blue Plains Advanced WWTP nitrification basin, and immediately transported to Virginia Tech with aquarium-pump aeration (Figure 2.1). A 25-L reactor was set up in a constant temperature room and aeration was controlled by a HACH SC100 sensor controller coupled with LDO^{TM} dissolved oxygen sensor (HACH, Loveland, CO) to maintain an oxygen level between 2.5 and 4 mg/L. Throughout the experiment pH was adjusted within a range of 7.2-7.8 using $NaHCO_3$. Samples were collected from the reactor for DNA and cDNA analyses and for nitrifying microorganism activity tests using NPR/NO_xPR batch reactors. Initial trials were run at three temperatures commonly experienced by the Blue Plains Advanced WWTP throughout normal seasonality (14 °C, 20 °C, and 30 °C) and were run for 16-18 days. In order to better understand how nitrifying microorganisms recover from starvation, follow-up trials were conducted at similar temperatures (14 °C, 20 °C, and 27 °C) in which at the conclusion of the starvation experiment (18 days of starvation), ammonium was fed to the reactor and the concentration of ammonium was maintained between 20-50 mg/L NH_3-N. In these recovery experiments, influent of the DC Water nitrification basin was also sampled in order to compare the lab microbial communities to the field condition. The seed sludge was also sampled directly from the basin in these recovery experiments and are denoted here as “Day 0” samples. See Table S1 for sludge collection dates and details on sampling frequency for each trial.

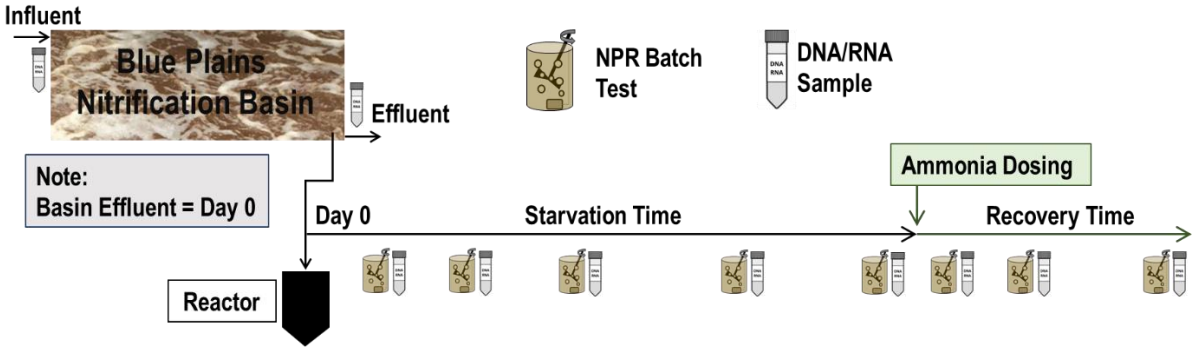

Figure 2. 1 Schematic for experimental trials. First three trials (14-1, 20-1, and 30-1) included reactor seeding and starvation time, while recovery trials (14-2, 20-2, and 27-1) all included basin influent and Day 0 sampling, as well as recovery time portions of schematic.

2.3.2 NPR Batch Tests for Metabolic Activity Evaluation

After a ≈36 h acclimation time, 1300 mL of liquor was withdrawn from the reactor and used to run ammonia and NPR activity tests in duplicate. $(NH_4)_2SO_4$ and $NaNO_2$ were dosed to aerated batch activity reactors to reach an initial concentration of ≈50 and ≈15 mg-N/L, respectively. DO was maintained at 2 to 4 mg/L during the batch tests by adjusting the air flow. Ammonium, nitrite, and nitrate were monitored every 20 min for 2 hours. pH was also monitored and maintained between 7.2 to 7.9 using $NaHCO_3$. The batch activity tests were repeated seven times throughout starvation experiments. Water samples for ammonia, nitrite and nitrate were filtered through 0.45 µm VWR Polyethersulfone membrane filters (Arlington Heights, IL). Nitrate was measured using a Dionex (Sunnyvale, CA) DX-120 ion chromatography (IC) according to Standard Method 4110[81]. Ammonia and nitrite were measured using HACH Salicylate Method (TNTplus 832) and HACH Diazotiaztion method (TNTplus 840), respectively. In the follow-up recovery trials, after feeding in the reactor began, nitrifying microorganism activity was monitored by dosing $(NH_4)_2SO_4$ and $NaNO_2$ into the reactor at a concentration of ≈50 and ≈15 mg-N/L, respectively and then ammonia, nitrite and nitrate were measured every 20 min for 2 hours.

2.3.3 DNA and RNA Extraction

Activated sludge samples for DNA and RNA extraction were preserved with RNAlater® solution (Life technologies, Grand Island, NY) upon sampling, flash frozen

using a dry ice- ethanol bath, and stored at -80 ˚C until further processing. DNA was extracted from 175 µL of preserved sludge samples using a FastDNA® Spin kit for soil (MP Biomedicals, Solon, OH) according to the manufacturer's protocol. RNA was extracted from same amount of sample using a MagMAX® Total Nucleic Acid Isolation Kit (Life technologies, Grand Island, NY) and was transcribed to cDNA using iScript™ cDNA synthesis kit (Bio-Rad, Hercules, CA) on the same day according to the manufacturer's instruction. See Table B.1 for sampling frequency.

2.3.4 Quantitative Polymerase Chain Reaction

Ammonia oxidizing bacteria (as represented by the bacterial ammonia monooxygenase gene (*amoA*)), *Nitrospira*, *Nitrobacter*, and total bacteria were enumerated by qPCR using previously published methods[47]. Reactions were performed in triplicate in 10 µl volumes containing 1×SsoFast® Probes or Evagreen® supermix (Bio-Rad, Hercules, CA), 400 nM primers, and 1 µl template. Samples were analyzed at 1:10 or 1:50 dilutions to minimize qPCR inhibition based on dilution curves.

2.3.5 Amplicon Sequencing and Analysis

A representative cross-section of samples was selected from the experimental trials (see Table A.1 for sample selection) and submitted for 16S rRNA amplicon sequencing on an Illumina MiSeq platform. All samples were subject to PCR amplication of the V4 region of the 16S rRNA gene from DNA and cDNA samples using universal bacterial/archaeal barcoded primers 515F/806R[18] and following the earth microbiome project 16S Illumina amplification protocol (http://www.earthmicrobiome.org). For QA/QC purposes, a DNA extraction blank, cDNA extraction blank, and PCR blank were subjected to sample processing in parallel and submitted for sequencing. Pooled samples were submitted to the Biocomplexity Institute's Genomics Research Laboratory (Blacksburg, Virginia) for paired-end 250 Illumina sequencing. Paired-end sequence reads were joined using PANDAseq[82] and then processed using Quantitative Insights Into Microbial Ecology (QIIME) version 1.8.0[83]. The *pick_de_novo_otus.py* script was used to perform *de novo* operational taxonomic unit (OTU) picking using the uclust_ref method and taxonomy assignments of OTUs were generated using Greengenes 13_8

reference database, aligned at 97%. The resulting OTU table was filtered to remove chimeric sequences using the Chimera Slayer method[84], and singletons and organelle sequences using the *filter_taxa_from_otu_table.py* script. This procedure produced an OTU table consisting of 12 million sequences from 84 samples and 3 blank controls. The lowest number of sequences in a sample was 38,561 and therefore the OTU table was rarefied to 38,000 sequences per sample for all analysis unless otherwise stated. Similarity of microbial community compositions was quantified using weighted UniFrac distances computed using the Greengenes reference tree within QIIME[85]. A weighted UniFrac distance matrix was exported to Primer 6 software (Primer-E, Plymouth, UK) where multidimensional scaling (MDS) ordination was conducted.

2.4 RESULTS:

2.4.1 Shifts in Microbial Community

MDS ordination based on the weighted unifrac distance matrix revealed general trends in activated sludge microbial community compositions throughout the trials (Figure 2.2). The complete MDS plot (Figure A.1) shows that genomic-based (DNA) samples grouped separately from transcriptomic-based (cDNA) samples with two cDNA samples clustering separately (20 °C trial 2, fed 12 hrs and fed 48 hrs). Figure 2.2 shows that the microbial communities in the starvation portion of all trials (panels a-c) shifted in a similar trajectory for both DNA and cDNA. The starting points of the starvation experiments (light-shaded red) are in similar locations on the MDS plot, and then as the starvation experiment progressed (darker-shaded reds) the microbial community compositions shifted toward the upper right of the plot. An interesting trend emerged in the recovery trials at each temperature. While the microbial community characterized by DNA after ammonia dosing remained relatively similar to the Day 18, the cDNA was much more variable. In the 14 °C and 20 °C experiments (Figure 2.2, panels a and b), this cDNA shift after feeding was farther away from the influent microbial community activity (see open blue triangle and open blue circle respectively). However, in the 27 °C experiment (Figure 2.2, panel c) the cDNA shift after feeding shifted the microbial community activity back such that it resembled the influent microbial community activity (see open upside-down blue triangles).

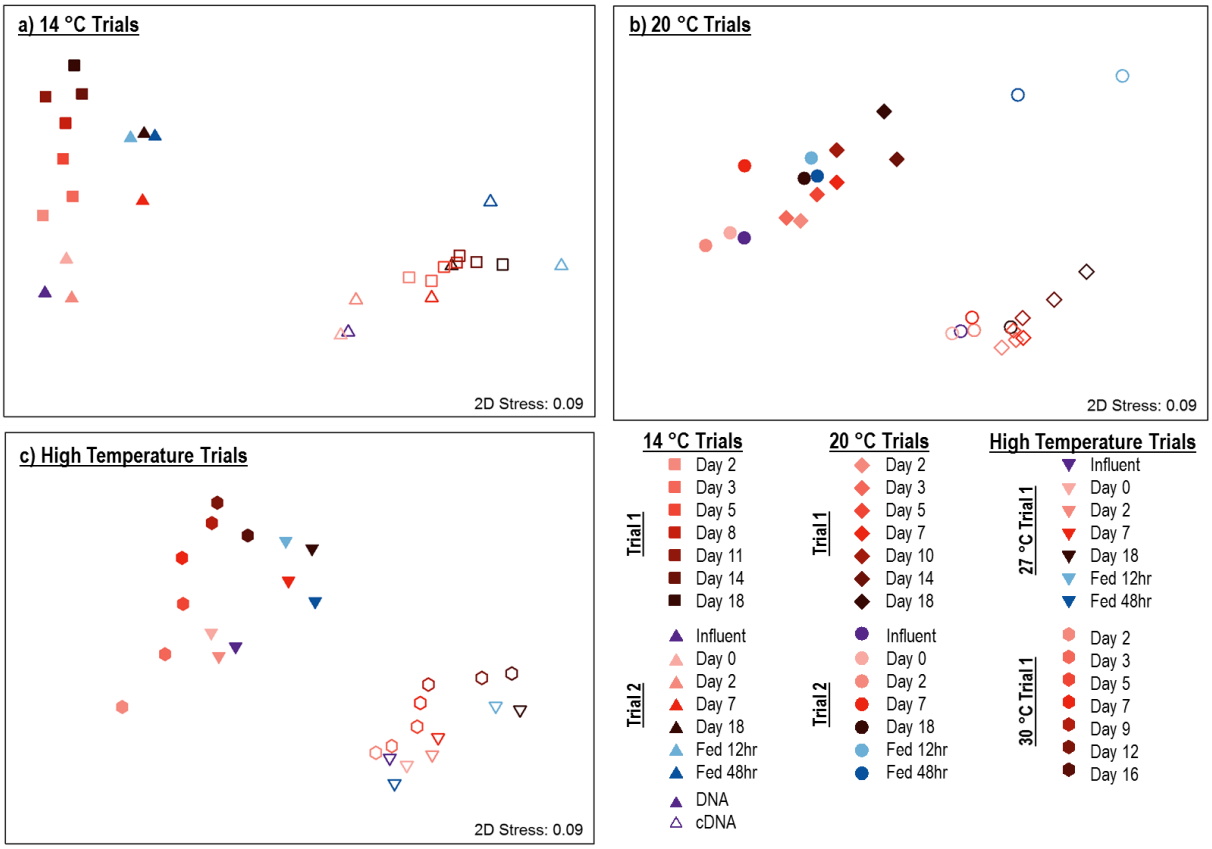

Figure 2. 2 MDS ordination of unifrac distance matrix of OTU table rarefied to lowest sample sequence number (38,000 sequences). Overall MDS has been broken into three panels for easier visualization (a: 14 °C trials b: 20 °C trials c: high temperature trials at 27 °C and 30 °C) complete plot can be seen in SI (Figure A.1). Darkness of red shading increases with time in starvation reactor, purple points indicate samples collected from the influent of the DC Water nitrification basin, blue points represent samples collected after feeding of ammonium to reactor.

Examining the relative abundance of the phyla (Figure 2.3) gives insight into potential underlying factors driving the common trajectory of microbial community shifts within the trial reactors through time, as well as the bifurcation of DNA and cDNA-based analyses shown in Figure 2.2. In Figure 2.2, DNA and cDNA consistently group separately. Likewise, a trend of distinct phyla relative abundance is seen between DNA and cDNA groups in all trials, with DNA-based measurements consistently indicating increased *Bacteroidetes* and decreased *Proteobacteria* compared to cDNA-based measurements (Figure 2.3). Other phyla, such as *Planctomycetes* and *Cyanobacteria*, also showed differentiating trends in DNA and cDNA datasets having greater relative

abundance in the cDNA dataset compared to the DNA dataset especially at 20 °C and high temperature trials.

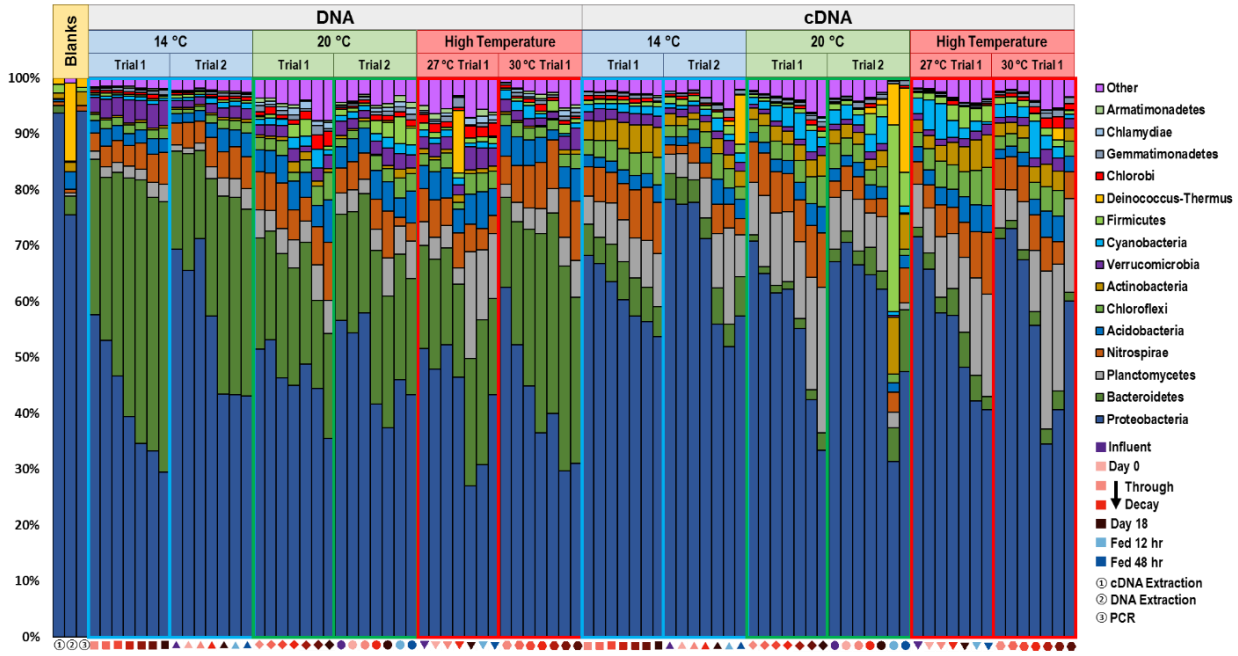

Figure 2. 3 Stacked bar chart of relative abundance of phyla in samples. Data is not rarefied so that blanks could be shown with sample data. Symbols along x-axis match those in Figure 2.2 where darkness of red shading increases with time in starvation reactor, purple points indicate samples collected from the influent of DC Water nitrification basin, blue points represent samples collected after feeding of ammonium to reactor.

In an attempt to determine the OTUs most responsible for driving the observed trends, the variance of the OTU relative abundances within each trial and nucleic acid type were calculated and then ranked (Figure A.2). This also demonstrated substantial differences in the ten most variable OTUs in DNA and cDNA datasets for every trial. For example, in the 14 °C trials Bacteroidetes and Betaproteobacteria OTUs were among the most variable OTUs compared to mainly Deltaproteobacteria OTUs being the most variable in the cDNA dataset. Of particular interest in this study, a *Nitropira* OTU was among the top ten most variable OTUs in 5 of the 6 trials for the DNA dataset (all but trial 14C-2), and 4 of the 6 trials for the cDNA dataset (all but trials 20C-2 and 27C-1). PICRUSt analysis was also conducted to determine fluctuations in predicted functional genes throughout the starvation process. This analysis involves predicting the functional content of a metagenome based on the taxonomy present in a sample, and a database of

reference genomes.[86] Here PICRUSt indicated little variation in the functional gene composition across all trials and time points within trials (see Figure A.3).

2.4.2 Nitrifiers Revealed by 16S rRNA Amplicon Sequencing

After OTU taxonomic identification using the Greengenes reference database, nitrifying microorganisms were searched for in the resulting OTU table. AOB genera searched for included *Nitrosomonas, Nitrosospira, Nitrosococcus, Nitrosolobus,* and *Nitrosovibrio*,[87] and NOB genera searched for included *Nitrospira, Nitrobacter, Nitrococcus, Nitrospina, Nitrotoga, Nitrolancea,* and *Nitromaritima*.[88] Since no OTUs were identified as *Crenarchaeota*, which is thought to be the only kingdom containing ammonia oxidizing archaea,[87] archaea were not thought to play a significant role in nitrification in our system. *Nitrosomonas* were detected in only four samples out of the rarefied dataset (84 samples), and were found at low relative abundance (less than 10^{-3}) (Figure 2.4). *Nitrospira*, however, were detected at high relative abundance in all trials across temperature variations and remained relatively stable throughout starvation experiments with a minimum of $10^{-1.85}$ and a maximum of $10^{-0.97}$. AOB, *Nitrospira*, and *Nitrobacter* were also examined using qPCR to quantify gene markers amoA (bacterial), *Nitrospira* 16S rRNA, and *Nitrobacter* 16S rRNA, respectively (Figure A.4). *Nitrospira* 16S rRNA gene copies were consistently greater than amoA gene copies, which supports the findings from 16S rRNA Amplicon Sequencing. *Nitrobacter* 16S rRNA was consistently detected at sufficiently high abundance to be detected using 16S rRNA amplicon sequencing; however this was not observed in our OTU table.

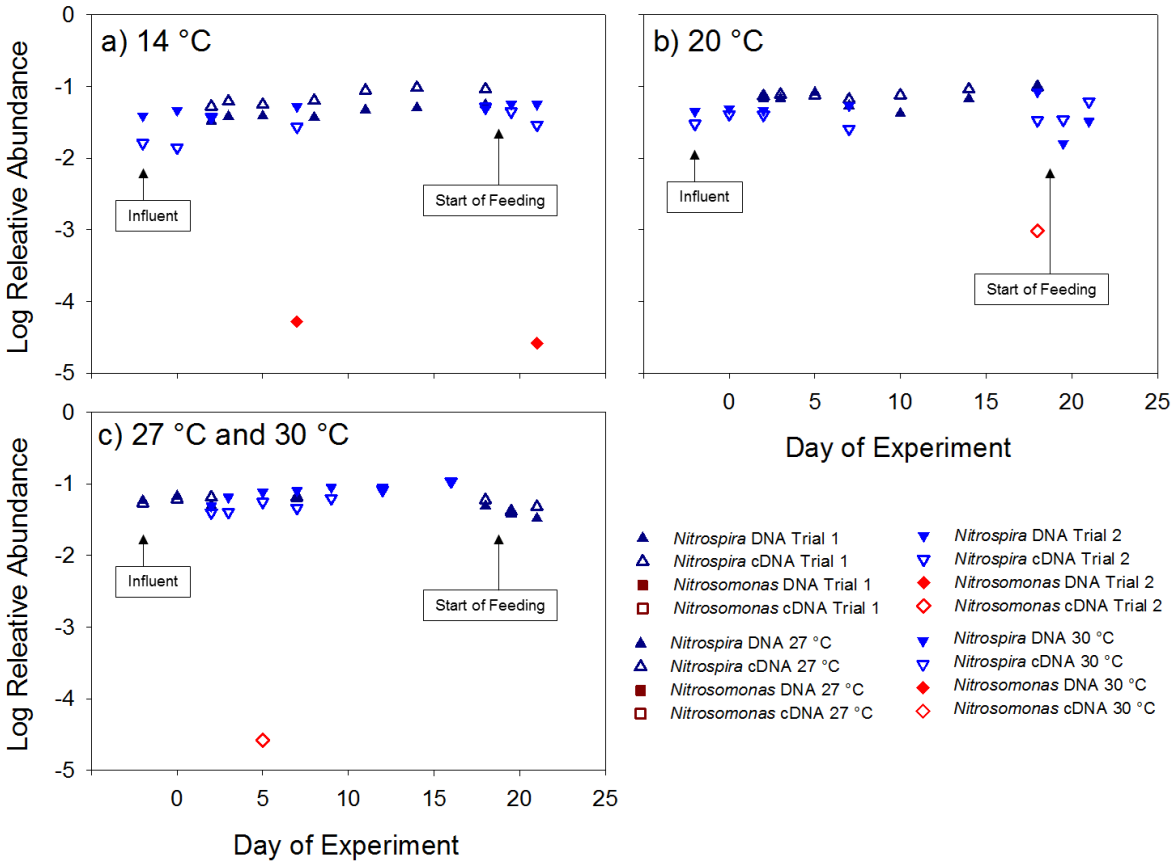

Figure 2. 4 Nitrifying genera relative abundance in starvation experiments based on Illumina 16S rRNA amplicon sequencing. Relative abundance was calculated based on abundance in rarefied OTU table, normalized to total rarefied sequences (38,000 sequences). Influent samples were plotted and labeled as a reference to starvation samples, and ammonium dosing in reactor started at about day 18.5 of the experiment which is marked on plots.

2.4.3 *Nitrospira* OTU Variability

The *Nitrospira* genus was composed of 159 unique OTUs in this dataset, but two were consistently more abundant (greater than 1 log) than the others (OTU ID# 4460870 (henceforth called *Nitrospira* OTU-A) and OTU ID# 1491 (called *Nitrospira* OTU-B)) (data not shown). OTU-A was consistently more abundant than OTU-B with a few exceptions (See Figure 2.5). In the 14 °C trials *Nitrospira* OTU-A and OTU-B trends are similar to each other, however, the cDNA relative abundance for OTU-A decreased after 48 hrs of feeding, while the cDNA relative abundance for OTU-B increased at the same

time. Similarly, in the 20 °C trials, both OTUs were stable throughout the starvation period, but after 12 hrs and 48 hrs of feeding, cDNA relative abundance of OTU-A sharply decreased while the relative abundance of OTU-B cDNA increased. In the 27 °C and 30 °C trials *Nitrospira* abundance and activity seemed to be controlled by OTU-A, with the exception of Day 7 of the 27 °C experiment in which the relative abundance of OTU-A DNA decreased, and the relative abundance of OTU-B increased to control *Nitrospira* trends at that point.

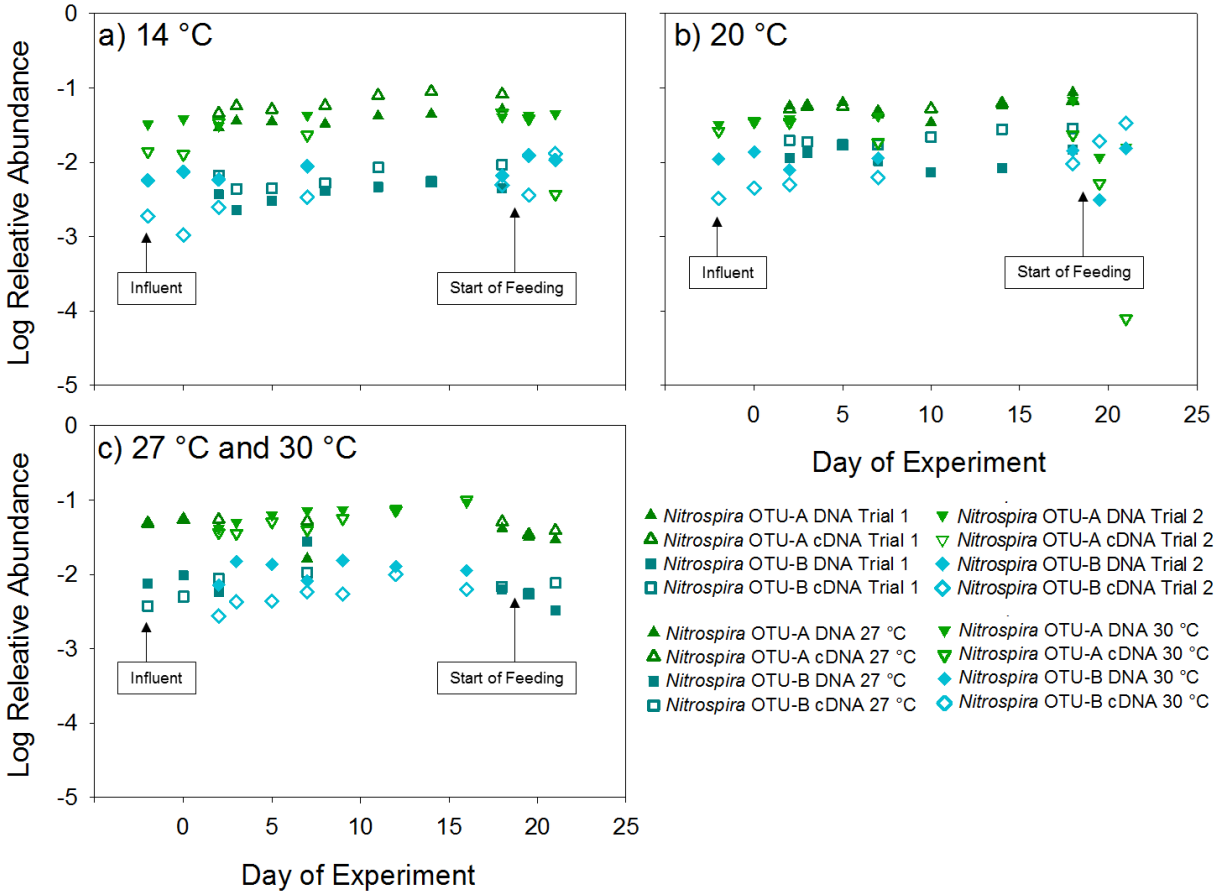

Figure 2. 5 Relative abundance of dominant *Nitrospira* OTUs based on Illumina 16S rRNA amplicon sequencing. Relative abundance was calculated based on abundance in the rarefied OTU table, normalized to total rarefied sequences (38,000 sequences). Influent samples were plotted and labeled as a reference to starvation samples, and ammonium dosing in reactor started at about day 18.5 of the experiment which is marked on plots.

2.4.4 Nitrifying Microbial Community Activity

Activity of the nitrifying microbial community was determined throughout the trials by removing an aliquot of biomass, spiking with ammonia, and measuring the NO_x production rate and NO_3 production rate. These values quantify how the activity potential of the AOB and NOB, respectively, shift with time as starvation ensues (Figure 2.5). NO_x production rates had a wide range of values at day 2 of each trial with 20 °C Trial 1 having the highest NO_x production rate (378 mg-N/L/d) and 14 °C Trial 2 having the lowest (38 mg-N/L/d). As expected, NOx production rates decreased with time and all trials ended with similar NO_x production rates by day 16-18 (range 13-58 mg-N/L/d). NO_3 production rate decay behaved similarly to NO_x production rate decay with high variability in activity during the first several days of starvation, and a convergence of activity at the end of the starvation period (Day 16-18).

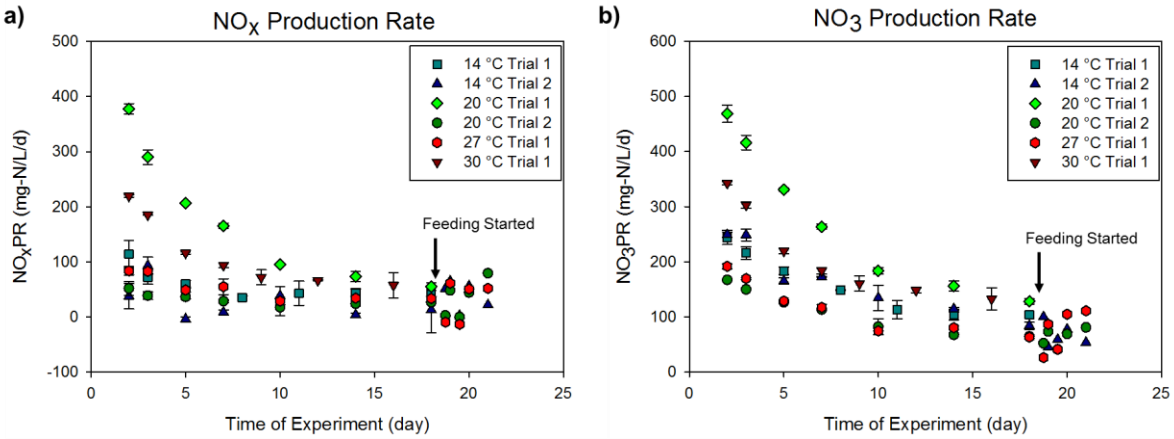

Figure 2. 6 Metabolic activity of nitrifying microorganisms. a) NO_x Production Rates indicative of ammonia oxidizing microorganisms and b) NO_3 production rates indicative of nitrite oxidizing bacteria. Error bars show standard deviation of duplicate small batch-decay reactor values, no replicates available after feeding of NH_4^+ started.

2.5 DISCUSSION:

2.5.1 Microbial Community Dynamics Throughout Experiment

The microbial communities characterized by DNA were dominated by *Proteobacteria* and *Bacteroidetes*, as is expected in activated sludge.[11,89,90] It was observed that the relative abundance of *Proteobacteria* decreased in both the DNA and

cDNA datasets. *Bacteroidetes* relative abundance in the DNA dataset increased throughout the starvation portion of trials, while the corresponding relative abundance in the cDNA dataset was much lower and less variable. This observation is thought to be due to the high abundance of *Bacteroidetes* in fecal matter explaining the high presence in the DNA pool, while an aeration basin is not an ideal environment for most *Bacteroidetes* species since most are obligate anaerobes, explaining their low activity.[91] The perceived increase of *Bacteroidetes* relative abundance in the DNA dataset may be indicative of higher resilience to decay compared to other phyla present in the reactor, such as *Proteobacteria*. The trends observed in Figure 2.3 are supported by the 10 most variable OTUs in each trial for DNA and cDNA (Figure A.2). In general most of these OTUs are involved in carbon degradation, with the exception of OTUs in the *Nitrospira* genus. It has been shown that influent COD and carbon source correlate with activated sludge microbial communities.[15] Therefore, the variation in microbial community throughout the starvation trials may simply be due to the activated sludge microbial community acclimating to a new carbon substrate source. Although the taxonomy varied considerably throughout starvation, PICRUSt analysis revealed very little difference in functional capability of the microbial community (Figure A.3). This may be due to PICRUSt only assigning functional genes based on organisms in the reference databases,[86] which likely exclude several difficult to culture microorganisms in activated sludge.

The difference in relative abundance between DNA and cDNA datasets demonstrates the usefulness of both techniques used to characterize the microbial community. The higher *Bacteriodetes* relative abundances in the DNA dataset compared to the cDNA dataset is a good example of how microorganism presence and activity can be measured by comparting these datasets.

2.5.2 Nitrifying Microbial Community

Several studies have investigated the microbial community composition of nitrifying microorganisms using methods that target only a finite number of nitrifying microorganisms such as qPCR, PCR, FISH, and amplicon sequencing on functional genes. In this study, we utilized Illumina 16S rRNA amplicon sequencing to characterize

shifts in nitrifying microbial communities throughout starvation in order to not restrict taxonomy detected. *Nitrospira* and *Nitrosomonas* were the only known nitrifying genera detected using this assay (Figure 2.4), and *Nitrospira* was the only nitrifying genus detected consistently.

Pyrosequencing of a lab-scale nitrifying reactor, and a wastewater treatment plant similarly revealed dominance of *Nitrosomonas* and *Nitrospira*; however, in that study *Nitrosomonas* represented 15.54% of sequences (in the reactor).[90] Another study determined that relatively fast-growing nitrifiers, *Nitrosomonas and Nitrobacter*, were dominant in an alternating aerobic/anoxic sequening batch reactor, while slower growing *Nitrosospira and Nitrospira* were dominant in a strictly aerobic reactor.[22] Therefore, reactor configuration at DC Water and our trials likely played a role in shaping the microbial community. It was also previously found that *Nitrospira* was sensitive to changes in temperature,[76] however in this study *Nitrospira* had consistent relative abundance and dominant OTU (*Nitrospira* OUT-A) across seasonal temperature variation. This observed stability may be due to the lack of competition as there were no other nitrifying microorganisms detected. These studies demonstrate the complexity of nitrifying microbial communities and the presence of *Nitrospira* as the dominant nitrite oxidizing bacteria; however, to our knowledge this is the first study to observe *Nitrospira* as the only nitrifying genera detected in activated sludge communities using Illumina 16S rRNA amplicon sequencing, as was the case in most of our samples.

There are several plausible explanations for the dominance of *Nitrospira* observed in the 16S rRNA amplicon OTU table. The assumed interdependence between AOM and NOB has recently been challenged by the discovery of *Nitrospira* species capable of ammonia oxidation[21], and *Nitrospira* species capable of ureolytic and heterotrophic activity using oxygen or nitrate as electron acceptors.[92] These recent discoveries highlight the possibility for *Nitrospira* to be the dominant or sole nitrifying genera in this system. To our knowledge however, *Nitrospira* have not been observed to be the dominant AOM in a wastewater treatment plant. *Nitrospira* dominance has been observed in drinking water environments and the presence of commamox *Nitrospira* was inferred.[93,94] This theory is also supported by qPCR data in which we observed low *amoA* abundance using

primers designed for traditional AOB *amoA* detection (Figure A.4), which differ phylogenetically from *amoA* in comammox *Nitrospira*.[95]

However, it is also possible that this observation is a result of the limitations of 16S rRNA amplicon sequencing. The AOM responsible for ammonia oxidation may be extremely diverse and at low abundances, and therefore are not being sequenced. Also, there may be other nitrifying archaea or bacteria present in adequate abundance to be sequenced, but are not being identified due to limitations of genomic data in the reference database.[96] In this study, *Nitrobacter* was detected in abundances close to *Nitrospira* (within 1 log) using qPCR (Figure A.4) but was not detected in the 16S rRNA amplicon sequencing dataset. This suggests error in amplicon sequencing and further research is needed to determine why *Nitrospira* was the only nitrifying microorganism consistently detected.

2.5.3 Variations in *Nitrospira* OTUs

Although *Nitrospira* were the only nitrifying microorganisms consistently detected, analysis into *Nitrospira* OTUs yielded interesting trends in the starvation of this important nitrifying genus. In the entire dataset, there were 159 unique *Nitrospira* OTUs detected, however *Nitrospira* abundance was dominating mainly by two of these OTUs (*Nitrospira* OTU-A and *Nitrospira* OTU-B). This high number of unique *Nitrospira* OTUs in activated sludge is consistent with a previous study that found 120 unique *Nitrospira* OTUs.[97] During the starvation portion of the experiments relative abundance of both of these OTUs are relatively stable (Figure 2.4). However, the abundance of total 16S rRNA is decaying over the same time period (Figure A.4), therefore total abundance of these *Nitrospira* OTUs are decaying as well as confirmed by qPCR (Figure A.4). The stability of *Nitrospira* relative abundance during starvation is a surprising finding considering the only nitrogen available as a substrate would come from decaying organisms. Recently recognized metabolic diversity in *Nitrospira* species[21,92,97] may have allowed these organisms to compete with traditional heterotrophic organisms dominating the activated sludge microbial community, leading to the relative abundance stability observed.

The feeding of ammonia in the follow-up recovery trials seemed to affect *Nitrospira* OTUs in unique ways. Figure 2.5 shows that in both the 14 °C Trial 2 (panel a) and 20 °C Trial 2 (panel b), *Nitrospira* OTU-A DNA and *Nitrospira* OTU-B DNA relative abundance reacts similarly to introduced ammonia. However, cDNA relative abundance of these OTUs had opposing reactions to introduced ammonia. While *Nitrospira* OTU-A was dominant during starvation, after feeding started the relative abundane of *Nitrospira* OTU-A cDNA decreased, while *Nitrospira* OTU-B cDNA relative abundance increased and became the dominant *Nitrospira* OTU in the cDNA dataset. This effect was not observed at the high temperature trials (Figure 2.5 panel C), which suggests different selective pressures between these two OTUs at high temperatures. This observed differences in *Nitrospira* OTU reaction to environmental changes is believed to be the product of physiological differences between the OTUs leading to differing competitive advantages, as has been observed previously within the *Nitrospira* genus in activated sludge[97].

2.6 CONCLUSION:

Here we observed *Nitrospira* to be the dominant nitrifying microorganism in activated sludge. The dominance of *Nitrospira*, and continued AOM and NOB activity is indicative of comammox *Nitrospira* species being present and driving ammonia oxidation in activated sludge. We also observed high diversity and apparent temperature dependent differentiation in selective advantages within the *Nitrospira* genus with variations of dominant OTU transcription of 16S rRNA as a result of varying environmental conditions. This observation was seen in the cDNA dataset, but was far less apparent in the DNA dataset, demonstrating the importance of evaluating cDNA when characterizing microbial communities in order to determine variations in OTU activity as well as presence. This study supports recent observations and notions that nitrification in wastewater treatment plants is more complex than the traditional model of AOB oxidize ammonia and NOB oxidize nitrite. In order to more accurately model and therefore design for nitrification systems with activated sludge increased understanding is needed of how nitrifying microbial community variations, especially those that undermine the traditional model, will affect important key nitrification parameters.

REFERENCES

1. Whiteley, A. S., Manefield, M. & Lueders, T. Unlocking the ‘microbial black box’ using RNA-based stable isotope probing technologies. *Curr. Opin. Biotechnol.* **17,** 67–71 (2006).
2. Ju, F. & Zhang, T. 16S rRNA gene high-throughput sequencing data mining of microbial diversity and interactions. *Appl. Microbiol. Biotechnol.* **99,** 4119–4129 (2015).
3. Park, H.-D., Wells, G. F., Bae, H., Criddle, C. S. & Francis, C. a. Occurrence of ammonia-oxidizing archaea in wastewater treatment plant bioreactors. *Appl. Environ. Microbiol.* **72,** 5643–7 (2006).
4. Lackner, S. *et al.* Full-scale partial nitritation / anammox experiences e An application survey. *Water Res.* **55,** 292–303 (2014).
5. Nunes-alves, C. Do it yourself nitrification. *Nat. Publ. Gr.* **16461,** 16461 (2015).
6. Love, N. G. & Bott, C. B. Evaluating the role of microbial stress reponse mechanims in causing biological treatment system upset. *Water Sci. Technol.* **46,** 11–18 (2002).
7. Huang, Z., Gedalanga, P. B., Asvapathanagul, P. & Olson, B. H. Influence of physicochemical and operational parameters on Nitrobacter and Nitrospira communities in an aerobic activated sludge bioreactor. *Water Res.* **44,** 4351–4358 (2010).
8. Wang, Z. *et al.* Response of performance and ammonia oxidizing bacteria community to high salinity stress in membrane bioreactor with elevated ammonia loading. *Bioresour. Technol.* **216,** 714–721 (2016).
9. Antoniou, P. *et al.* Effect of temperature and ph on the effective maximum specific growth rate of nitrifying bacteria. *Water Res.* **24,** 97–101 (1990).
10. Bollmann, A. & Laanbroek, J. Growth at Low Ammonium Concentrations and Starvation Response as Potential Factors Involved in Niche Differentiation among Ammonia-Oxidizing Bacteria Growth at Low Ammonium Concentrations and Starvation Response as Potential Factors Involved in Niche Diff. *Appl. Environ. Microbiol.* **68,** 4751–4757 (2002).
11. Schmidt, I., Look, C., Bock, E. & Jetten, M. S. M. Ammonium and hydroxylamine uptake and accumulation in Nitrosomonas. *Microbiology* **150,** 1405–1412 (2004).

12. Tappe, W. *et al.* Maintenance energy demand and starvation recovery dynamics of Nitrosomonas europaea and Nitrobacter winogradskyi cultivated in a retentostat with complete biomass retention. *Appl. Environ. Microbiol.* **65,** 2471–7 (1999).
13. Tappe, W., Tomaschewski, C., Rittershaus, S. & Groeneweg, J. Cultivation of nitrifying bacteria in the retentostat, a simple fermenter with internal biomass retention. *FEMS Microbiol. Ecol.* **19,** 47–52 (1996).
14. Johnstone, B. & Jones, R. Physiological effects of long-term energy-source deprivation on the survival of a marine chemolithotrophic ammonium-oxidizing bacterium. *Mar. Ecol. Prog. Ser.* **49,** 295–303 (1988).
15. Stein, L. Y., Sayavedra-Soto, L. a., Hommes, N. G. & Arp, D. J. Differential regulation of amoA and amoB gene copies in Nitrosomonas europaea. *FEMS Microbiol. Lett.* **192,** 163–168 (2000).
16. Yuan, Z., Oehmen, A., Peng, Y., Ma, Y. & Keller, J. Sludge population optimisation in biological nutrient removal wastewater treatment systems through on-line process control: A re/view. *Rev. Environ. Sci. Biotechnol.* **7,** 243–254 (2008).
17. Dytczak, M. a., Londry, K. L. & Oleszkiewicz, J. a. Activated sludge operational regime has significant impact on the type of nitrifying community and its nitrification rates. *Water Res.* **42,** 2320–2328 (2008).
18. Caporaso, J. G. *et al.* Global patterns of 16S rRNA diversity at a depth of millions of sequences per sample. (2010). doi:10.1073/pnas.1000080107/-/DCSupplemental.www.pnas.org/cgi/doi/10.1073/pnas.1000080107
19. Americnan Public Health Association (APHA). *Standard Methods for the Examination of Water and Wastewater*. (American Water Works Association and Water Environment Federation, 1998).
20. Ma, Y. *et al.* Microbial community response of nitrifying sequencing batch reactors to silver, zero-valent iron, titanium dioxide and cerium dioxide nanomaterials. *Water Res.* **68,** 87–97 (2015).
21. Masella, A. P., Bartram, A. K., Truszkowski, J. M., Brown, D. G. & Neufeld, J. D. PANDAseq: paired-end assembler for illumina sequences. *BMC Bioinformatics* **13,** 31 (2012).

22. Caporaso, J. G. *et al.* correspondence QIIME allows analysis of high- throughput community sequencing data Intensity normalization improves color calling in SOLiD sequencing. *Nat. Publ. Gr.* **7,** 335–336 (2010).
23. Haas, B. J. *et al.* Chimeric 16S rRNA sequence formation and detection in Sanger and 454-pyrosequenced PCR amplicons. *Genome Res.* **21,** 494–504 (2011).
24. Lozupone, C. & Knight, R. UniFrac : a New Phylogenetic Method for Comparing Microbial Communities UniFrac : a New Phylogenetic Method for Comparing Microbial Communities. *Appl. Environ. Microbiol.* **71,** 8228–8235 (2005).
25. Langille, M. *et al.* Predictive functional profiling of microbial communities using 16S rRNA marker gene sequences. *Nat. Biotechnol.* **31,** 814–21 (2013).
26. You, J., Das, A., Dolan, E. M. & Hu, Z. Ammonia-oxidizing archaea involved in nitrogen removal. *Water Res.* **43,** 1801–9 (2009).
27. Daims, H., L??cker, S. & Wagner, M. A New Perspective on Microbes Formerly Known as Nitrite-Oxidizing Bacteria. *Trends Microbiol.* **24,** 699–712 (2016).
28. Zhang, T., Shao, M.-F. & Ye, L. 454 Pyrosequencing Reveals Bacterial Diversity of Activated Sludge From 14 Sewage Treatment Plants. *ISME J.* **6,** 1137–47 (2012).
29. Yu, K. & Zhang, T. Metagenomic and Metatranscriptomic Analysis of Microbial Community Structure and Gene Expression of Activated Sludge. *PLoS One* **7,** e38183 (2012).
30. Ye, L. *et al.* Analysis of the bacterial community in a laboratory-scale nitrification reactor and a wastewater treatment plant by. *Water Res.* **45,** 4390–4398 (2011).
31. Trosvik, P. & de Muinck, E. J. Ecology of bacteria in the human gastrointestinal tract--identification of keystone and foundation taxa. *Microbiome* **3,** 44 (2015).
32. Gao, P. *et al.* Correlating microbial community compositions with environmental factors in activated sludge from four full-scale municipal wastewater treatment plants in Shanghai, China. *Appl. Microbiol. Biotechnol.* **100,** 4663–4673 (2016).
33. Koch, H. *et al.* Expanded metabolic versatility of ubiquitous nitrite-oxidizing bacteria from the genus Nitrospira. **112,** 11371–11376 (2015).
34. Palomo, A. *et al.* Metagenomic analysis of rapid gravity sand filter microbial communities suggests novel physiology of Nitrospira spp. *ISME J.* 1–13 (2016). doi:10.1038/ismej.2016.63

35. Pinto, A. J., Marcus, D. N. & Ijaz, Z. Metagenomic Evidence for the Presence of Comammox Nitrospira -Like Bacteria in a Drinking Water System. **1,** 1–8
36. Kessel, M. A. H. J. Van *et al.* Complete nitrification by a single microorganism. *Nature* **528,** 555–559 (2015).
37. Brooks, J. P. *et al.* The truth about metagenomics: quantifying and counteracting bias in 16S rRNA studies. *BMC Microbiol.* **15,** 66 (2015).
38. Gruber-Dorninger, C. *et al.* Functionally relevant diversity of closely related Nitrospira in activated sludge. *ISME J.* **9,** 643–55 (2014).

APPENDIX A: SUPPORTING INFORMATION FOR CHAPTER 2

A.1 SUPPORTING TABLES

Table A. 1 Seed sludge collection dates, temperatures and sampling details

Trial	Experimental Temp (°C)	Date of Collection	Collection Temp (°C)	Frequency of NPR tests	Samples selected for 16S rRNA amplicon sequencing
14 °C Trial 1	14	4/7/2014	15.17	Days 2, 3, 5, 8, 11, 14, 18	Days 2, 3, 5, 8, 11, 14, 18
20 °C Trial 1	20	12/2/2013	18.38	Days 2, 3, 5, 7, 10, 14, 18	Days 2, 3, 5, 7, 10, 14, 18
30 °C Trial 1	30	2/19/2014	15.17	Days 2, 3, 5, 7, 9, 12, 16	Days 2, 3, 5, 7, 9, 12, 16
14 °C Trial 2	14	3/20/2015	14.36	Days 2, 3, 5, 7, 10, 14, 18 Fed for 6hr, 12hr, 24hr, 36hr, 48hr	INF, Days 0, 2, 7, 18, Fed for 12hr, 48hr
20 °C Trial 2	20	5/11/2015	20.49	Days 2, 3, 5, 7, 10, 14, 18 Fed for 6hr, 12hr, 24hr, 36hr, 48hr	INF, Days 0, 2, 7, 18, Fed for 12hr, 48hr
27 °C Trial 1	27	6/23/2015	23.72	Days 2, 3, 5, 7, 10, 14, 18 Fed for 6hr, 12hr, 24hr, 36hr, 48hr	INF, Days 0, 2, 7, 18, Fed for 12hr, 48hr
Note: INF- sample taken at influent of DC Water nitrification basin, "Fed for" samples are those taken after reactor was dosed with ammonia					

A.2 SUPPORTING FIGURES

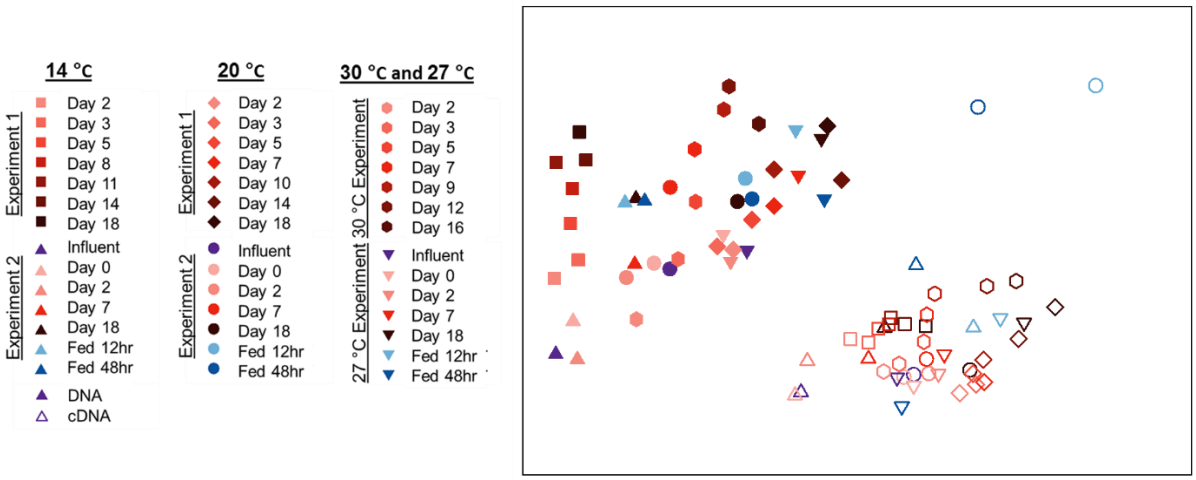

Figure A. 1 Overall MDS ordination of unifrac distance matrix of OTU table rarefied to lowest sample sequence number (38,000 sequences). Darkness of red shading increases with time in starvation reactor, purple points indicate samples taken from the influent of DC Water nitrification basin, blue points represent samples taken after feeding of ammonium to reactor.

Log Relative Abundance

14 °C Experiment 1

DNA								cDNA							
Taxonomy	D2	D3	D5	D8	D11	D14	D18	Taxonomy	D2	D3	D5	D8	D11	D14	D18
(f)Methylophilaceae	-0.80	-0.87	-0.91	-1.03	-1.12	-1.20	-1.29	(g)Nannocystis	-1.62	-1.32	-1.40	-1.62	-2.40	-2.93	-3.47
(f)Chitinophagaceae	-1.33	-1.34	-1.18	-1.20	-0.98	-0.99	-0.92	(g)Nitrospira	-1.34	-1.25	-1.29	-1.24	-1.10	-1.05	-1.09
(o)Sphingobacteriales	-1.30	-1.23	-1.13	-1.08	-1.23	-1.48	-1.70	(f)Methylocystaceae	-1.06	-1.05	-1.12	-1.10	-1.00	-0.99	-0.96
(g,s)Methylotenera, mobilis	-1.16	-1.22	-1.37	-1.56	-1.57	-1.66	-1.70	(o)Myxococcales	-1.49	-1.63	-1.71	-1.88	-2.07	-2.34	-2.19
(c)Betaproteobacteria	-1.39	-1.45	-1.68	-2.06	-2.17	-2.18	-2.36	(f)Methylophilaceae	-1.52	-1.59	-1.71	-1.88	-1.96	-2.02	-2.08
(f)Cytophagaceae	-1.83	-1.70	-1.71	-1.43	-1.40	-1.46	-1.33	(c)Betaproteobacteria	-1.74	-1.85	-2.17	-2.36	-2.38	-2.74	-2.87
(g,s)Methylotenera, mobilis	-1.50	-1.54	-1.68	-1.90	-2.01	-2.01	-2.04	(o)Myxococcales	-1.71	-1.85	-1.87	-2.02	-2.36	-2.37	-2.65
(g)Nitrospira	-1.54	-1.45	-1.45	-1.49	-1.38	-1.35	-1.29	(o)Myxococcales	-1.72	-1.87	-1.60	-1.63	-1.81	-1.95	-2.07
(o)Sphingobacteriales	-2.29	-2.30	-2.04	-1.80	-1.76	-1.64	-1.67	(o)Myxococcales	-1.78	-1.80	-1.86	-1.96	-2.20	-2.41	-2.67
(g)Niabella	-2.28	-2.18	-2.11	-1.91	-1.82	-1.76	-1.62	(o)HOC36	-1.43	-1.53	-1.53	-1.64	-1.63	-1.62	-1.56

14 °C Experiment 2

DNA								cDNA							
Taxonomy	INF	D0	D2	D7	D18	F12	F48	Taxonomyonomy	INF	D0	D2	D7	D18	F12	F48
(f)Methylophilaceae	-0.72	-0.81	-0.71	-0.87	-1.12	-1.09	-1.11	(o)Myxococcales	-1.32	-1.33	-1.20	-1.20	-2.07	-2.12	-2.44
(f)Saprospiraceae	-2.44	-2.33	-2.34	-1.89	-0.98	-0.98	-1.01	(o)Myxococcales	-1.43	-1.41	-1.10	-1.43	-2.02	-2.34	-2.14
(c)Betaproteobacteria	-1.02	-1.03	-0.93	-1.31	-1.43	-1.37	-1.41	(c)Betaproteobacteria	-1.26	-1.27	-1.22	-1.61	-1.74	-2.42	-2.19
(c)Deltaproteobacteria	-2.43	-2.42	-2.15	-1.54	-1.87	-1.89	-1.82	(c)Deltaproteobacteria	-1.99	-1.91	-1.67	-1.28	-1.65	-1.26	-1.41
(g)Rhodoferax	-1.38	-1.43	-1.43	-1.59	-1.68	-1.59	-1.66	(g)Thermus	ND	ND	ND	-3.07	-3.54	-2.64	-1.32
(o)Myxococcales	-2.02	-1.88	-1.72	-1.84	-2.96	-2.89	-3.12	(o)Phycisphaerales	-2.32	-2.42	-2.55	-1.96	-1.89	-1.28	-1.83
(f)Saprospiraceae	-2.08	-2.01	-2.06	-1.76	-1.60	-1.70	-1.68	(g)Nitrospira	-1.85	-1.89	-1.46	-1.63	-1.33	-1.41	-2.43
(f)Flavobacteriaceae	-1.84	-1.80	-2.22	-2.60	-3.35	-3.40	-3.15	(g)Pseudomonas	-3.16	-3.28	-3.09	-2.69	-2.49	-2.00	-1.40
(c)Betaproteobacteria	-1.84	-1.84	-2.00	-2.69	-3.02	-3.32	-3.06	(g)Meiothermus	-4.28	-4.58	#####	-3.43	-3.80	-2.46	-1.43
(f)Chitinophagaceae	-2.08	-1.93	-1.86	-1.63	-1.65	-1.63	-1.64	(g)Nannocystis	-1.88	-1.77	-1.92	-1.42	-2.99	-3.50	-2.98

20 °C Experiment 1

DNA								cDNA							
Taxonomy	D2	D3	D5	D7	D10	D14	D18	Taxonomy	D2	D3	D5	D7	D10	D14	D18
(g)Pseudomonas	-1.87	-1.39	-1.49	-0.92	-0.94	-1.17	-1.19	(f)Methylocystaceae	-0.48	-0.53	-0.56	-0.49	-0.63	-1.02	-1.57
(f)Methylophilaceae	-1.06	-0.99	-1.21	-1.39	-1.52	-1.64	-1.74	(o)MLE1-12	-2.24	-2.13	-1.78	-1.64	-1.47	-1.60	-2.17
(g)Bdellovibrio	-2.45	-3.15	-2.22	-2.18	-1.36	-1.11	-1.73	(o)Myxococcales	-1.61	-1.64	-1.71	-1.81	-1.98	-2.15	-2.58
(f)Methylocystaceae	-1.21	-1.25	-1.36	-1.59	-1.58	-2.20	-3.15	(o)HOC36	-1.51	-1.55	-1.68	-1.77	-1.79	-1.89	-2.07
(g)Nitrospira	-1.24	-1.27	-1.19	-1.36	-1.47	-1.25	-1.06	(o)Myxococcales	-1.66	-2.03	-2.46	-2.82	-2.86	-3.63	-4.28
(g)Bdellovibrio	-1.60	-1.54	-1.94	-2.19	-2.48	-2.56	ND	(g)Nitrospira	-1.29	-1.25	-1.25	-1.33	-1.28	-1.21	-1.18
(f)Saprospiraceae	-1.73	-1.57	-1.88	-2.02	ND	-2.03	-2.57	(g)Rhizobiales	-1.68	-1.75	-1.83	-1.76	-1.92	-2.15	-2.44
(f)Saprospiraceae	-1.78	-1.77	-1.69	-1.50	-1.66	-2.45	-1.93	(g)Nitrospira	-1.71	-1.73	-1.77	-1.77	-1.66	-1.56	-1.55
(o)Sphingobacteriales	-2.13	-2.30	-1.83	-1.73	ND	ND	-4.58	(g)Bdellovibrio	-3.54	-3.98	-3.13	-2.74	-2.09	-1.91	-2.52
(c)Betaproteobacteria	-1.67	-1.78	-2.12	-2.27	-2.49	-2.17	-3.38	(k)Bacteria	-2.51	-2.35	-2.18	-2.07	-2.30	-1.92	-1.94

20 °C Experiment 2

DNA								cDNA							
Taxonomy	INF	D0	D2	D7	D18	F12	F48	Taxonomy	INF	D0	D2	D7	D18	F12	F48
(f)Methylophilaceae	-0.95	-0.88	-0.75	-1.05	-1.27	-1.47	-1.31	(g)Staphylococcus	ND	-4.58	ND	-3.15	ND	-0.77	-3.05
(c)Betaproteobacteria	-1.23	-1.12	-1.09	-1.43	-1.63	-1.76	-1.57	(f)Methylocystaceae	-0.96	-0.92	-1.03	-0.91	-0.80	-2.30	-4.58
(g)Pseudomonas	-1.58	-2.31	-2.42	-2.15	-2.32	-1.23	-1.56	(o)Rhizobiales	-1.09	-1.04	-0.93	-0.93	-0.88	-1.51	ND
(g)Nitrospira	-1.49	-1.46	-1.42	-1.38	-1.16	-1.94	-1.80	(o)HOC36	-1.16	-1.12	-1.09	-1.53	-2.09	-3.28	ND
(g,s)Bacillus, cereus	ND	ND	ND	-1.73	-1.78	-1.46	-1.86	(g)Meiothermus	ND	-3.98	-4.58	-2.52	-2.51	-1.32	-1.13
(o)Sphingobacteriales	-2.21	-1.82	-1.73	-1.55	-1.95	ND	-2.32	(g)Thermus	-3.80	-4.10	-4.10	-2.12	-2.19	-1.61	-1.18
(o)HOC36	-1.75	-1.66	-1.83	-2.44	-2.61	-3.22	-3.24	(g)Corynebacterium	ND	ND	ND	ND	ND	-1.20	ND
(g,s)Methylotenera, mobilis	-1.70	-1.68	-1.66	-1.87	-2.19	-2.44	-2.33	(g)Pseudomonas	-2.76	-3.68	-3.63	-1.59	-1.58	-1.24	-1.32
(o)Sphingobacteriales	-2.61	-2.52	-2.50	-1.92	-1.64	-1.91	-2.32	(g)Anaerococcus	ND	ND	ND	ND	ND	-1.30	ND
(p)Proteobacteria	-2.94	-3.12	-3.02	-2.34	-1.82	-1.95	-1.78	(c)Betaproteobacteria	ND	ND	ND	-2.12	-3.24	-1.65	-1.39

27 °C Experiment

DNA								cDNA							
Taxonomy	INF	D0	D2	D7	D18	F12	F48	Taxonomy	INF	D0	D2	D7	D18	F12	F48
(o)DH61	-4.28	ND	ND	ND	-0.91	-1.16	-1.20	(f)Methylocystaceae	-0.82	-0.69	-0.72	-0.87	-1.84	-1.98	-2.28
(g)Pseudomonas	ND	-4.28	ND	-3.18	ND	-2.64	-1.00	(g)Pseudomonas	-4.58	ND	ND	-3.88	-3.63	-2.55	-1.00
(f)Methylophilaceae	-1.15	-1.12	-1.06	-1.50	-1.71	-1.88	-1.78	(o)HOC36	-1.08	-1.09	-1.19	-1.48	-2.17	-2.42	-2.47
(f)Methylocystaceae	-1.20	-1.20	-1.23	-1.51	-2.53	-3.20	-3.68	(o)DH61	ND	ND	ND	-4.58	-1.06	-1.64	-1.38
(g)Meiothermus	ND	ND	ND	-1.24	ND	ND	-2.91	(o)Rhizobiales	-1.18	-1.17	-1.16	-1.27	-1.97	-1.88	-2.17
(g)Thermus	ND	ND	ND	-1.31	ND	ND	ND	(g)Hyphomicrobium	-2.60	-2.50	-2.45	-2.44	-1.85	-1.36	-1.12
(f)Cytophagaceae	-2.04	-2.14	-1.93	-1.91	-1.37	-1.31	-1.70	(o)Myxococcales	-1.36	-1.45	-1.41	-1.52	-2.37	-2.47	-2.82
(c)Betaproteobacteria	ND	ND	ND	-1.43	-3.80	ND	ND	(o)MLE1-12	-2.29	-2.39	-2.31	-1.34	-2.21	-2.32	-2.86
(f)Saprospiraceae	-1.96	-1.87	-1.77	-2.04	-1.40	-1.40	-1.48	(f)Rhodocyclaceae	-3.98	-3.35	-3.80	-3.80	-4.58	-2.52	-1.52
(g)Nitrospira	-1.30	-1.25	-1.37	-1.79	-1.38	-1.50	-1.53	(g,s)Hyphomicrobium, zavarzinii	-2.22	-2.01	-1.98	-2.05	-1.97	-1.73	-1.43

30 °C Experiment

DNA								cDNA							
Taxonomy	D2	D3	D5	D7	D9	D12	D16	Taxonomy	D2	D3	D5	D7	D9	D12	D16
(f)Methylophilaceae	-0.76	-0.98	-1.31	-1.47	-1.79	-1.67	-2.04	(f)Methylocystaceae	-0.80	-0.77	-0.94	-1.12	-1.30	-1.77	-2.40
(f)Sphingobacteriaceae	ND	ND	ND	ND	-0.91	-1.11	-1.30	(g)Nitrospira	-1.44	-1.45	-1.29	-1.40	-1.25	-1.14	-1.00
(g)Pseudomonas	-1.79	-1.60	-1.02	-1.49	-0.81	-1.13	-1.16	(g)Pseudomonas	-2.96	-2.44	-2.09	-1.26	-1.45	-1.40	-1.39
(g,s)Methylotenera, mobilis	-1.35	-1.45	-1.84	-2.58	-2.47	-2.90	-2.95	(o)MLE1-12	-1.63	-1.31	-1.28	-1.62	-1.86	-2.02	-2.76
(g)Nitrospira	-1.38	-1.30	-1.20	-1.14	-1.13	-1.11	-1.03	(o)Myxococcales	-1.28	-1.80	-2.17	-2.76	-2.96	-2.98	-2.82
(f)Methylocystaceae	-1.58	-1.54	-1.97	-1.95	-2.10	-3.00	-4.58	(o)Myxococcales	-1.38	-1.36	-1.50	-1.74	-2.27	-2.61	-2.63
(g,s)Methylotenera, mobilis	-1.50	-1.61	-1.88	-2.13	-2.12	-2.48	-2.39	(o)HOC36	-1.41	-1.65	-1.77	-1.79	-1.88	-2.10	-2.27
(g)Geothrix	-1.49	-1.60	-1.68	-2.00	-2.24	-2.34	-2.09	(o)Myxococcales	-1.90	-1.70	-1.61	-1.49	-1.75	-2.22	-2.75
(o)Sphingobacteriales	-2.73	ND	ND	-1.84	-1.57	-2.11	ND	(g)Nannocystis	-2.06	-1.78	-1.74	-1.74	-1.82	-3.40	ND
(f)Sphingobacteriaceae	ND	ND	-2.15	-1.58	-2.14	-2.13	ND	(g,s)Bacillus, cereus	ND	ND	-3.63	-1.80	-1.74	-1.96	-1.89

	Alphaproteobacteria
	Betaproteobacteria
	Deltaproteobacteria
	Gammaproteobacteria
	Unclassified Proteorbacteria
	Acidobacteria
	Actinobacteria
	Bacteroidetes
	Cyanobacteria
	Deinococcus-Thermus
	Firmicutes
	Nitrospirae
	Planctomycetes
	Unidentified
(k)	kingdom
(p)	phylum
(c)	class
(o)	order
(f)	family
(g)	genus
(g,s)	genus, species

INF	Influent
D#	Days
F#	Hours after feeding

Least Relative Abundance
Most Relative Abundance

Figure A. 2 Ten most variable OTUs in each trial and nucleic acid type. Values in cells are log relative abundance (normalized to number of sequences per samples (38,000)). Heat

mapping for each OTU indicates behavior of OTU in that trial (darker color indicates greater relative abundance.

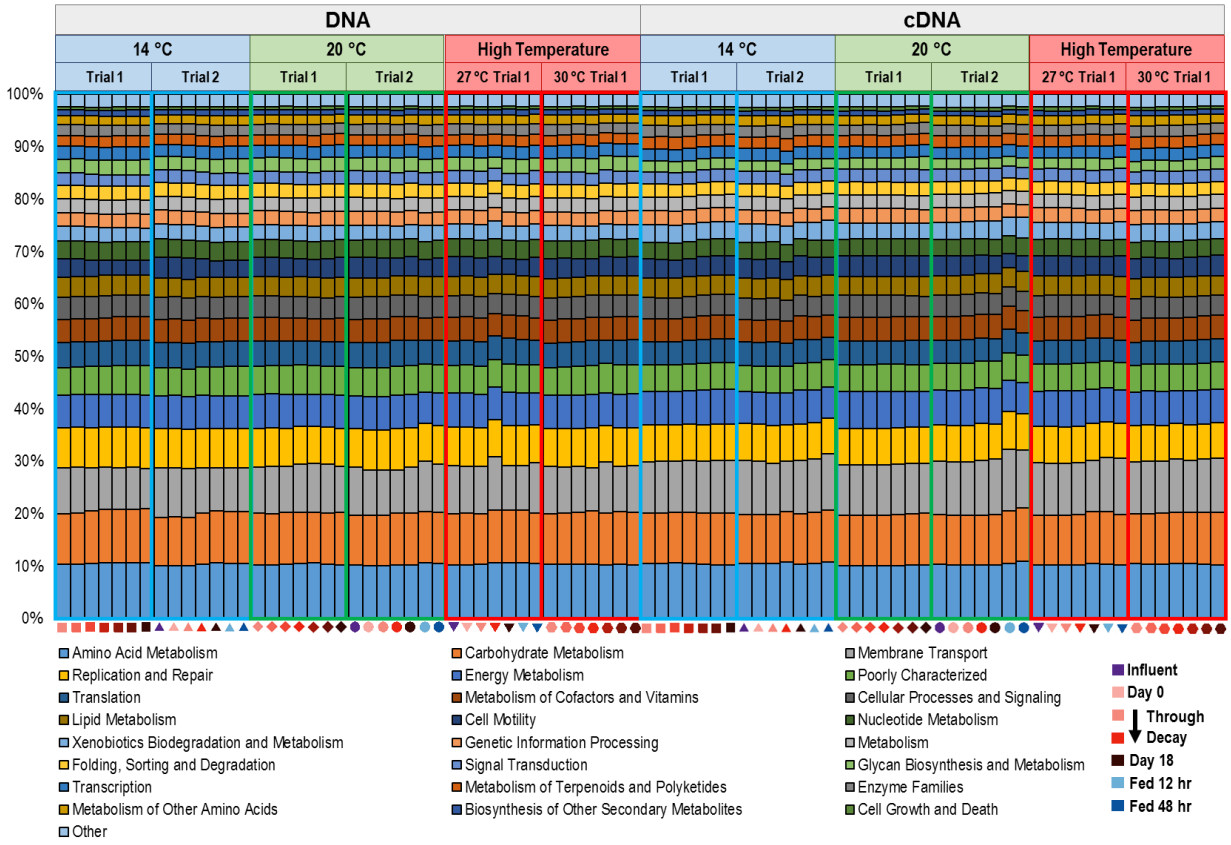

Figure A. 3 Stacked bar chart of the kegg level 2 predicted metagenome as analyzed using PICRUSt. Symbols along x-axis match those in Figure 2.2 where darkness of red shading increases with time in starvation reactor, purple points indicate samples taken from the influent of DC Water nitrification basin, blue points represent samples taken after feeding of ammonium to reactor.

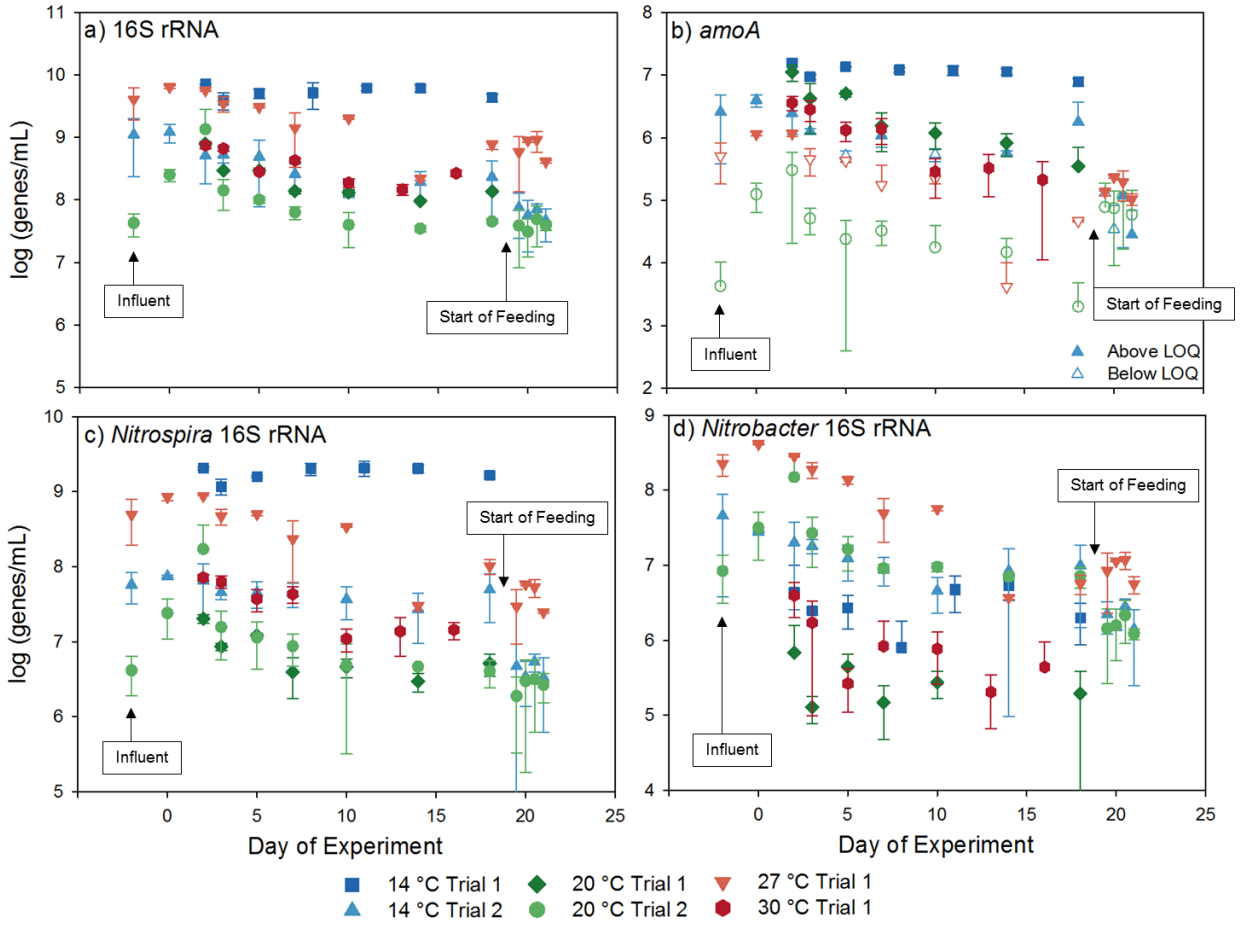

Figure A. 4 Genes quantified using qPCR of a) total 16S rRNA using universal primers b) *amoA* gene encoding the ammonia monooxygenase enzyme used by bacteria for oxidizing ammonia c) *Nitrospira* 16S rRNA targeting only *Nitrospira* species and d) *Nitrobacter* 16S rRNA targeting only *Nitrobacter* species.

CHAPTER 3: METAGENOMIC ANALYSIS OF MICROBIAL COMMUNITIES YIELDS INSIGHT INTO IMPACTS OF NANOPARTICLE DESIGN

Jacob W. Metch, Nathan D. Burrows, Catherine J. Murphy, Amy Pruden,
Peter J. Vikesland

3.1 ABSTRACT

Design of nanoparticles with consideration of environmental impacts is needed and with next generation DNA sequencing and metagenomic analysis of nanoparticle impacts on microbial communities, this may be a possibility. Herein we demonstrate this approach using a model community of environmental microbes (i.e., wastewater activated sludge) dosed with gold nanoparticles of varying surface coating and morphology. Metagenomic analysis was highly sensitive in detecting microbial community response to gold nanospheres and nanorods with either cetyltrimethylammonium bromide or polyacrylic acid surface coatings. We observed that gold nanoparticle morphology imposes a stronger force in shaping microbial community structure than surface coating. Trends were consistent both in terms of composition of taxonomic and functional genes, including antibiotic resistance genes, metal resistance genes, and gene transfer elements associated with cell stress that are relevant to public health. Given that nanoparticle morphology remained constant the potential influence of gold dissolution was minimal. Surface coating governed nanoparticle partitioning between the bioparticulate and aqueous phases.

3.2 INTRODUCTION

Novel entities, such as nanomaterials, could elicit unintended environmental consequences if they are persistent, widely distributed, and impact critical global processes or subsystems[1]. For the nanotechnology industry to develop sustainably, sensitive means of screening environmental impacts are required[2,3]. Recent advances in DNA sequencing and metagenomic analysis of microbial communities provide a powerful means to achieve this purpose by informing "environmentally friendly" nanomaterial design by analyzing and limiting the impact these nanoparticle have to vital microbial communities, which are a foundational component of all natural[4] and

engineered[5] ecosystems. Specifically, wastewater treatment plants harbor interdependent microbial communities that carry out vital functions for pollutant (pathogen, pharmaceuticals, etc.) removal[6,7] and are increasingly exposed to measurable nanoparticle fluxes[2]. To date, most microbial nanotoxicity studies have used pure-cultures[8]; however, assaying nanoparticle impacts to real-world microbial communities has greater potential to capture ecological interactions. For instance, recent studies have shown that microbial community structure can subtly change in response to nanosilver exposure[9,10].

Metagenomics entails high-throughput sequencing of microbial community DNA extracts enabling high-resolution taxonomic and functional characterization[11,12]. Metagenomics circumvents *a priori* target gene selection by directly sequencing extracted DNA and can access functional gene information therefore making this approach a powerful tool for discovery[12]. Herein we demonstrate the use of metagenomics for sensitive assessment of the environmental impacts of nanoparticles. Nanoparticle surface coating and morphology are important properties that impact the nano-bio interface and nanotoxicity[13–15]; however, potential impacts beyond single organism-single target receptors need to be evaluated. To date, few studies have examined the impacts of morphology, surface charge, or coating on bacterial populations. A positive correlation was found between surface charge and toxicity in mixed *Bacillus* spp. cultures[16] and morphology impacted nanotoxicity of silver[17] and titanium dioxide[18] nanoparticles in pure culture studies. Likewise, prior studies have shown that surface coatings determine nanomaterial partitioning to biofilm and sediments[19] and affect transport through aquatic food webs[20]. However, these studies provide neither a comprehensive assessment of how nanomaterials influence important ecological-scale microbial environmental processes, nor the influence of individual nanomaterial properties, for informative environmentally-friendly design.

Herein we utilized gold nanoparticles as a flexible platform with an inert core to gain generalizable insight into the influence of surface coating and morphology on microbial communities. It was hypothesized that surface coating would be the driver of nanoparticle impact in such a system. Gold nanorods were functionalized with cetyltrimethylammonium bromide (CTAB) or polyacrylic acid (PAA) for which environmental partitioning has previously been studied[19,20] and CTAB-coated

nanospheres were used as a morphology control. Nitrifying activated sludge sequencing batch reactor (SBR) microbial communities were then exposed to these particles (see Figure B.1). Undosed and CTAB-dosed control SBRs were examined in parallel to account for ambient microbial community drift and the potential toxicity of free CTAB, respectively. Metagenomic analysis revealed nanoparticle morphology had a dominant effect on microbial community structure and function. In contrast, surface coating dictated nanoparticle partitioning into sludge versus bulk water. This study demonstrates metagenomics as a powerful means to screen for environmental impacts of nanomaterials and supports proactive environmentally-friendly design.

3.3 RESULTS AND DISCUSSION

3.3.1 Characterization of Gold Nanoparticles

Because of their chemical stability, gold nanoparticles are an ideal platform to generically manipulate nanoparticle properties[21]. This capacity enabled the independent study of surface coating and morphological effects. The chemical stability of the nanoparticles was confirmed using transmission election microscopy (TEM) showing consistent particle size distribution throughout dosing (Figure 3.1a and 3.1b). Electrophoretic mobility (EM) measurements were used to determine nanoparticle surface charge both in the original particle suspensions and in SBR effluent (Figure 3.1c). As expected, starting CTAB-coated particles carried a positive charge (spheres: EM = 3.1 μm-cm/V-s, rods: EM = 2.5 μm-cm/V-s) and starting PAA-coated particles had a negative charge (EM = -2.2 μm-cm/V-s). Following addition to filtered control SBR effluent, the surface charges of all three nanoparticle types shifted towards the charge of the particulates in the filtered effluent. This finding suggests the nanoparticles became covered with organic matter present in the effluent, a result consistent with the notion that nanoparticles are readily coated by biomolecular ‘coronas’ in the presence of organic molecules, which reduces their surface energy[22]. Consistent with previous observations[23], PAA-coated rods carried a greater negative charge than CTAB-coated particles, a result suggesting the differential affinity of protein and organic matter based on the original surface coating of the particle.

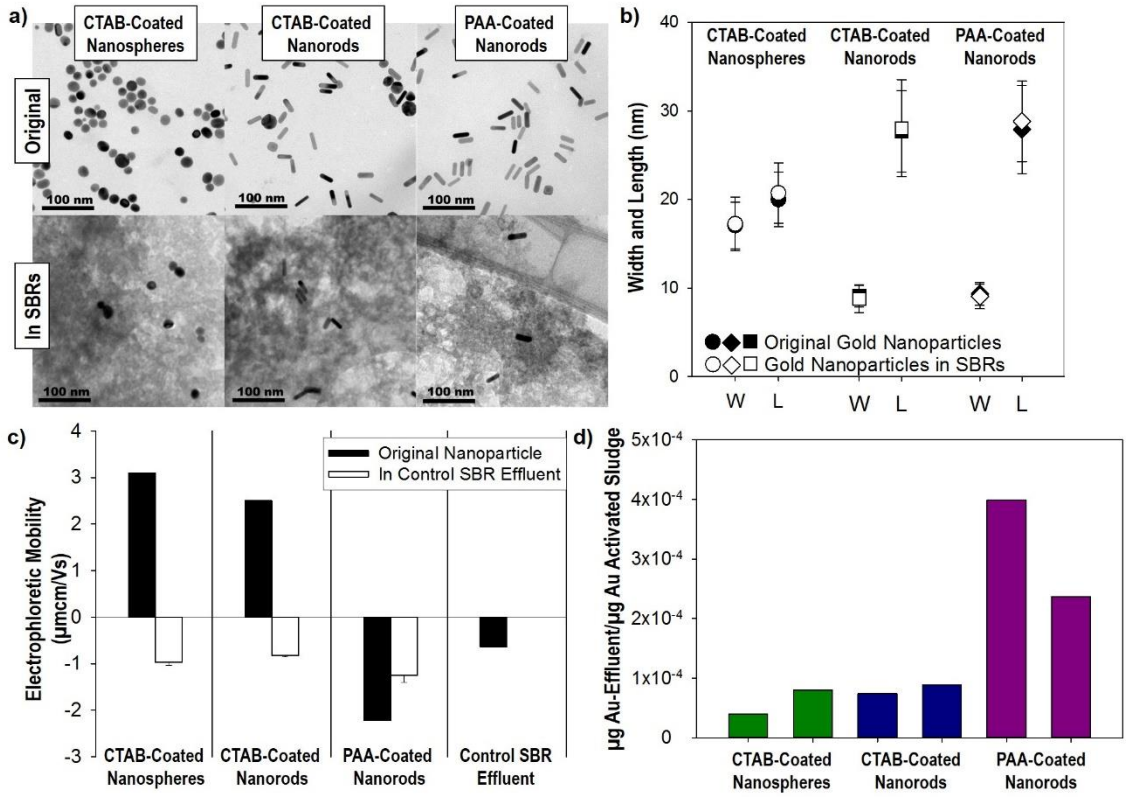

Figure 3.1: Characterization of gold nanoparticles before and after addition to SBRs. a) TEM images of original suspensions of nanoparticles (upper row) and nanoparticles in SBRs sampled upon completion of the study on day 56 (lower row); b) size distribution of original nanoparticles (filled) and nanoparticles in SBRs upon completion of the study (open), comparing width (W) and length (L). Error bars represent one standard deviation of sized particles (n as follows: Original CTAB-Coated Nanospheres-211, CTAB-Coated Nanospheres in SBRs-175, Original CTAB-Coated Nanorods-188, CTAB-Coated Nanorods in SBRs-188, Original PAA-Coated Nanorods-139, PAA-Coated Nanorods in SBRs-123); c) Comparison of electrophoretic mobility of nanoparticles before (filled) and after (open) addition to control SBR effluent. Error bars represent the EM range measured for nanoparticles in SBR effluent (n=3), replicates were not conducted for original nanoparticle suspensions or control SBR effluent; d) Ratio of gold in effluent to gold associated with biomass upon experiment completion. Duplicate bars represent replicate SBRs.

3.3.2 Fate of Gold Nanoparticles in Sequencing Batch Reactors

Nanoparticle characteristics, such as surface coating and functionalization, have previously been reported to play an important role in sorption to activated sludge[24] and therefore fate in the environment[2,25]. Gold nanoparticles were dosed into reactors in

synthetic wastewater feed at a concentration of 200 µg/L, which is more reasonable that previous similar experiments, but still higher than concentrations of gold nanoparticles predicted to enter wastewater treatment plants by a recent probabilistic modeling exercise[3]. Dosed surface area and number of particles were calculated based on gold unit cell volume (See Table 3.1). Upon completion of the study after 56 days the effluent and sludge samples were digested and analyzed for gold using inductively-coupled plasma mass spectroscopy (ICP-MS). The ratio of gold in the effluent to gold in the sludge was determined and all ratios were extremely low due to high gold concentrations in sludge (Figure B.2). However, there is a relative increase in the ratio for PAA-coated nanorods compared to the CTAB-coated nanoparticles (Figure 3.1d) indicating the original surface coating continued to influence nanoparticle affinity towards the bioparticulate sludge despite the presence of the biomolecular corona. Electrostatic forces are one possible driver for this differentiation as PAA-coated nanorods carried a greater negative charge than CTAB-coated nanoparticles after addition to SBR effluent, and therefore may have had decreased affinity for biomass, which largely carries a negative charge.

Table 3.1: Gold dosed to SBRs throughout the entire 56 day experiment

	Mass Dosed (µg)	**# Particles Dosed**	**Surface Area Dosed (nm^2)**
CTAB-Coated Nanospheres	2.24×10^3	3.56×10^{14}	3.81×10^{17}
CTAB-Coated Nanorods	2.24×10^3	7.24×10^{14}	5.73×10^{17}
PAA-Coated Nanorods	2.24×10^3	6.85×10^{14}	5.61×10^{17}
Note: Gold dosed to SBRs in synthetic wastewater at 200 µg-Au/L			

3.3.3 Metagenomics Reveals Variations in Gold Nanoparticle Impact

Nitrification is a multi-step process carried out by slow-growing autotrophic bacteria and serves as a key component of a delicate ecological balance driving nutrient removal in wastewater treatment plants[26]. Ammonia-oxidizing bacteria (AOB) convert ammonia to nitrite, while nitrite-oxidizing bacteria (NOB) transform nitrite to nitrate and comammox bacteria are capable of both ammonia and nitrite oxidation. As this is an aerobic process, nitrifiers often compete for oxygen and other nutrients with faster growing heterotrophs[7]. Nitrifiers are known to be sensitive to various toxins[27], including some nanomaterials[28,29].

Here we quantified ammonia removal, effluent nitrate (Figure B.3), and marker genes indicative of nitrifying bacteria (Figure B.4) which collectively suggest no impact of the nanomaterials on nitrification. Metagenomic analysis derived from the M5RNA database in MG-RAST[30] which annotates against several databases and assigns taxonomy based on both functional and 16S rRNA genes and the SEED Subsystems database confirmed no discernable trends in nitrifying bacteria genera, or functional genes related to nitrogen cycling, as a result of nanoparticle exposure (Figure B.5).

Indicators of live biomass (mixed liquor volatile suspended solids (MLVSS)), total suspended solids (mixed liquor suspended solids (MLSS)) and pH remained constant throughout nanoparticle exposure (Figure B.6). These results are consistent with a prior study[9] in which high doses of silver nanoparticles (20 mg/L) in similar SBRs did not impact nitrification function[9]. However, in that study, application of 16S rRNA gene amplicon sequencing did reveal taxonomic shifts in the SBR microbial community structure that were attributed to nanoparticle dosing[9]. In this effort, we utilized lower doses of nanomaterials with controlled properties and applied metagenomics as a powerful tool capable of revealing both taxonomic and functional shifts in microbial community structure.

To gain insight into functional impacts of the nanomaterials, DNA extracts from all reactors on the final day of dosing (representing long-term effects) and a week after the start of dosing (representing short term effects) as well as two DNA extracts from before dosing were selected for Illumina high-throughput sequencing and metagenomic analysis (Illumina, Inc., San Diego, California). Multidimensional scaling (MDS) ordination of Bray-Curtis similarity at the taxonomic level of genus annotated using the M5RNA in MGRAST[30] indicate that nanomaterials had a discernable influence on the microbial community composition over time (Figure 3.2a). High initial similarity (85%) in SBR taxonomic composition was noted based on the clustering of day 0 and day 7 points; however, microbial communities underwent successive shifts with time. After 56 days (the final day of dosing), SBRs dosed with CTAB-coated nanospheres clustered together, while SBRs dosed with nanorods were more similar to each other, regardless of surface coating, and clustered with control SBRs. Changes in abundance at the phylum taxonomic level were observed as a result of nanoparticle dosing (Figure 3.2b). In all

SBRs, *Proteobacteria*, *Actinobacteria*, and *Bacteroidetes* were the dominant phyla as expected based on previous studies of activated sludge microbial ecology[31,32]. Compared to the control SBRs, *Proteobacteria*, *Bacteroidetes*, and *Firmicutes* abundances were enhanced by CTAB-coated nanospheres, and to a lesser extent by both nanorod types, whereas *Actinobacteria* abundance decreased as a result of CTAB-coated nanosphere dosing.

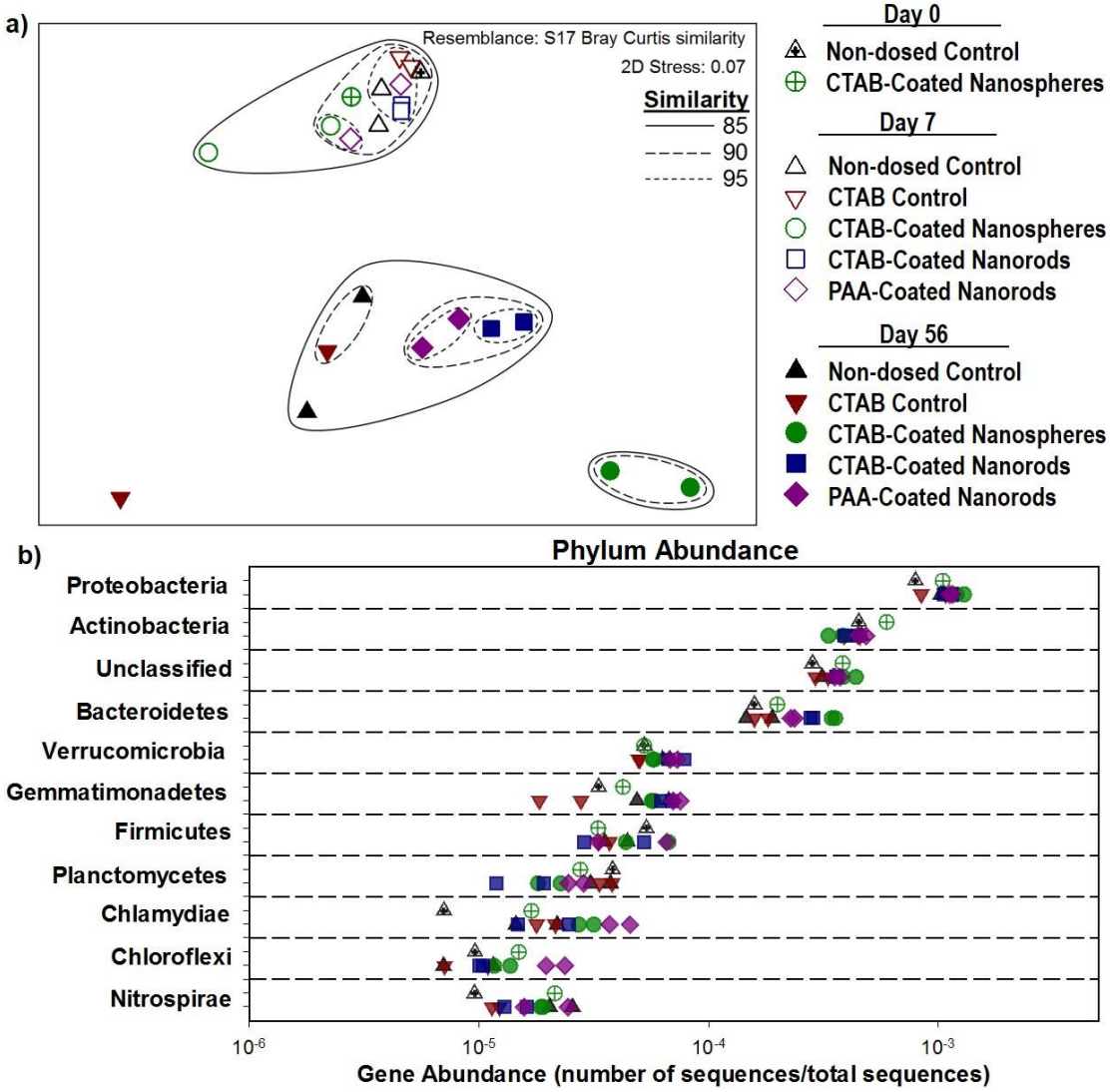

Figure 3.2: Taxonomic shifts in SBR microbial community structure throughout the nanoparticle-dosing period. a) MDS ordination of Bray-Curtis similarity of microbial community phylogenetic distance at the genus level. The relative proximity of points in 2D space is indicative of relative similarity in taxonomic structure of the microbial communities. Group-average Bray-Curtis similarity clustering was superimposed on MDS obtained from the same similarities; b) Comparison

of absolute abundance at the Phylum level expressed as number of sequences corresponding to each phylum normalized to the total number of sequences passing quality control. Duplicate SBRs are represented with similar symbols.

Annotation of functional genes using MG-RAST[30] and the SEED Subsystem database revealed similar trends to those observed based on taxonomic analysis. Although most SBRs maintained similar functional gene composition throughout dosing (Similarity > 90%), SBRs dosed with CTAB-coated nanospheres clustered together, while SBRs dosed with nanorods were more similar to each other, regardless of surface coating (See Figure B.7).

To examine community-scale effects on specific functions of interest we focused on genes associated with microbial stress and public health concern: antibiotic resistance genes (ARGs), metal resistance genes (MRGs), and plasmids involved in the sharing of these genes among bacteria. Wastewater treatment plants have been identified as important reservoirs for receiving and disseminating ARGs to the environment[33], and metals have been widely implicated as potential co-selective agents[34]. One recent study implicated nanoparticles in stimulating shifts in ARG profiles (the "resistome")[35] and stress in general is known to stimulate transfer and proliferation of ARGs[36], including plasmid-mediated transfer[37]. A new online metagenomics analysis server, MetaStorm[38], was utilized to annotate our metagenomics data against the Comprehensive Antibiotic Resistance Database[39], BacMET[40], and ACLAME[41], databases that contain ARG, MRG, and plasmid sequences, respectively. Similar trends were observed for all three of these functional gene categories as observed in the broader taxonomic and functional gene profiling; namely, SBRs receiving CTAB-coated nanospheres were distinct from SBRs receiving nanorods after 56 days of dosing (Figure 3.3).

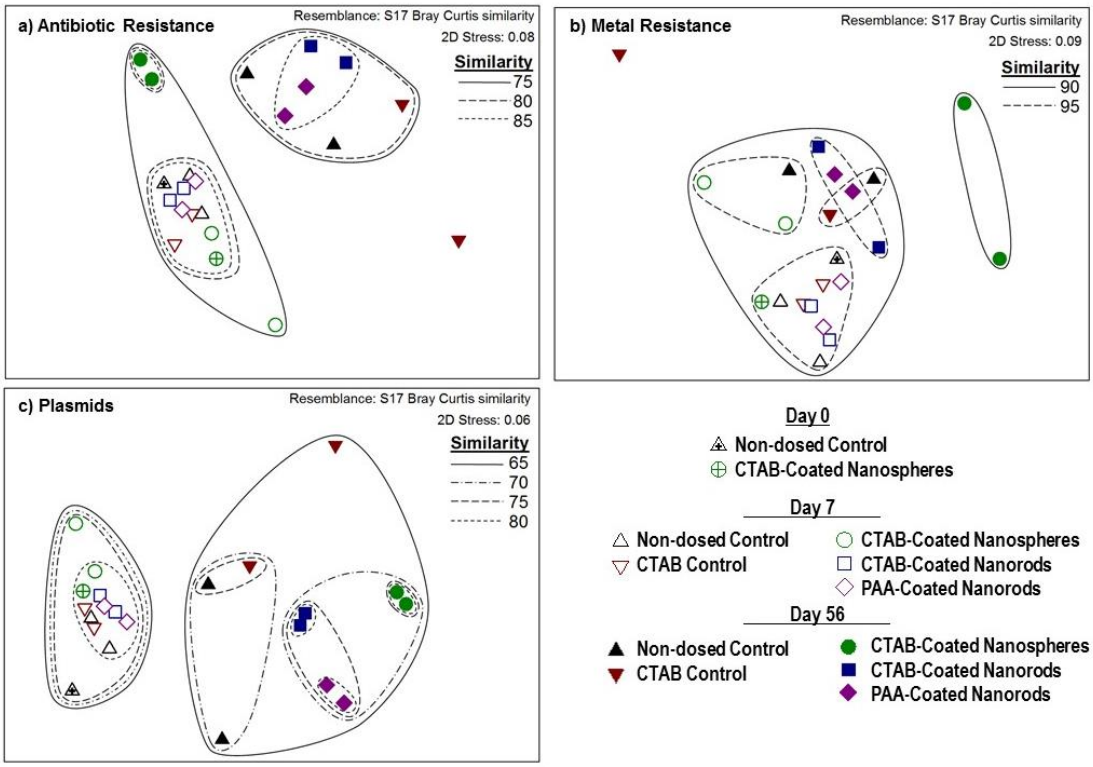

Figure 3.3: MDS ordination of Bray-Curtis similarity of a) antibiotic resistance b) metal resistance c) plasmid genes. The relative proximity of points in 2D space is indicative of relative similarity in taxonomic structure of the microbial communities. Group-average Bray-Curtis similarity clustering was superimposed on MDS obtained from the same similarities. Duplicate SBRs are represented with similar symbols.

Interestingly, SBRs receiving nanospheres displayed a less distinct shift in ARG profiles with time than did SBRs receiving nanorods or controls (Figure 3.3a). Still, several classes of ARGs increased following CTAB-coated nanosphere exposure, relative to nanorod-dosed SBRs or controls, including tetracycline, trimethoprim, chloramphenicol, fluoroquinolone, phenicol, macrolide, and aminocoumarin resistance genes; while, sulfonamide ARGs decreased comparatively in abundance (Figure 3.4). ARG abundances in SBRs dosed with either type of nanorod were not distinguishable from that of control SBRs, with the exception of sulfonamide resistance genes, which appeared to increase in SBRs dosed with nanorods (Figure 3.4). Thus, the overall trend observed was a generally consistent total abundance of ARGs in the SBRs, with individual resistance classes shifting in association with the dosed nanoparticles.

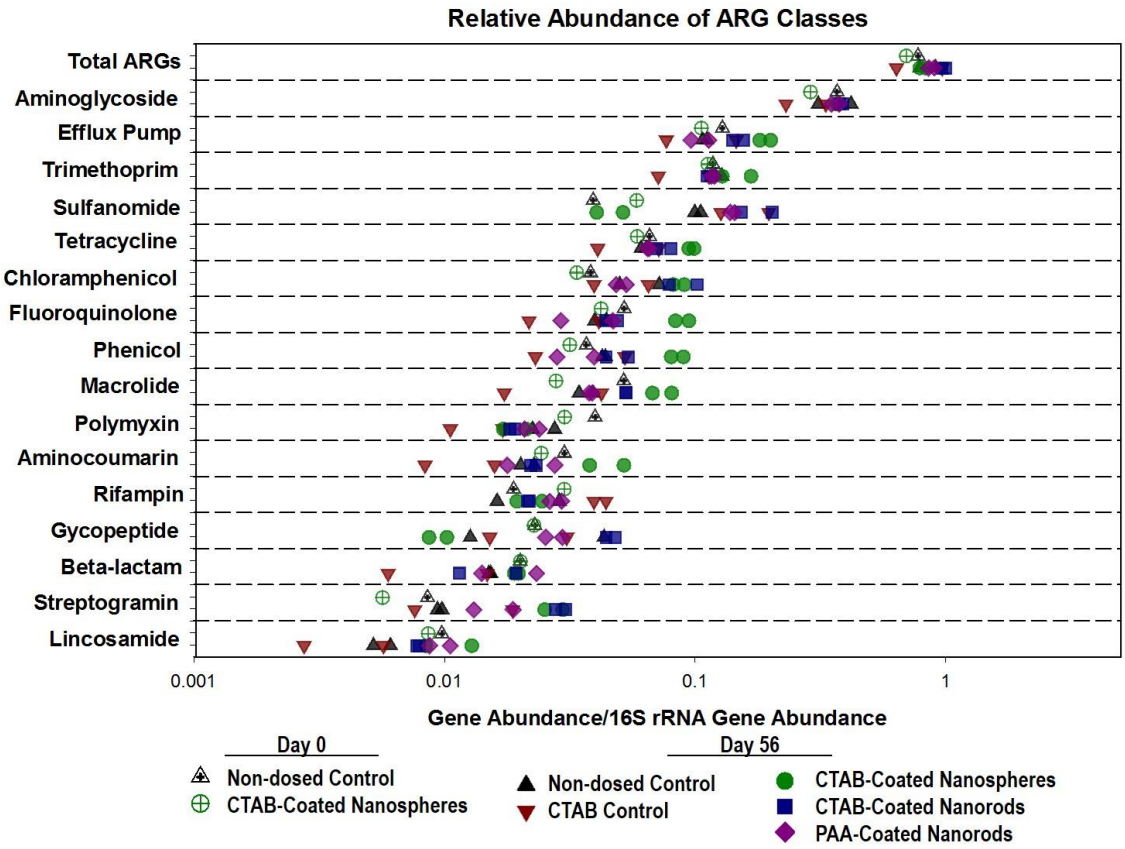

Figure 3.4: Relative abundance of ARG classes normalized to 16S rRNA gene abundance. ARG composition of SBRs on the final day of dosing (day 56) and two SBRs from day 0, as a reference, are represented. Duplicate SBRs are represented with similar symbols and SBRs with no hits are not shown. (For day 7 data see Figure B.8)

Genes associated with metal resistance in control and nanorod-dosed SBRs remained similar upon completion of the experiment (>90%) to SBRs sampled on days 0 and 7 of dosing, indicating little change in overall composition (Figure 3.3b). However, by the end of the experiment, SBRs dosed with CTAB-coated nanospheres shifted in a distinct manner relative to all other SBRs. This shift corresponded with SBRs dosed with CTAB-coated nanospheres having a slight increase in total MRG abundance as well as containing the greatest abundance of several MRG classes, including chromium, arsenic, tellurium, cadmium, lead, antimony, and gold resistance (Figure 3.5). Enrichment of some MRG classes were also observed in SBRs dosed with CTAB-coated nanorods for chromium, tellurium, and selenium resistance genes, when compared to control SBRs. PAA-coated nanorods did not display this trend.

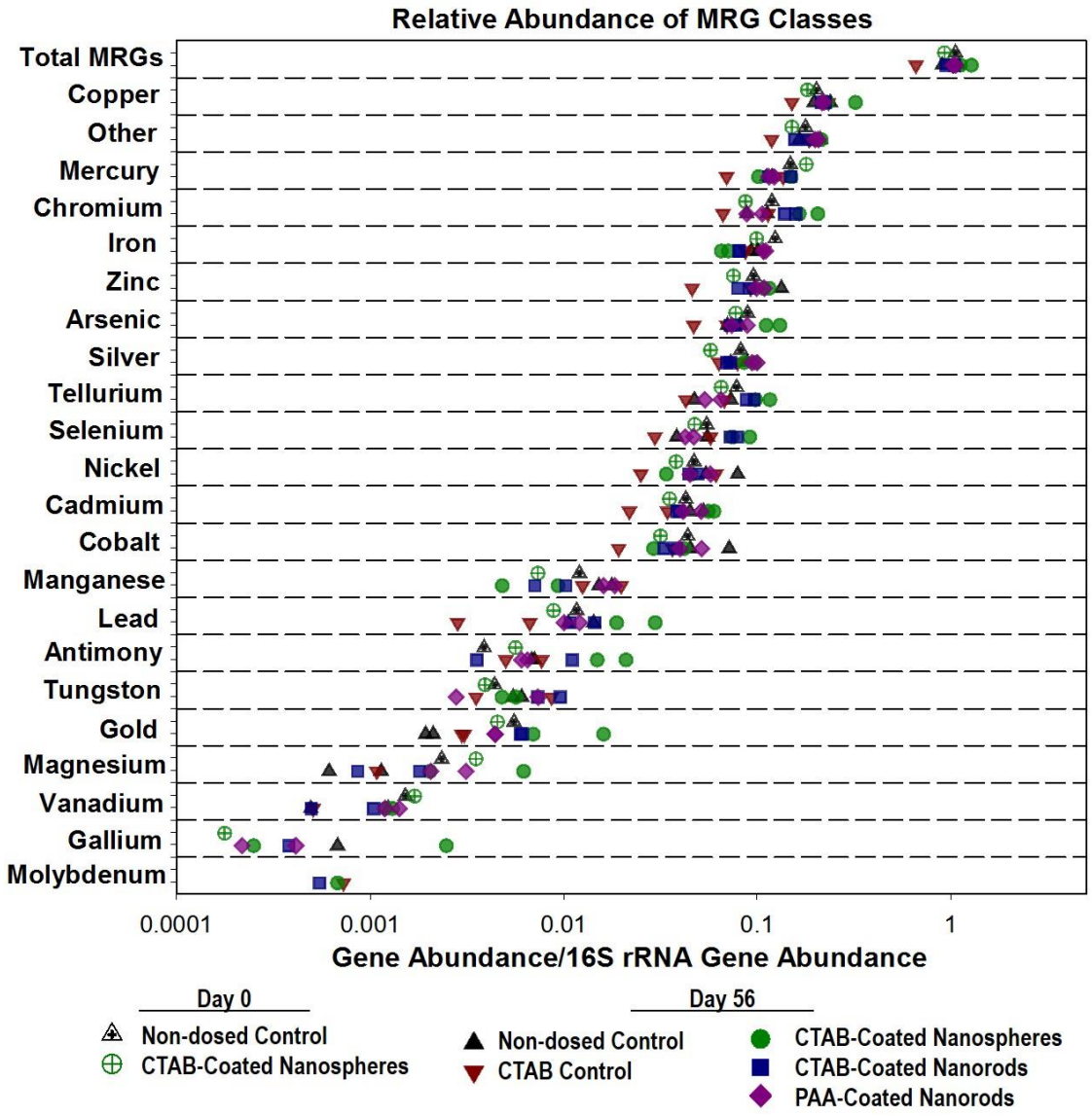

Figure 3.5: Relative abundance of MRG classes (number of MRGs of each class normalized to 16S rRNA gene abundance). MRG composition of SBRs on the final day of dosing and two SBRs from day 0, as a reference, are represented. Duplicate SBRs are represented with similar symbols and SBRs with no hits are not shown. (For day 7 data see Figure B.9)

The plasmid composition of SBRs dosed with nanoparticles clustered together, with nanospheres being distinct from nanorods (similarity >70%) and CTAB and PAA-coated nanorods clustering separately within the larger nanorod cluster (similarity >80%) (Figure 3.3c). However, there was not a discernable difference in total plasmid abundance in SBRs. These results indicate that there is potential for nanomaterial morphology, and to a lesser extent, surface coating, to influence gene exchange, which is

a key process for disseminating drug resistance and an important driver of microbial ecological function.

To our knowledge, there has been no prior investigation into the effects of nanoparticle surface coating or morphology on microbial community response using a metagenomics approach. However, previous studies have investigated the impacts of these properties on mammalian cells. CTAB-coated nanorods were shown to have greater toxicity than poly(allylamine hydrochloride)-coated nanorods using human colon carcinoma cells, which was attributed to free CTAB in solution[42]. In the present study, however, it appears that free CTAB was not the driver of gold nanosphere impacts on SBR microbial communities, as demonstrated by dissimilarity of SBRs dosed with CTAB-coated nanoparticles versus an equivalent concentration of free CTAB. Furthermore, free-CTAB-dosed controls were largely similar to undosed controls. The lack of CTAB toxicity observed in this study may be due to the activated sludge microbial community's ability to utilize surfactants similar to CTAB as a growth substrate[43], thereby removing free CTAB from the system.

One possible driver of selective pressure as a result of particle morphology may be differences in the organic coating that forms on the nanoparticles after dosing. Gagner et al. (2011) determined that coronas formed by two independent proteins on nanorods were more dense than those on nanospheres and speculated that this difference was due to a combination of surface curvature and crystal facet (nanospheres having Au(111) facets and nanrods having Au(100) at tips and Au(110) on cylinder) differences[44]. Similar mechanisms may be relevant in the SBR system, causing variations in materials sorbed to nanoparticles that can alter local concentrations of important biomolecules, as was shown to play a key role in fibroblast cell response to gold nanoparticles[45].

Another possible driver of selective pressure may be extracellular polymeric substances (EPS)-nanoparticle interactions. Production of EPS has been identified as an important stress response mechanism of bacteria to nanosilver[46,47]. EPS serves as a physical barrier between nanoparticles and cells and not only protects EPS-producing cells, but all cells within biofilms[46]. EPS is also important in activated sludge, providing floc structure and playing a crucial role protecting bacteria from toxins in wastewater[48]. Possible variations in nanoparticle mobility due through EPS as a result of morphology,

similar to differences in diffusion through nanopure water between nanospheres and nanorods, could lead to differences in bioavailability of nanoparticles and therefore distinct selective pressures as a function of morphology.

While there was a shift in microbial community taxonomy, no influence on reactor performance in terms of gross functional measures (e.g., N removal, MLSS, MLVSS) was observed. However, the capacity of the dosed nanoparticles to shift resistance genes and gene transfer elements raises potential concerns considering the increase in antibiotic resistant infections[49] coupled with the increase in nanoparticle application and therefore dissemination into sewers[25]. It is also important to note that there was a different number of particles and surface area dosed based on particle morphology (See Table 3.1). This study highlights a need for a better understanding of the selection pressures imparted by nanoparticles in complex microbial populations. Such an understanding is not only important for wastewater treatment, but other relevant receptors that may be impacted by nanoparticles such as aquatic environments, soils, and the guts of organisms ingesting nanoparticles[50]. Of particular interest would be to evaluate how nanoparticle based therapies affect the human gut microbiome following prophylaxis.

3.4 CONCLUSIONS

To our knowledge, this is the first effort to characterize the metagenomic response of a complex microbial community to variations in nanoparticle surface coating and morphology. Our results demonstrate metagenomics as a powerful tool for identifying potential environmental impacts of nanoparticles, with gold nanoparticles serving as a highly suitable platform for systematically differentiating effects of nanoparticle design. Metagenomic analysis effectively revealed shifts in taxonomic and functional aspects of microbial community structure associated with gold nanoparticle exposure. Functional gene analysis revealed detectable shifts in functional gene profiles as indicators of microbial stress and public health concern. Overall, morphology of the gold nanoparticles was found to be the strongest driver of taxonomic and functional composition, while there were subtler effects of surface coating as well. Shifts in microbial community structure even though initial nanoparticle morphology remained

stable indicates a selective pressure independent of potential dissolution of metal ions or production of reactive oxygen species from the nanoparticles. The fate of the nanoparticles dosed appeared to be controlled by the particle surface coating with PAA-coated particles remaining in the water column to a greater extent than CTAB-coated particles.

As nanomaterial use in consumer products increases, it will be critical to develop comprehensive means of identifying and screening potential environmental and human impacts to guide their design in a manner that avoids unintended consequences. In particular, this study demonstrated that metagenomics provides a highly sensitive indicator of potential effects of nanoparticle design that could be used as a conservative guideline. Focus on genes of public health concern may be of particular value in such an approach. An understanding of the relationship between morphology, surface coating, fate, stress response, and resistance genes may become important for water sustainability. The subtle impacts imparted here by relatively low concentrations, although still higher than current environmental relevance, of inert gold nanoparticles indicates that although high concentrations of nanoparticles are often required to either exert a response in traditional toxicity assays or disrupt system functionality, much lower concentrations may have unforeseen and possibly negative consequences.

3.5 METHODS

3.5.1 Reactor Configuration and Dosing

Nitrifying SBRs were maintained in 3 L beakers, with an operating volume of 2 L, and were run in a 20 °C controlled temperature room as previously described by Ma et al. (2015)[9]. SBRs were fed a synthetic wastewater (Table B.1) with a 14 d mean cell residence time. Sequential operation consisted of 0.1 h of feeding, 10.82 h aeration, 0.05 h mixed solids wasting, 0.75 h settling and 0.33 h decant, for a total 12 h cycle (Figure B.1). Experimental dosing began once SBRs achieved stable pH, mixed liquor suspended solids (MLSS) concentration, mixed liquor volatile suspended solids (MLVSS) concentration, and ammonia removal (greater than 98%). Reactors were dosed in duplicate, with five conditions as follows: non-dosed control receiving only synthetic wastewater, CTAB control receiving free CTAB solution at 800 µM (equivalent

concentration of CTAB in CTAB-coated particle stock solutions), CTAB-coated gold nanospheres in synthetic wastewater at 200 µg-Au/L, CTAB-coated gold nanorods in synthetic wastewater at 200 µg-Au/L, PAA-coated gold nanorods in synthetic wastewater at 200 µg-Au/L. The experiment was conducted for 56 d (4 mean cell residence times). SBR effluent was sampled throughout dosing and analyzed for ammonia concentration using an Ammonia Nitrogen Test Kit (Hach, Loveland, CO), and nitrate nitrogen (NO_3^--N) and nitrite nitrogen (NO_2^--N) using ion chromatography (Thermo Scientific, Tewksbury, MA). Reactor performance was also monitored using pH, MLSS, and MLVSS using standard methods[51].

DNA was extracted weekly in duplicate from 175 µL activated sludge using Fast DNA Spin Kit for Soil (MP Biomedicals LLC, Chicago, IL) according to manufacturer protocol. Using quantitative polymerase chain reaction, ammonia oxidizing bacteria were quantified through amplification of the *amoA* gene encoding the ammonia monooxygenase polypeptide activation site, nitrite oxidizing bacteria were quantified by targeting *Nitrobacter* and *Nitrospira* 16S rRNA genes, and total bacterial abundance was estimated using universal bacterial 16S rRNA gene primers. Primers and reaction conditions used can be found in Appendix B (Tables B.3 and B.4).

3.5.2 Nanoparticle Synthesis and Characterization

Nanoparticles were synthesized according to published procedures[52,53]. Stock nanoparticle concentrations were determined using ICP-MS (Thermo Scientific, Tewksbury, MA) and then diluted to similar concentrations before dosing. CTAB-coated nanoparticles were diluted with 800 µM CTAB solution. Spin coating TEM grid preparation was performed on activated sludge samples from SBRs dosed with nanoparticles at the conclusion of dosing. TEM images of nanoparticles in sludge were collected using a JEOL 2100 TEM operated at 200 kV, and sizing of nanoparticles was performed using Image-J (National Institutes of Health; Table B.5). Nanoparticle electrophoretic mobilities were measured using a Zetasizer NanoZS (Malvern Instruments)[54]. Stock nanoparticle solutions were diluted 1:10 with nanopure water for original nanoparticle measurement, and diluted 1:10 with 0.45 µm filtered non-dosed control SBR effluent to acquire the "In Control SBR Effluent" value.

3.5.3 Digestion and ICP analysis of Au

SBR activated sludge and effluent was sampled at the conclusion of dosing and stored at -80 °C until further analysis. Digestion of activated sludge to quantify Au concentration was as follows: 5 mL of activated sludge was dried at 100 °C overnight in a 50 ml beaker, ashed at 450 °C for 1.5 hours, acidified with 10 mL concentrated nitric acid, covered with a ribbed watchglass, and heated (but not boiled) until only a residue remained. Next, 10 mL freshly prepared aqua regia was added and incubated overnight, 500 µL of the aqua regia solution was diluted with 9.5 mL nanopure water and analyzed via ICP-MS. Effluent samples were subjected to 5% aqua regia digestion before analysis. Standard checks and blanks were used to verify digestion techniques.

3.5.4 Metagenomic and Statistical Analysis

DNA extracts from all reactors on the final day of dosing (representing long-term effects) and a week after the start of dosing (representing short term effects) as well as two DNA extracts from before dosing as a reference starting point were selected for metagenomics analysis. DNA Chip-Seq library preparation and Illumina paired-end HiSeq, 100 cycle, 101 bp read length, multiplexed sequencing was performed by the Biocomplexity Institute Genomics Research Laboratory (Blacksburg, VA). Sequencing reads were uploaded to MG-RAST[30] and annotated for taxonomy using the M5RNA database, a cutoff E value of $1e^{-5}$, 60% amino acid identity, and alignment length ≥15. Functional genes were also annotated using the SEED Subsystems database with identical parameters as taxonomy. Values were normalized to number of sequences passing MG-RAST default quality control per sample. A new online metagenomics analysis server, MetaStorm[38], was used to annotate ARGs, MRGs, and plasmids using the Comprehensive Antibiotic Resistance Database[39], BacMet Experimentally Confirmed Metal Resistance Genes Dataset[40], and ACLAME[41] respectively; annotated using a cutoff E value of $1e^{-5}$, 90% amino acid identity, and alignment length ≥25, and normalized to total 16S rRNA reads, using the Green Genes[55] database. Abundance tables were exported to Primer 6 software (Primer-E, Plymouth, UK) where Bray-Curtis dissimilarity was calculated and used for computing clustering and MDS plots.

3.6 ACKNOWLEDGEMENTS

This research was funded by the U.S. Environmental Protection Agency Star Grant #834856, the National Science Foundation (NSF) Center for the Environmental Implications of Nanotechnology (CEINT) (EF-0830093), the Water Environment Research Foundation Paul L. Busch Award, NSF PIRE: Halting Environmental Antimicrobial Resistance Dissemination (HEARD) (award number 1545756) and the Virginia Tech Institute for Critical Technology and Applied Science (ICTAS). The authors would also like to thank Rebecca Jones for help maintaining SBRs, Matt Chan for assisting in electrophloretic mobility measurements and Weinan Leng for assistance in TEM sample preparation.

REFERENCES

1. Steffen, W. *et al.* Planetary boundaries: Guiding human development on a changing planet. *Science* **347,** 6223 (2015).
2. Gottschalk, F., Sonderer, T., Scholz, R. W. & Nowack, B. Modeled environmental concentrations of engineered nanomaterials (TiO2, ZnO, Ag, CNT, fullerenes) for different regions. *Environ. Sci. Technol.* **43,** 9216–9222 (2009).
3. Mahapatra, I. *et al.* Probabilistic modelling of prospective environmental concentrations of gold nanoparticles from medical applications as a basis for risk assessment. *J. Nanobiotechnology* **13,** 93 (2015).
4. Schimel, J., Balser, T. C. & Wallenstein, M. Microbial stress-response physiology and its implications for ecosystem function. *Ecology* **88,** 1386–1394 (2007).
5. Briones, A. & Raskin, L. Diversity and dynamics of microbial communities in engineered environments and their implications for process stability. *Curr. Opin. Biotechnol.* **14,** 270–276 (2003).
6. Zhang, T., Shao, M. F. & Ye, L. 454 Pyrosequencing Reveals Bacterial Diversity of Activated Sludge From 14 Sewage Treatment Plants. *ISME J.* **6,** 1137–1147 (2012).
7. Grady Jr, C. L., Daigger, G. T., Love, N. G. & Filipe, C. D. *Biological Wastewater Treatment* (CRC Publishing, Boca Raton, FL 2011)
8. Hajipour, M. J. *et al.* Antibacterial properties of nanoparticles. *Trends Biotechnol.* **30,** 499–511 (2012).

9. Ma, Y. *et al.* Microbial community response of nitrifying sequencing batch reactors to silver, zero-valent iron, titanium dioxide and cerium dioxide nanomaterials. *Water Res.* **68,** 87–97 (2015).
10. Yang, Y. *et al.* Pyrosequencing reveals higher impact of silver nanoparticles than Ag+ on the microbial community structure of activated sludge. *Water Res.* **48,** 317–325 (2014).
11. Loman, N. J. *et al.* High-throughput bacterial genome sequencing: an embarrassment of choice, a world of opportunity. *Nat. Rev. Microbiol.* **10,** 599–606 (2012).
12. Simon, C. & Daniel, R. Metagenomic analyses: Past and future trends. *Appl. Environ. Microbiol.* **77,** 1153–1161 (2011).
13. Suresh, A. K., Pelletier, D. A. & Doktycz, M. J. Relating nanomaterial properties and microbial toxicity. *Nanoscale* **5,** 463–474 (2013).
14. Nel, A. E. *et al.* Understanding biophysicochemical interactions at the nano-bio interface. *Nat. Mater.* **8,** 543–557 (2009).
15. Gorka, D. E. *et al.* Reducing Environmental Toxicity of Silver Nanoparticles through Shape Control. *Environ. Sci. Technol.* **49,** 10093–10098 (2015).
16. El Badawy, A. M. *et al.* Surface charge-dependent toxicity of silver nanoparticles. *Environ. Sci. Technol.* **45,** 283–287 (2011).
17. Pal, S., Tak, Y. K. & Song, J. M. Does the antibacterial activity of silver nanoparticles depend on the shape of the nanoparticle? A study of the Gram-negative bacterium Escherichia coli. *Appl. Environ. Microbiol.* **73,** 1712–1720 (2007).
18. Tong, T. *et al.* Effects of material morphology on the phototoxicity of nano-TiO2 to bacteria. *Environ. Sci. Technol.* **47,** 12486–12495 (2013).
19. Burns, J. M. *et al.* Surface charge controls the fate of Au nanorods in saline estuaries. *Environ. Sci. Technol.* **47,** 12844–12851 (2013).
20. Ferry, J. L. *et al.* Transfer of gold nanoparticles from the water column to the estuarine food web. *Nat. Nanotech.* **4,** 441–444 (2009).
21. Alkilany, A. M. & Murphy, C. J. Toxicity and cellular uptake of gold nanoparticles: what we have learned so far? *J. Nanopart. Res.* **12,** 2313–2333 (2010).
22. Monopoli, M. P., Bombelli, F. B. & Dawson, K. A. Nanobiotechnology: nanoparticle coronas take shape. *Nat. Nanotech.* **6,** 11–12 (2011).

23. Tenzer, S. *et al.* Rapid formation of plasma protein corona critically affects nanoparticle pathophysiology. *Nat. Nanotech.* **8,** 772–781 (2013).
24. Kaegi, R. Behavior of silver nanoparticles in a pilot wastewater treatment plant SI. *Environ. Sci. Technol.* **45,** 3902-3908 (2011).
25. Keller, A. A. & Lazareva, A. Predicted Releases of Engineered Nanomaterials: From Global to Regional to Local. *Environ. Sci. Technol. Lett.* **1,** 65–70 (2014).
26. Siripong, S. & Rittmann, B. E. Diversity study of nitrifying bacteria in full-scale municipal wastewater treatment plants. *Water Res.* **41,** 1110–1120 (2007).
27. Tomlinson, T. G., Boon, A. G. & Trotman, C. N. Inhibition of nitrification in the activated sludge process of sewage disposal. *J. Appl. Bacteriol.* **29,** 266–291 (1966).
28. Choi, O. & Hu, Z. Size dependent and reactive oxygen species related nanosilver toxicity to nitrifying bacteria. *Environ. Sci. Technol.* **42,** 4583–4588 (2008).
29. Arnaout, C. L. & Gunsch, C. K. Impacts of Silver Nanoparticle Coating on the Nitri fi cation Potential of Nitrosomonas europaea. *Environ. Sci. Technol.* **46,** 5387-5395 (2012).
30. Meyer, F. *et al*. The metagenomics RAST server—a public resource for the automatic phylo- genetic and functional analysis of metagenomes. *BMC Bioinformatics* **9,** 386 (2008).
31. Ju, F., Guo, F., Ye, L., Xia, Y. & Zhang, T. Metagenomic analysis on seasonal microbial variations of activated sludge from a full-scale wastewater treatment plant over 4 years. *Environ. Microbiol. Rep.* **6,** 80–89 (2014).
32. Yang, C. *et al.* Phylogenetic diversity and metabolic potential of activated sludge microbial communities in full-scale wastewater treatment plants. *Environ. Sci. Technol.* **45,** 7408–7415 (2011).
33. Pruden, A., Pei, R., Storteboom, H. & Carlson, K. H. Antibiotic resistance genes as emerging contaminants: Studies in northern Colorado. *Environ. Sci. Technol.* **40,** 7445–7450 (2006).
34. Baker-Austin, C., Wright, M. S., Stepanauskas, R. & McArthur, J. V. Co-selection of antibiotic and metal resistance. *Trends Microbiol.* **14,** 176–182 (2006).
35. Ma, Y., Metch, J. W., Yang, Y., Pruden, A. & Zhang, T. Shift in antibiotic resistance gene profiles associated with nanosilver during wastewater treatment. 1–8 (2016).

36. Poole, K. Stress responses as determinants of antimicrobial resistance in Gram-negative bacteria. *Trends Microbiol.* **20,** 227–234 (2012).
37. Zhang, T., Zhang, X. X. & Ye, L. Plasmid metagenome reveals high levels of antibiotic resistance genes and mobile genetic elements in activated sludge. *PLoS One* **6,** e26041 (2011).
38. Arango-Argoty, G. *et al.* MetaStorm: A Public Resource for Customizable Metagenomic Annotation. *PLoS One* **11,** e0162442 (2016).
39. McArthur, A. G. *et al.* The comprehensive antibiotic resistance database. *Antimicrob. Agents Chemother.* **57,** 3348–3357 (2013).
40. Pal, C., Bengtsson-Palme, J., Rensing, C., Kristiansson, E. & Larsson, D. G. J. BacMet: Antibacterial biocide and metal resistance genes database. *Nucleic Acids Res.* **42,** 737–743 (2014).
41. Leplae, R., Lima-Mendez, G. & Toussaint, A. ACLAME: A CLAssification of mobile genetic elements, update 2010. *Nucleic Acids Res.* **38,** D57-61 (2009).
42. Alkilany, A. M. *et al.* Cellular uptake and cytotoxicity of gold nanorods: molecular origin of cytotoxicity and surface effects. *Small* **5,** 701–708 (2009).
43. González, S., Petrovic, M. & Barceló, D. Removal of a broad range of surfactants from municipal wastewater - Comparison between membrane bioreactor and conventional activated sludge treatment. *Chemosphere* **67,** 335–343 (2007).
44. Gagner, J. E., Lopez, M. D., Dordick, J. S. & Siegel, R. W. Effect of gold nanoparticle morphology on adsorbed protein structure and function. *Biomaterials* **32,** 7241–7252 (2011).
45. Sisco, P. N. *et al.* Adsorption of Cellular Proteins to Polyelectrolyte-Functionalized Gold Nanorods : A Mechanism for Nanoparticle Regulation of Cell Phenotype? **9,** e86670 (2014).
46. Joshi, N., Ngwenya, B. T. & French, C. E. Enhanced resistance to nanoparticle toxicity is conferred by overproduction of extracellular polymeric substances. *J. Hazard. Mater.* **241,** 363–370 (2012).
47. Yang, Y. & Alvarez, P. J. J. Sublethal Concentrations of Silver Nanoparticles Stimulate Biofilm Development. *Environ. Sci. Technol. Lett.* **2,** 221–226 (2015).

48. McSwain, B. S., Irvine, R. L., Hausner, M. & Wilderer, P. A. Composition and Distribution of Extracellular Polymeric Substances in Aerobic Flocs and Granular Sludge Composition and Distribution of Extracellular Polymeric Substances in Aerobic Flocs and Granular Sludge. *Appl. Environ. Microbiol.* **71,** 1051–1057 (2005).
49. Center for Disease Control and Prevention. Antibiotic resistance threats in the United States. http://www.cdc.gov/drugresistance/threat-report-2013/ (US Department of Health and Human Services, 2013).
50. Klaine, S. J. *et al.* Nanomaterials in the Environment: Behavior, Fate, Bioavailability, and Effects. *Environ. Toxicol. Chem.* **27,** 1825–1851 (2008).
51. Americnan Public Health Association (APHA). *Standard Methods for the Examination of Water and Wastewater*. (American Water Works Association and Water Environment Federation, 1998).
52. Murphy, C. J., Gole, A. M., Hunyadi, S. E. & Orendorff, C. J. One-dimensional colloidal gold and silver nanostructures. *Inorg. Chem.* **45,** 7544–7554 (2006).
53. Sau, T. K. & Murphy, C. J. Seeded high yield synthesis of short Au nanorods in aqueous solution. *Langmuir* **20,** 6414–6420 (2004).
54. Chan, M. Y. & Vikesland, P. J. Porous media-induced aggregation of protein-stabilized gold nanoparticles. *Environ. Sci. Technol.* **48,** 1532–1540 (2014).
55. Bowman, J. L., Floyd, S. K. & Sakakibara, K. Green Genes-Comparative Genomics of the Green Branch of Life. *Cell* **129,** 229–234 (2007).

APPENDIX B: SUPPORTING INFORMATION FOR CHAPTER 3

B.1 SUPPORTING TABLES

Table B. 1 Composition of synthetic wastewater

Chemical	Formula	Concentration (g/L)
Bactopeptone	/	0.30
Linoleic acid	$C_{18}H_{32}O_2$	0.09
Ammonium sulfate	$(NH_4)_2SO_4$	0.03
Aluminum sulfate octadecahydrate	$Al_2(SO_4)_3 \cdot 18H_2O$	0.04
Calcium chloride dihydrate	$CaCl_2 \cdot 2H_2O$	0.11
Iron chloride	$FeCl_3$	0.02
Magnesium sulfate	$MgSO_4$	0.09
Potassium hydrogen phosphate	K_2HPO_4	0.11
Sodium acetate	NaAc	0.14
Sodium bicarbonate	$NaHCO_3$	0.22
Micronutients	Table S2	0.1% (v/v)
Synthetic wastewater composition identical to Ma et al. (2015)[9]		

Table B. 2 Composition of micronutrients

Chemical	Formula	Concentration (g/L)
Citric acid	$C_6H_8O_7$	2.73
Hippuric acid	$C_9H_9NO_3$	2.00
Trisodium ethylenediaminetetraacetic acid tetrahydrate	$Na_3(EDTA) \cdot 4H_2O$	1.50
Boric acid	H_3BO_3	0.25
Zinc sulfate heptahydrate	$ZnSO_4 \cdot 7H_2O$	0.15
Manganese chloride tetrahydrate	$MnCl_2 \cdot 4H_2O$	0.12
Copper sulfate pentahydrate	$CuSO_4 \cdot 5H_2O$	0.06
Potassium iodide	KI	0.03
Sodium molybdate dehydrate	$Na_2MoO_4 \cdot 2H_2O$	0.03
Cobalt chloride hexahydrate	$CoCl_2 \cdot 6H_2O$	0.03

Nickel chloride hexahydrate	$NiCl_2 \cdot 6H_2O$	0.03
Sodium tungstate tetrahydrate	$NaWO_4 \cdot 2H_2O$	0.03
Synthetic wastewater composition identical to Ma et al. (2015)[9]		

Table B. 3 Primer sequences and annealing temperatures of quantitative polymerase chain reaction assays

Primer	Target gene	Primer Sequence (5'-3')	Annealing Temp. (°C)	Reference*
amoA-1F	*amoA*	GGGGTTTCTACTGGTGGT	60	Rotthauwe et al. 1997
amoA-2R		CCCCTCKGSAAAGCCTTCTTC		
FGPS1269	*Nitrobacter* 16S rRNA	TTTTTTGAGATTTGCTAG	50	Degrange and Bardin, 1995
FGPS872		CTAAAACTCAAAGGAATTGA		
EUB338f	*Nitrospira* 16S rRNA	ACTCCTACGGGAGGCAGC	50	Regan et al., 2002
Ntspa0685M		CGGGAATTCCGCGCTC		
1369F	Universal bacterial 16S rRNA	CGGTGAATACGTTCYCGG	60	Suzuki et al., 2000
1492R		GGWTACCTTGTTACGACTT		

***Reference**

Degrange, V. and Bardin, R., 1995. Detection and Counting of Nitrobacter Populations in Soil by PCR. Applied and Environmental Microbiology 61(6), 2093-2098.

Regan, J.M., Harrington, G.W. and Noguera, D.R., 2002. Ammonia- and nitrite-oxidizing bacterial communities in a pilot-scale chloraminated drinking water distribution system. Applied and Environmental Microbiology 68(1), 73-81.

Rotthauwe, J.H., Witzel, K.P. and Liesack, W., 1997. The ammonia monooxygenase structural gene amoA as a functional marker: Molecular fine-scale analysis of natural ammonia-oxidizing populations. Applied and Environmental Microbiology 63(12), 4704-4712.

Suzuki, M.T., Taylor, L.T. and DeLong, E.F., 2000. Quantitative analysis of small-subunit rRNA genes in mixed microbial populations via 5 '-nuclease assays. Applied and Environmental Microbiology 66(11), 4605-4614.

Table B. 4 Reaction matrix of quantitative polymerase chain reaction

Reaction Component	In 10 µL reaction mix
Forward and reverse primers	0.3 µM
SsoFast EvaGreen Supermix (Bio-Rad Laboratories, Hercules, CA)	1x
DNA sample	1 µL

Table B. 5 TEM Sizing of Nanoparticles

Nanoparticle	n	Width (nm)		Length (nm)		Aspect Ratio	
		Average	St. Dev.	Average	St. Dev.	Average	St. Dev
Original CTAB-Coated Nanospheres	211	17.06	2.62	19.99	3.09	1.18	0.18
Original CTAB-Coated Nanorods	188	9.11	1.27	27.68	4.61	3.06	0.49
Original PAA-Coated Nanorods	139	9.33	1.28	27.90	4.97	3.00	0.43
CTAB-Coated Nanospheres in SBRs	175	17.24	3.02	20.73	3.42	1.21	0.16
CTAB-Coated Nanorods in SBRs	188	8.75	1.55	28.05	5.47	3.29	0.81
PAA-Coated Nanorods in SBRs	123	9.03	1.39	28.81	4.55	3.24	0.57

B.2 SUPPLEMENTARY FIGURES

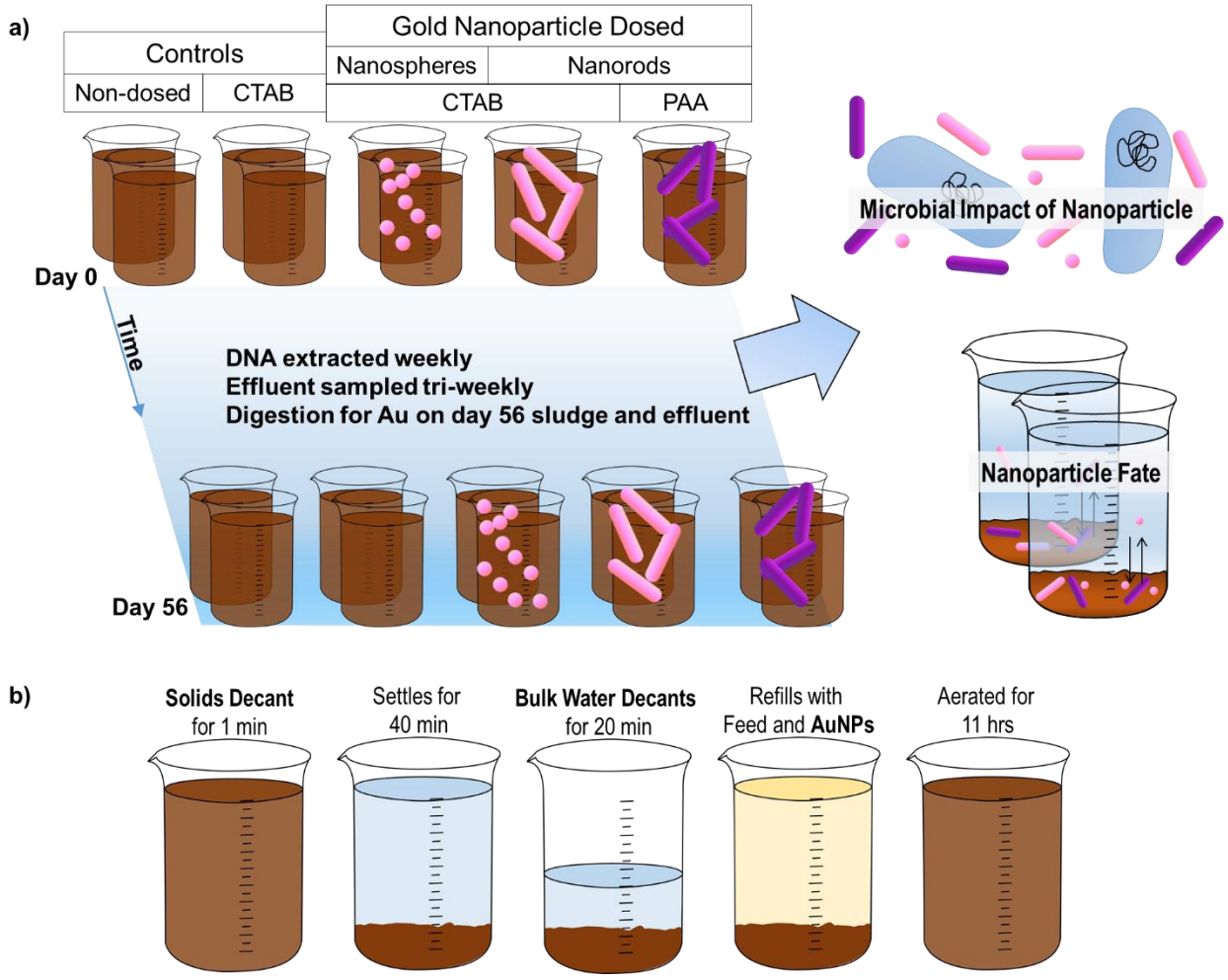

Figure B. 1 Experimental schematic of a) SBR dosing and sampling events b) the stages of the SBR 12 hour cycle.

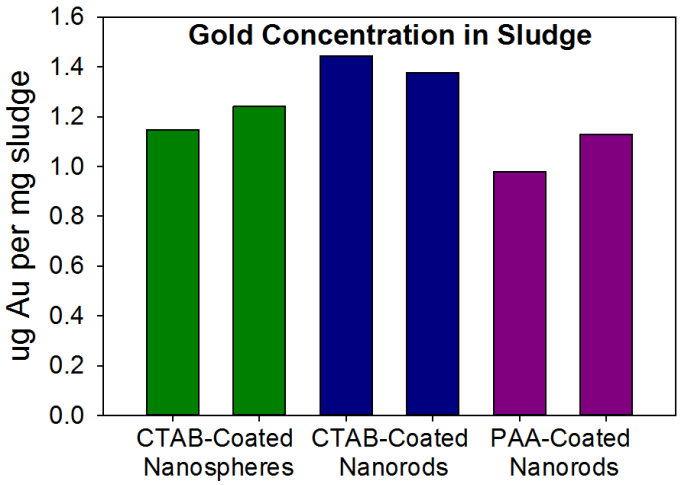

Figure B. 2 Concentration of gold in sludge on day 56 of dosing. Duplicate bars represent replicate SBRs.

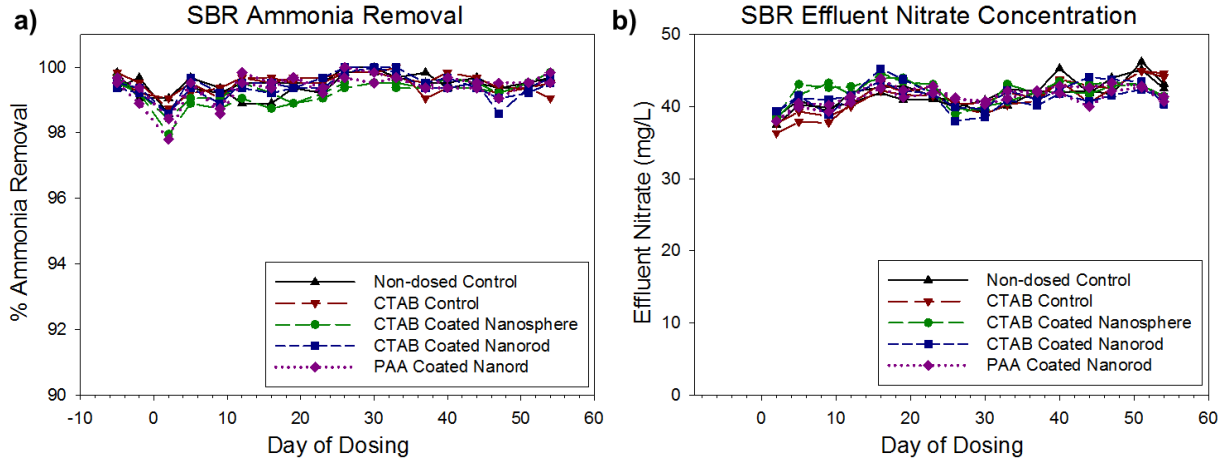

Figure B. 3 Nitrification performance of SBRs throughout dosing as measured by a) percent ammonia removal and b) effluent nitrate concentration.

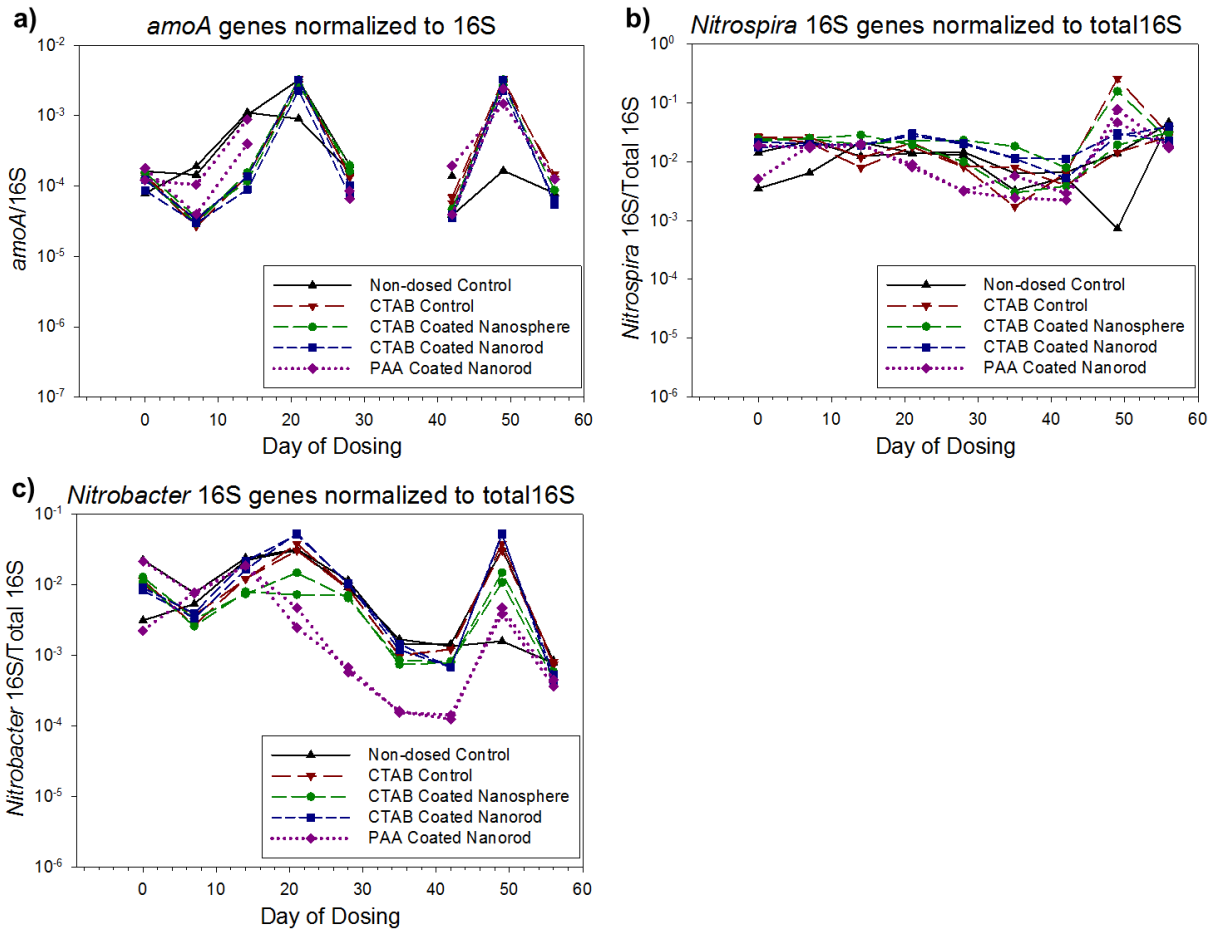

Figure B. 4 Quantitative polymerase chain reaction quantification of gene markers for nitrification in SBRs, normalized to total bacterial 16S rRNA genes; a) ammonia monoxygenase (*amoA*) used in ammonia oxidation and representative of ammonia oxidizing bacteria b) *Nitrospira* 16S rRNA genes and c) *Nitrobacter* 16S rRNA genes representing two key nitrite oxidizing bacteria.

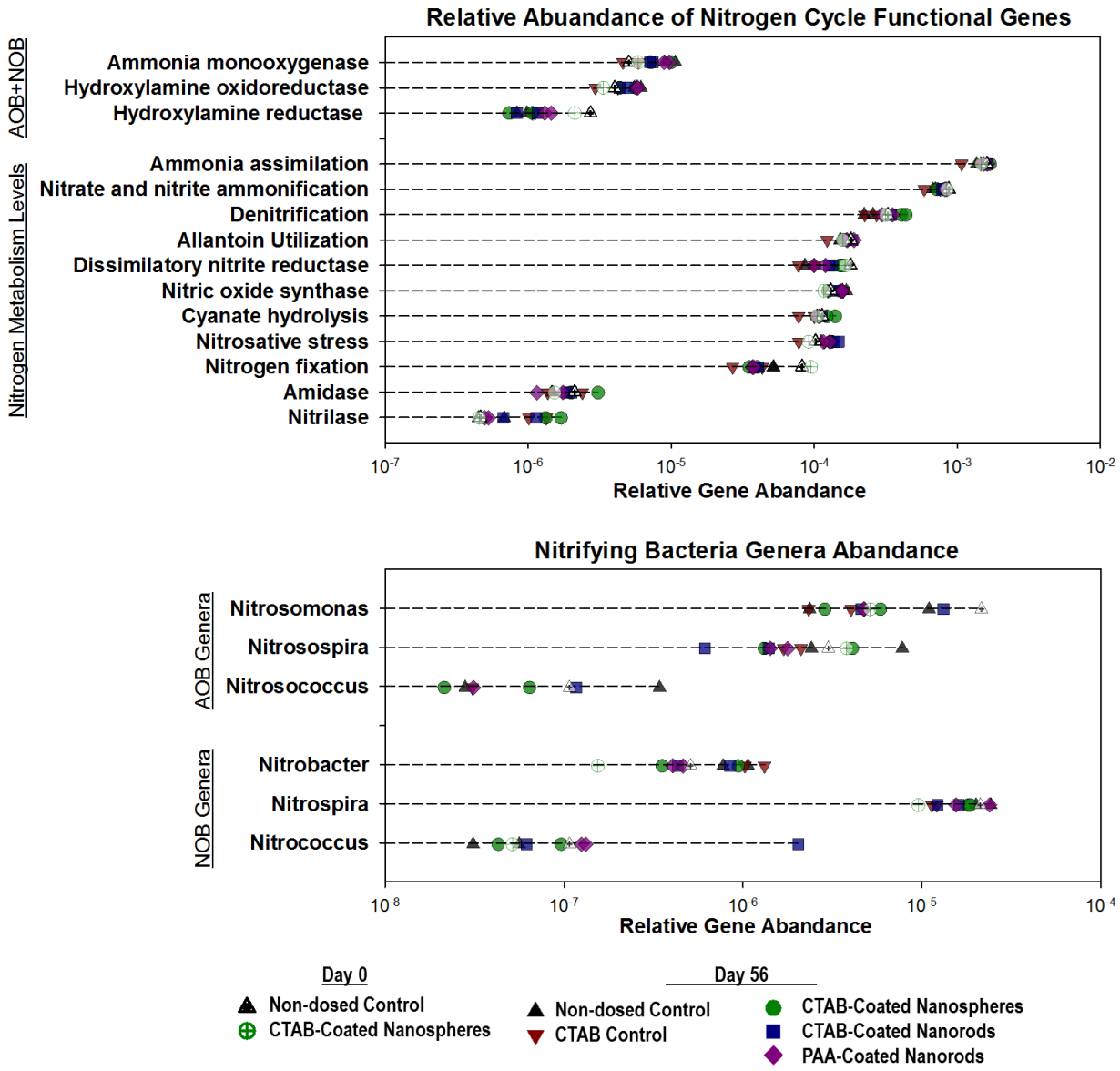

Figure B. 5 Metagenomic analysis of relative abundance of nitrifying and nitrogen metabolism functional genes (top panel), and relative abundance of genera typically attributed with nitrification in activated sludge (bottom panel). All annotated reads were normalized to the number of sequences passing QC.

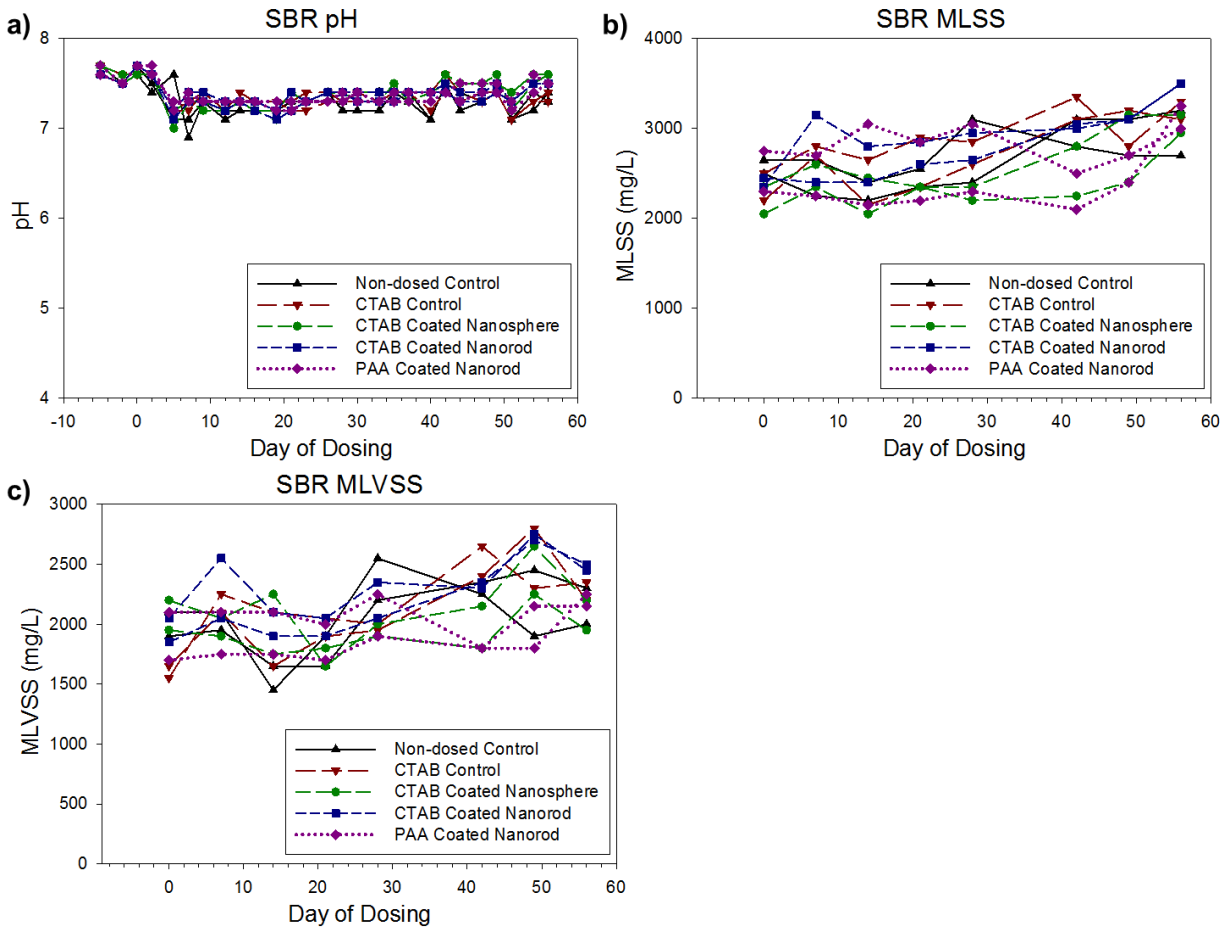

Figure B. 6 Activated sludge characterization in SBRs throughout dosing; a) pH of reactor measure with pH probe b) MLSS and c) MLVSS.

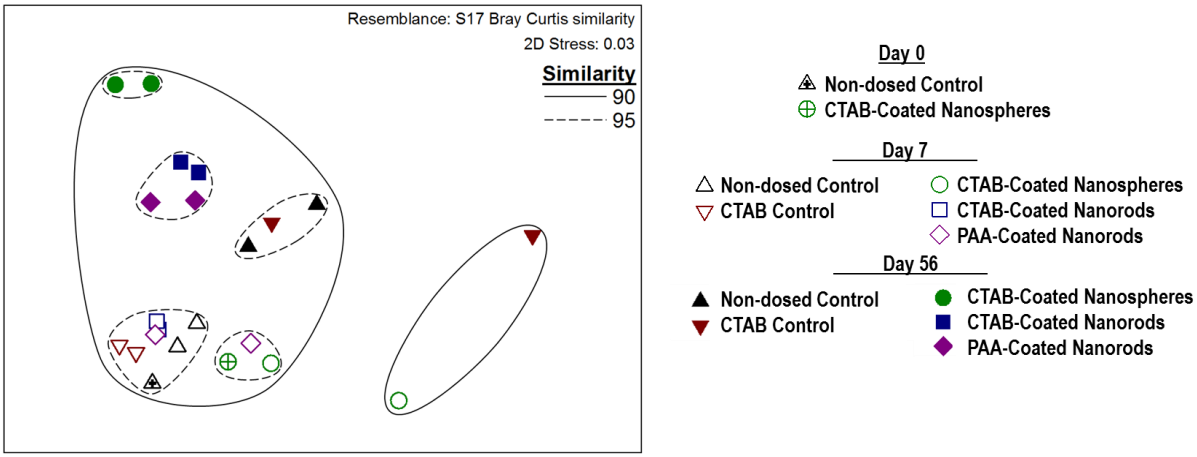

Figure B. 7 MDS ordination of Bray-Curtis similarity of functional genes. The relative proximity of points in 2D space is indicative of relative similarity in taxonomic structure of the microbial communities. Group-average clustering from Bray-Curtis similarity was superimposed on MDS obtained from the same similarities.

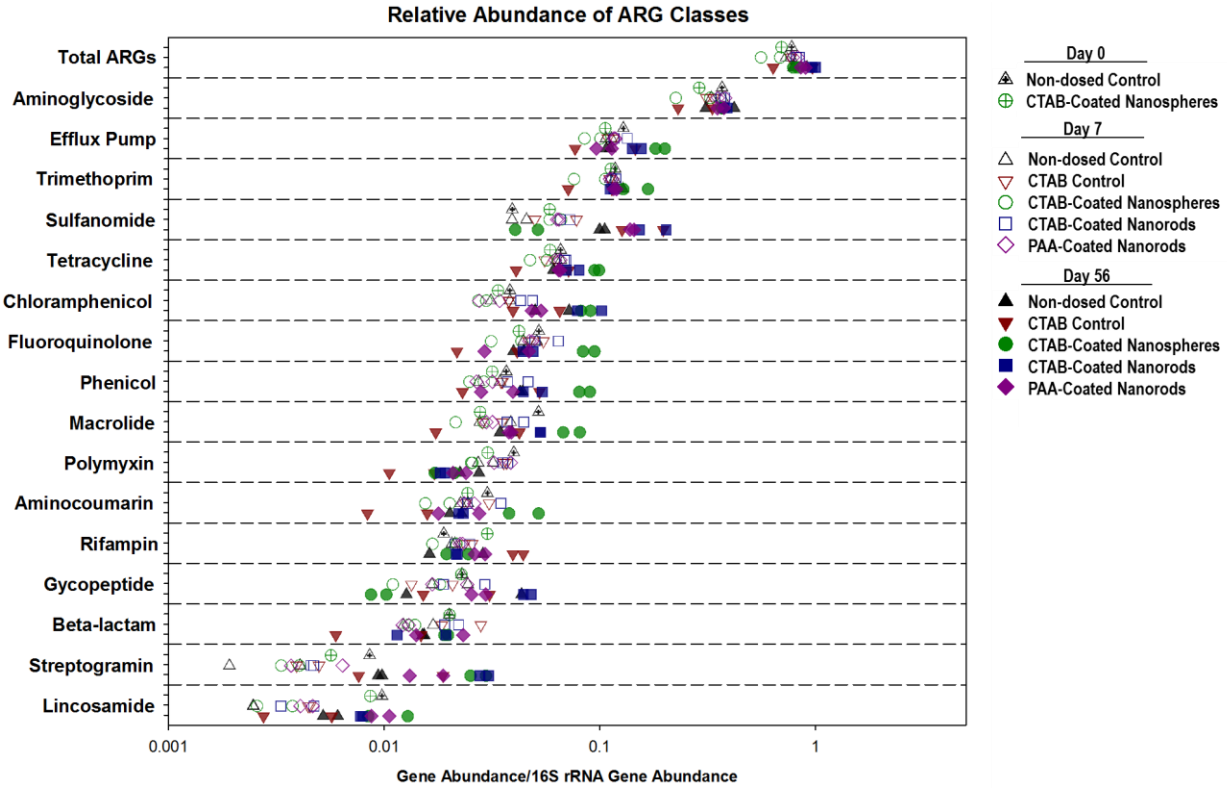

Figure B. 8 Relative abundance of ARG classes normalized to 16S rRNA gene abundance. ARG composition of SBRs on the final day of dosing (day 56), day 7 of dosing and two SBRs from day 0, as a reference, are represented. Duplicate SBRs are represented with similar symbols and SBRs with no hits are not shown.

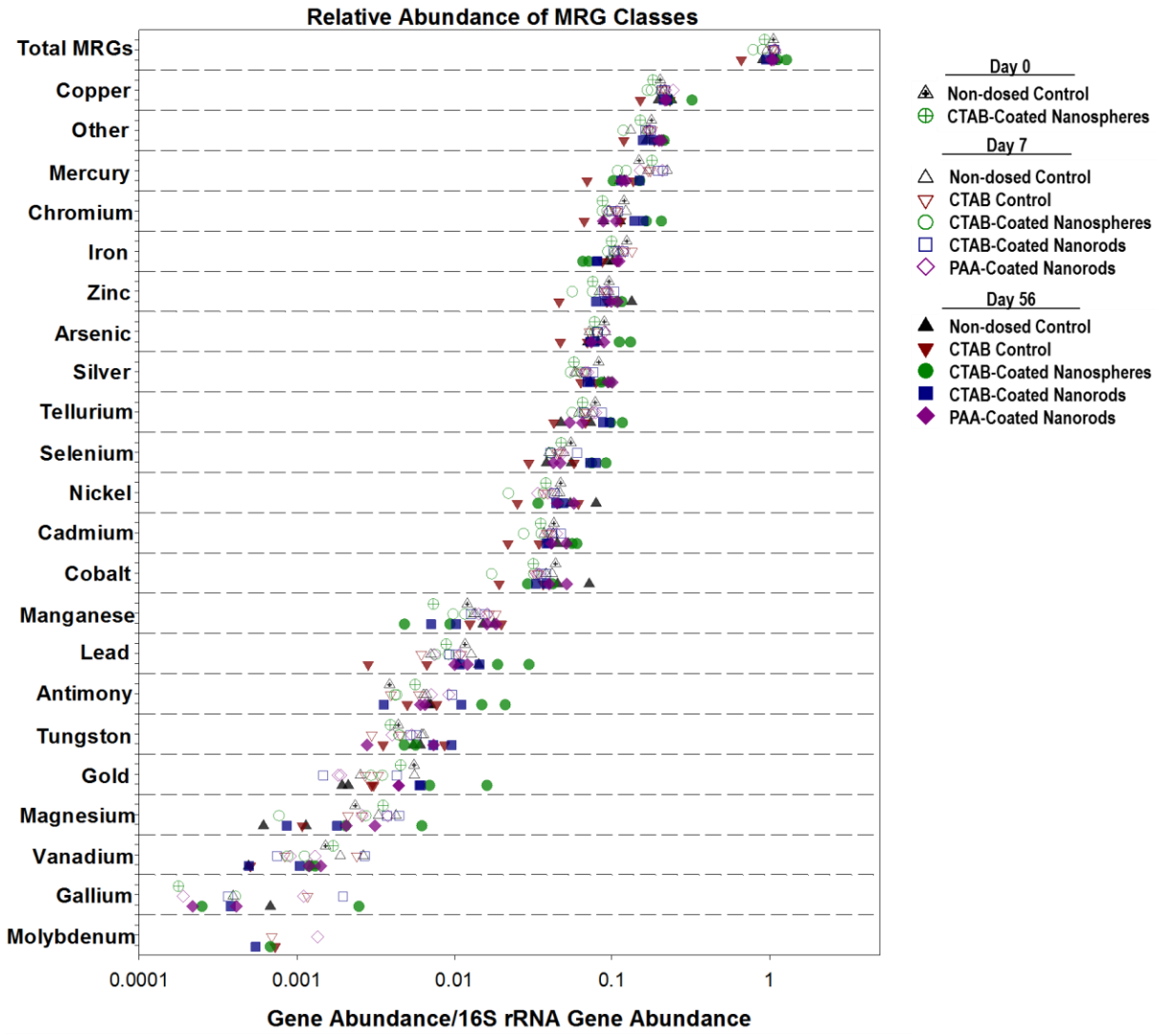

Figure B. 9 Relative abundance of MRG classes (number of MRGs of each class normalized to 16S rRNA gene abundance). MRG composition of SBRs on the final day of dosing (day 56), day 7 of dosing and two SBRs from day 0, as a reference, are represented. Duplicate SBRs are represented with similar symbols and SBRs with no hits are not shown.

CHAPTER 4: ENHANCED DISINFECTION BY-PRODUCT FORMATION DUE TO NANOPARTICLES IN WASTEWATER TREATMENT PLANT EFFLUENTS

Jacob W. Metch, Yanjun Ma, Peter J. Vikesland, Amy Pruden

4.1 ABSTRACT

Nanoparticles (NPs) are increasingly being incorporated into consumer products and are being used for industrial applications in ways that will lead to their environmental dissemination via wastewater treatment plants (WWTPs). Many NPs possess catalytic properties that could potentially enhance undesired chemical reactions such as the formation of disinfection by-products during disinfection of wastewater effluent. In this effort, silver (AgNPs), titanium dioxide (TiO_2), ceria (CeO_2), and nano zero valent iron (NZVI) NPs were investigated for their potential to enhance trihalomethane (THM) formation in three different disinfection regimes: UV alone, free chlorine, and UV + free chlorine. Of the test nanomaterials, only AgNPs demonstrated the capacity to enhance THM formation and thus they were subjected to additional study. AgNPs enhanced THM formation at all concentrations examined (1, 10, and 20 mg/L) even though the AgNPs were chemically unstable in the presence of free chlorine. The transformation of the AgNPs and the production of non-metallic silver species was observed via UV-Vis spectroscopy. The capacity for AgNPs to enhance THM formation was considerably increased in the UV + free chlorine disinfection regime. Although not the focus of the study, formation of AgNPs during UV disinfection of Ag^+ in effluent was also observed. This study illustrates the potential for NPs to catalyze unfavorable chemical reactions during disinfection of WWTP effluents. Such a result could prove detrimental to aquatic receiving environments and is especially of concern in water reuse scenarios where aggressive disinfection regimes may be utilized.

4.2 INTRODUCTION

The rapid development of nanotechnology has led to the incorporation of nanomaterials in numerous industrial and commercial products. Nanomaterials are being employed in these products due to their exceptional antimicrobial[1], photocatalytic[2], and

optical[3] properties, amongst others. The widespread application of nanomaterials in industrial and consumer products increases the likelihood that they will be released into the environment in ways that are uncontrolled and possibly detrimental.

The manner by which nanomaterial containing products are consumed or cleaned is expected to result in significant nanomaterial inputs to wastewater treatment plants (WWTPs)[4]. Consumer products, such as clothing and medical textiles, that contain embedded silver nanoparticles (AgNPs) have been found to release these nanomaterials during laundering[5,6]. Nanomaterials such as titanium dioxide (TiO_2) applied in food, lotions, and sunscreens have similar potential for transmission to sewer collection systems simply through industrial and consumer use[7]. Ceria (CeO_2) is used as a polishing agent in industry[8], and as a fuel additive to reduce harmful emissions from diesel engines[9]. Nano zero valent iron (NZVI) is also being developed for the oxidation of several water contaminants[10] and therefore may be introduced to the sewer system as well. The combination of their unique properties (relative to bulk materials) and the strong potential for nanomaterial dissemination to sewer systems has led to increased concern regarding the possible detrimental effects of nanomaterials to WWTP performance. Past studies by our group and others have shown that one unintended biological consequence of nanomaterial fluxes into WWTPs is a shift in the activated sludge microbial communities[11,12] and specifically, decreases in nitrifying bacteria[11,13]. To date, however, the potential implications of nanomaterials on the chemical processes used for wastewater disinfection have yet to be examined.

As a result of their unique properties, nanomaterials are widely applied as catalysts that can enhance the rates of a diverse array of chemical transformations[14]. For example, Vejerano et al. (2013) discovered that during waste incineration, total polycyclic aromatic hydrocarbon emissions were approximately six times higher in waste containing nanomaterials when compared to bulk controls[15]. Of concern to the present study was the potential for nanomaterials to catalyze undesirable reactions within a WWTP. Our particular focus was to evaluate the potential effects of nanomaterials on wastewater disinfection.

It is well known that high concentrations of organic matter can lead to elevated concentrations of toxic disinfection by products (DBPs) in chlorinated WWTP

effluents[16]. DBPs form when strong oxidants such as free chlorine oxidize organic matter, bromide, and iodide in water[17]. Similarly, UV irradiation is known to photorearrange organic matter and possibly increase its reactivity towards free chlorine[18], thus potentially increasing the DBP formation potential. Although it is acknowledged that DBP occurrence in WWTP effluents is important to water sustainability, and NPs will be transported to the environment via WWTPs, currently there are no studies investigating the effect of NPs on the formation of DBPs in WWTP effluents.

In this study, we assessed the potential for four common nanomaterials: Ag, TiO_2, NZVI, and CeO_2 to catalyze DBP formation with a focus on trihalomethanes (THMs) and chloropicrin. THMs are of immediate concern because of their relative ease of formation in chlorinated water, their mutagenicity and genotoxicity, as well as the regulatory standards placed on them by the US EPA[19]. Chloropicrin is also a concern due to its formation potential in chlorinated waters and its genotoxicity to mammalian cells[19]. Because AgNPs demonstrated an increased THM formation potential, follow up experiments were conducted to gain further insight into the mechanism by which AgNPs increased THM formation. These experiments monitored free chlorine demand, assessed THM formation at various AgNP concentrations, and used UV-Vis spectroscopy to investigate AgNP stability and material speciation throughout the disinfection process.

4.3 METHODS

4.3.1 Nanoparticle Source, Synthesis, and Characterization

AgNPs were synthesized by sodium citrate reduction, as described elsewhere[20]. NZVI dispersions were purchased with organic and inorganic stabilizers from NANO IRON s.o.r. (NANOFER 25S, Rajhrad, Czech Republic). Anatase TiO_2 and CeO_2 nanopowders were purchased from Sigma-Aldrich (St. Louis, Missouri, USA) and were suspended into nanopure water by sonication for 20 minutes (90 W, 20 KHz, 20 °C). Nanoparticle suspensions and bulk or ionic controls were prepared as stock suspensions of 100 mg/L and stored in the dark until use. The bulk or ionic controls for AgNP, TiO_2-NP, CeO_2-NP, and NZVI were silver nitrate (Fisher, Suwanee, GA), TiO_2 (≈44 µm) and

CeO_2 (≈5 µm) bulk powders (Sigma-Aldrich, Saint Louis, MO), and ferrous sulfate (Fisher), respectively.

The average sizes of the nanoparticles were determined by transmission electron microscopy (TEM) as previously described[21]. Nanoparticle suspensions were diluted 100x, then drop-cast onto a 200 mesh, lacey-carbon-coated copper TEM grid. Hydrocarbons that would cause interference were removed by heating under vacuum at 120 °C for 3 hr. A JEM 2100 TEM (JEOL Corporation) operated at 200 kV, equipped with an energy dispersive X-ray spectrometer and diffractometer was employed. Average nanoparticle sizes were determined by counting at least 70 particles per TEM image and then sizing via use of ImageJ software. Using this approach the AgNPs were determined to have a diameter of 52±12 nm, NZVI was 46±10 nm, TiO_2-NPs were 21±12 nm, and CeO_2-NPs were 33±12 nm.

4.3.2 WWTP Effluent Collection

Plant One (WWTP 1) received primarily domestic wastewater flow, while Plant Two (WWTP 2) received approximately 15% industrial wastewater flow along with domestic wastewater flow. Both WWTPs were conventional activated sludge plants and at the time of sample collection were not practicing denitrification processes. WWTP samples were collected immediately prior to disinfectant addition, transported immediately to the lab and stored at 4 °C until use (3 days or less). For general sample characteristics see SI Tables S1 and S2.

4.3.4 UV_{254} Disinfection

UV_{254} disinfection was carried using a collimated beam apparatus using our previously described setup[22]. A low pressure mercury lamp was used to produce UV light at a wavelength of 254 nm. A fluence dose of 200 mJ/cm^2 was achieved by measuring the fluence rate with a UVX Radiometer with a UVX-25 (UV_{254}) sensor (UVP, LLC, Upland, California, USA), and then calculating the contact time based on the fluence rate. Wastewater disinfection was carried out in 65 mL volumes in 9 cm diameter glass Petri dishes (depth of approximately 1 cm) with continuous mixing throughout the irradiation time.

4.3.5 Free Chlorine Disinfection

Three conditions (background control, bulk or ionic control, and NP) were subjected to free chlorine disinfection in triplicate using 20 mL amber vials. The free chlorine concentration of a commercial chlorine stock was determined via the colorimetric DPD method (HACH, Colorado, USA). A 2,000 mg/L stock free chlorine solution was prepared fresh for each experiment and then used to achieve an initial free chlorine concentration of 20 mg/L in the reaction vials. Although this chlorine dose is greater than what is practiced at most WWTPs, this dose was chosen to represent a worst case scenario and to investigate any potential DBP enhancement capability of nanoparticles. Final concentrations of the bulk or ionic controls as well as the nanoparticle conditions were set at 20 mg/L. For metal oxide particles this was measured as the mass of the nanoparticles and for zero valent metal particles, with respect to the concentration of the metal. As a background control the same volume of nanopure water was used to dilute the reaction matrix to the same volume (20 mL). In the experiments examining sequential disinfection by UV followed by free chlorine, the product of the UV disinfection was pipetted into 20 mL amber reaction vials in triplicate for each condition and then subjected to free chlorine disinfection. Following free chlorine addition the reaction vials were capped and mixed by inversion and then incubated at room temperature for 30 minutes. Excess citric acid was used to quench the reaction. Because the AgNPs enhanced DBP formation at 20 mg/L, the experiments were repeated at lower doses of NPs and repeated at 20 mg/L. In these follow-up experiments, the chlorine disinfection protocol was modified slightly as in previous studies[23]. Here a 5.6-6% sodium hypochlorite solution (Sigma Aldrich, St. Louis, Missouri, USA) was used as a chlorinating agent and diluted to prepare a 20,000 mg/L chlorine solution (concentration verified using DPD method as described above). A large batch of the background control, bulk or ionic control, or NP condition (180 mL) was prepared in an Erlenmeyer flask and mixed with a magnetic stir bar. In the UV + free chlorine disinfection regime; the product of UV disinfection was put into an Erlenmeyer flask. While mixing, the free chlorine solution was added to a final concentration of 20 mg/L, and the vial was then capped immediately. After 30 seconds of mixing, 20 mL amber vials were filled and capped with no head space, in triplicate, and incubated for 30

minutes at room temperature. Citric acid was added to the head space analysis vials so when the sample was added after 30 minutes, the reaction was quenched.

4.3.6 THM Analysis

Four THMs (trichloromethane, bromodichloromethane, dibromochloromethane, and tribromomethane) and chloropicrin were quantified using a Thermo Finnigan TraceGC Ultra gas chromatograph (Thermo Finnigan, San Jose, California, USA) with a SPB-624 Supelco fused silica capillary column (Sigma Aldrich, St. Louis, Missouri, USA) and equipped with a headspace autosampler and an electron capture detector as reported by a previous study[24]. Standards were diluted to known concentrations in headspace free glass syringes to limit loss of standard to volatilization, and concentrated stock standards were stored under water for up to one week. Samples were transferred from the reaction vials to 20 mL headspace vials and crimp sealed using an aluminum seal with septa (Restek Corporation, Bellefronte, Pennsylvania, USA). THM standards were purchased as a mixture (Restek Corporation, Bellefronte, Pennsylvania, USA). Chloropicrin was purchased (VWR International Inc., Suwanee, GA) and combined with THM standards during dilution. THMs were identified based upon elution times and quantified using calibration curves with reference to an internal standard of 1,2 dibromopropane (Crescent Chemical Company Inc., Islandia, New York, USA).

4.3.7 UV-Vis Spectrum Analysis

The UV-Vis spectrum was analyzed during the follow up experiments of varying concentrations of AgNPs. Samples were collected in 10 mL amber vials for background control, bulk/ion control, and NP conditions at four intervals of the follow up experiments (no disinfection, free chlorine disinfection, UV disinfection, and UV + free chlorine disinfection). Samples were stored at 4 °C for no longer than 2 days until analyzed using a Beckman DU-640 spectrophotometer (Beckman Instruments Inc., Fullerton, CA, USA).

4.3.8 Free Chlorine Demand

Free chlorine demand experiments were conducted with follow up experiments of varying NP concentrations. Samples for no disinfection and after UV disinfection were

collected in 20 mL amber vials in triplicate for background control, bulk/ion control, and NP conditions. These samples were chlorinated with sodium hypochlorite at 50 mg/L, after 24 hours of incubation in the dark at room temperature free chlorine was measured according to Standard Method 4500-Cl[25] using a DR2700 spectrophotometer (HACH, Loveland, CO). Chlorine demand was calculated as the difference between the initial free chlorine concentration and the final free chlorine concentration.

4.4 RESULTS AND DISCUSSION

4.4.1 Formation of Disinfection By-Products in the Presence of Nanoparticles

To ascertain whether our four tested nanomaterials were capable of enhancing DBP formation, our initial survey employed a high nanomaterial dose of 20 mg/L. Chloroform was the most abundant THM in all samples tested and therefore will be the focus of the following discussion as it drove THM trends. Of the four nanoparticles investigated, only the AgNPs resulted in increased chloroform formation relative to the bulk control, ion control, or the background controls (Figure 4.1). Chloropicrin was not quantifiable in most samples and no trends could be observed (Tables C.3, C.4, and C.6). Also, wastewater treatment plant effluent variations likely caused background formation of chloroform varied greatly between experiments as DBP formation has been found to vary temporally[26]. Interestingly, neither CeO_2 nor TiO_2 resulted in increased chloroform formation relative to the control conditions. This result was unexpected given the well-established capability of TiO_2 to catalyze a variety of reactions via UV light mediated formation of reactive oxygen species, as has been applied for wastewater disinfection[27]. Although not as reactive as TiO_2, CeO_2 also has demonstrated photocatalytic properties[28,29], however no such properties were displayed in this study. Similarly, there was also no significant increase in chloroform formation in effluent containing nano zero-valent iron relative to the background control. However, there was a significant decrease in chloroform formation in the ion control (ferrous sulfate). This result is likely because the ferrous sulfate incurred a significant free chlorine demand[30], thus limiting the opportunity for free chlorine to react with organic matter and produce chloroform. Interestingly, formation of chloroform in the presence of the AgNPs was considerably greater when subjected to UV + free chlorine disinfection relative to the free chlorine

only condition. There is considerable understanding of the photocatalytic properties of silver doped titanium dioxide[31]; however less is known about the photocatalytic ability of silver itself. Subsequent experiments attempted to identify the mechanisms driving this phenomenon.

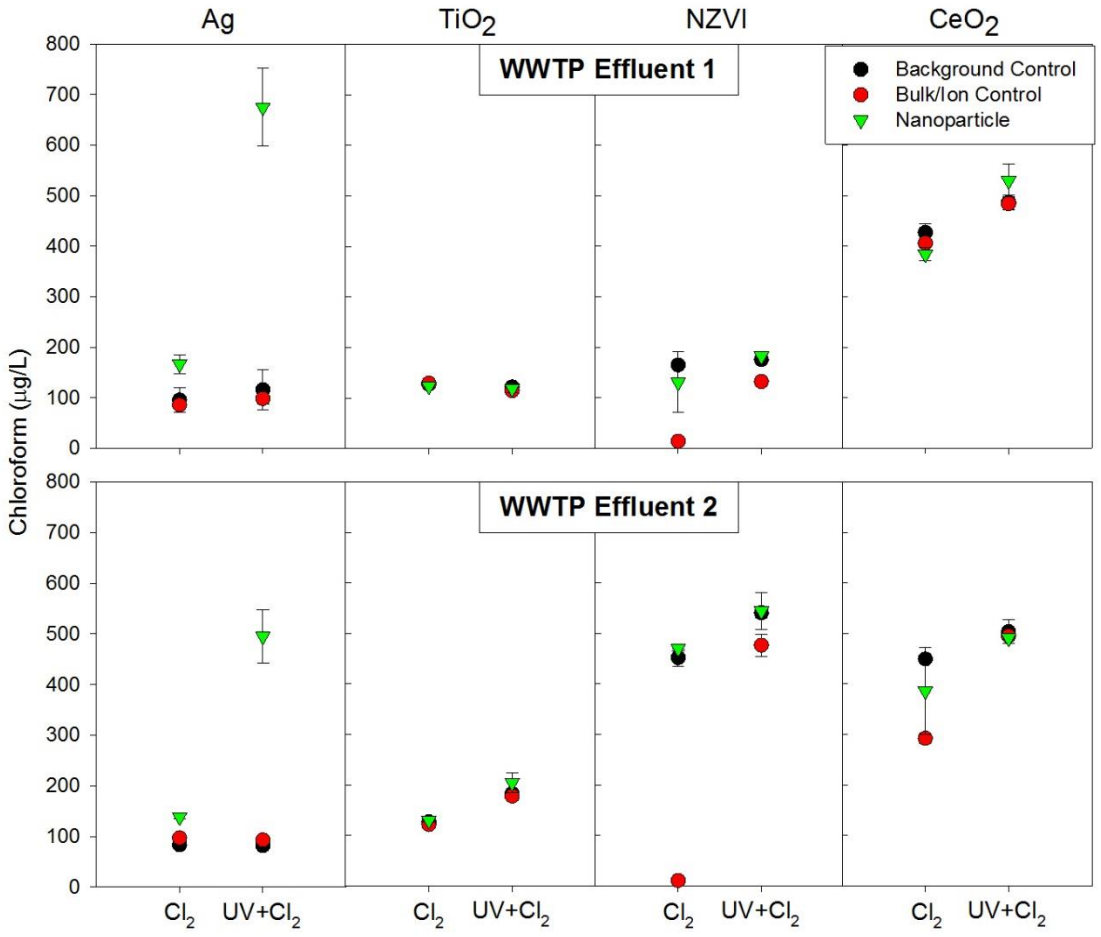

Figure 4. 1 Formation of chloroform in the presence of nanomaterials (indicated on x axis) relative to bulk/ion and background controls when subjected to either chlorine only (Cl_2) or UV + free Cl_2 disinfection. The bulk/ion controls for AgNP, TiO_2, NZVI, and CeO_2 were silver nitrate, bulk TiO_2, ferrous sulfate, and bulk CeO_2 respectively. Error bars represent one standard deviation of experimental triplicates.

4.4.2 AgNP Enhanced Chloroform Production

A second series of experiments focused specifically on further evaluation of the capability of AgNPs to catalyze disinfection by-product formation at 20 mg/L and at lower concentrations of 10 mg/L and 1 mg/L. Although these concentrations are still

higher than EPA freshwater discharge guidelines of 3.2 µg/L for silver[32], it is important to investigate the relationship between enhanced chloroform formation and concentration of AgNPs. Chloroform production was found to be enhanced in wastewater effluent amended with all three doses of AgNPs (Figure 4.2). The increase in chloroform production by AgNPs was consistently enhanced in the highly aggressive UV + free chlorine disinfection regime. Low amounts of chloropicrin were produced in experiments examining 1 mg/L silver; in experiments with either 10 or 20 mg/L of silver, chloropicrin was not quantifiable. No trends were discernible for AgNP mediated enhancement of chloropicrin formation. Brominated THMs were also produced in all samples tested with AgNPs having increased bromodichloromethane in some situations, however this was not consistent and no trend could be discerned (Tables C.8, C.9, and C.10).

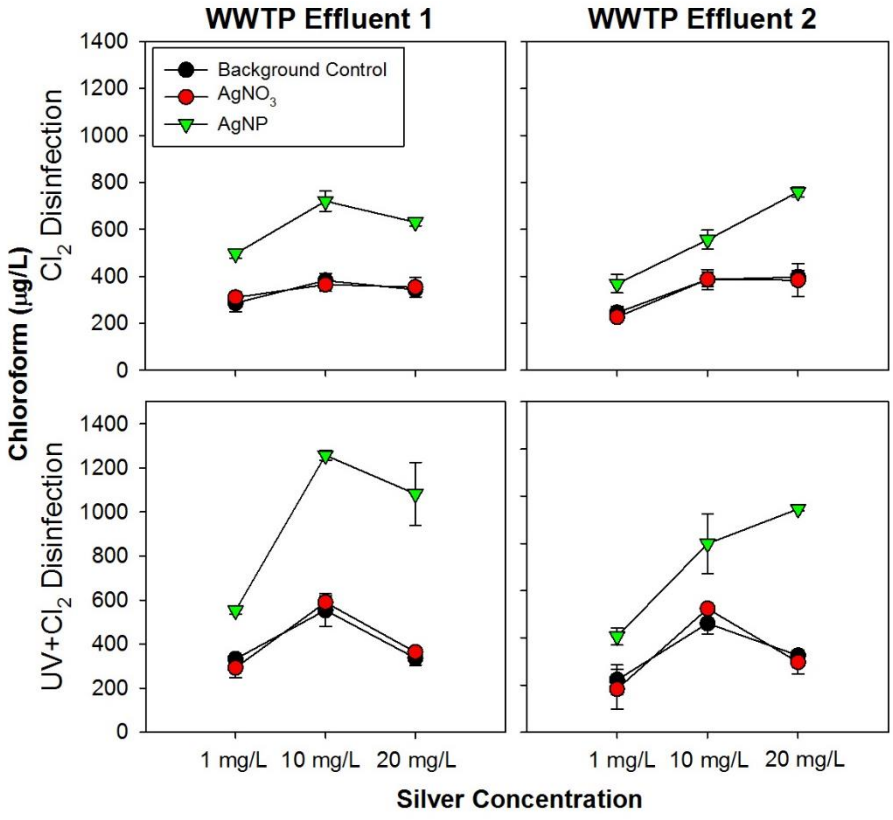

Figure 4. 2 Chloroform formation in the presence of varying concentrations of AgNPs, as well as ion (silver nitrate) and background controls in WWTP effluents disinfection using free chlorine or UV + free chlorine disinfection. Note: lines are intended to guide the eye

and not model the data. Error bars represent one standard deviation of analytical replicates.

The results of this study suggest that in most cases UV light influences wastewater chemistry in a manner that enhances disinfection by-product formation when the water is subsequently chlorinated. UV disinfection has been previously shown to photo-rearrange natural organic matter (NOM), which could increase its reactivity towards chlorine[18]. Also, it is known that NOM can form a thin layer or corona around metallic nanoparticles under many environmental conditions[33]. Specifically, NOM has been found to associate with both citrate coated nanoparticles[34], and AgNPs[35]. Therefore, it is possible that NOM coats the AgNPs and that this close proximity results in increased photo-rearrangement of NOM during UV disinfection due to availability of NOM to the AgNP surface, and thus increases its overall reactivity towards free chlorine.

Of interest in this study was the potential formation of disinfection by-products within the background matrix of treated wastewater effluent. Wastewater effluent is relatively rich in organic matter, relative to treated drinking water, which could enhance disinfection by-product formation. In this study, two WWTP effluents were examined, in order to capture a range of possible matrix effects. When the AgNPs were dosed to WWTP Effluent 1, there was no apparent trend between the concentration and the enhancement of chloroform production. Although there was increased enhancement in the 10 mg/L condition as compared to the 1 mg/L condition, there was not a significant increase in chloroform generation between the 10 mg/L and 20 mg/L conditions. When dosed to WWTP Effluent 2, however, there was a clear trend of an increase in chloroform production with an increase in AgNP dose. The differing trends observed with the two WWTP Effluent matrices indicates that variations in wastewater chemistry can influence the magnitude of the enhancement in chloroform formation caused by AgNPs. Based on the general characteristics of the effluents (Table C.1 and C.2), the most striking difference between the effluents is that the ionic strength was much higher in WWTP Effluent 2 (1,013 µS/cm) compared to WWTP Effluent 1 (594 µS/cm). Ionic strength has been demonstrated to affect nanoparticle stability and surface chemistry[36], which will likely impact reactivity and could account, at least in part, for the differing patterns of DBP production between the two effluents.

4.4.3 Potential Effects of Nanomaterial Coatings

Tugulea et al. (2013) recently investigated the effect of polyvinylpyrrolidone (PVP) coated AgNPs on DBP formation during drinking water disinfection and found they had no effect on the formation of several DBPs, including THMs[37]. This conclusion is in direct contrast to the findings of the present study, which indicated a significant increase in chloroform production in the presence of citrate coated AgNPs. Given that the main difference between the two studies is the AgNP coating, this difference suggests that the coating of the particle could play a crucial role in enhancing the formation of chloroform.

To investigate whether free citrate could be acting independently of the AgNPs to enhance formation of DBPs, an experiment was conducted to isolate the effect of the citrate. Citrate is oxidized during AgNP formation and is converted into a diverse suite of oxidation products such as formate and acetoacetate[38]. It is therefore difficult to discern the possible effects of these oxidation products on THM formation, however an experiment was conducted to evaluate how free citrate itself participates in THM formation. Citrate was dosed to both WWTP effluents and controls and subjected to the same disinfection regimes applied in the nanoparticle survey. No significant increase in chloroform formation was observed in either effluent in the presence of citrate (Table C.3). However, another experiment was conducted similarly with citrate coated gold nanoparticles, a similar effect was observed as has been described above with AgNPs (Table C.10). These results supports the conclusion that it is not free citrate in and of itself that is driving the enhanced formation of chloroform, rather it is an interactive effect of the association of citrate and its oxidation products with the AgNP surface than enhances chloroform formation.

4.4.4 Role of Free Chlorine Demand

Changes in chlorine demand mediated by AgNPs could potentially have played a role in the enhanced formation of DBPs. To explore this possibility, chlorine demand was measured while conducting the THM formation experiments with varying concentrations of AgNPs. However, there was no obvious difference in chlorine demand of the controls relative to the AgNP condition at 1 mg/L and 10 mg/L (Figure 4.3). This

is likely due to the fact that the majority of the chlorine demand in this system could be attributed to other materials present in the effluents, with minimal change in chlorine demand attributable to the presence of silver. In the 20 mg/L AgNP condition, however, a slight increase in chlorine demand was detected, likely resulting from chlorine directly reacting with AgNPs. In contrast, the effluent containing $AgNO_3$ had decreased chlorine demand, which was most likely due to the formation of silver sulfide complexes and therefore decreased reactivity with chlorine. This was especially apparent in the UV + free chlorine disinfection regime, in which silver nanoparticle formation likely occurred.

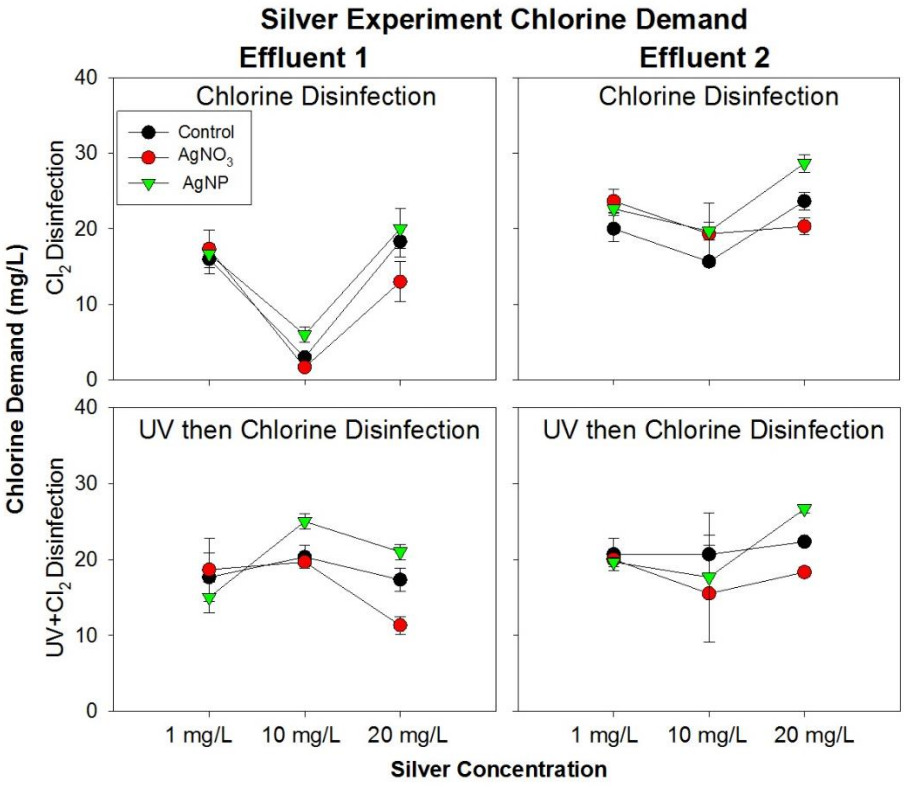

Figure 4. 3 Chlorine demand in the presence of varying concentrations of AgNPs, as well as ion (silver nitrate) and background controls in WWTP effluents disinfected using free chlorine or UV + free chlorine. Note: lines are intended to guide the eye and not model the data. Error bars represent experimental replicates.

4.4.5 Insight into Physiochemical Changes of AgNPs via UV-Vis Absorbance Spectra

To gain deeper insight into the complex interactions of the AgNPs during the disinfection treatments in the presence of wastewater we collected UV-Vis absorbance spectra for the samples both prior to and following disinfection. Past studies by our group and others have shown that UV-Vis spectral analysis is an appropriate means to capture the complexities of nanoparticle systems[39]. AgNPs exhibit a localized surface plasmon resonance (LSPR) that gives rise to a characteristic absorption band whose spectral location and width is a function of the nanoparticle size, nanoparticle aggregation state, and the solution chemistry[40].

As indicated in Figure 4, the AgNPs exhibit a characteristic absorption peak at ~400 nm whose intensity scales with the nanoparticle concentration. This peak was stable following UV disinfection; however, following free chlorine addition the peak was either completely eliminated, as seen when AgNP concentrations were 1 mg/L and 10 mg/L (Figures C.1 and C.2) or was dramatically diminished as in the AgNP concentration of 20 mg/L condition (Figure 4.4).

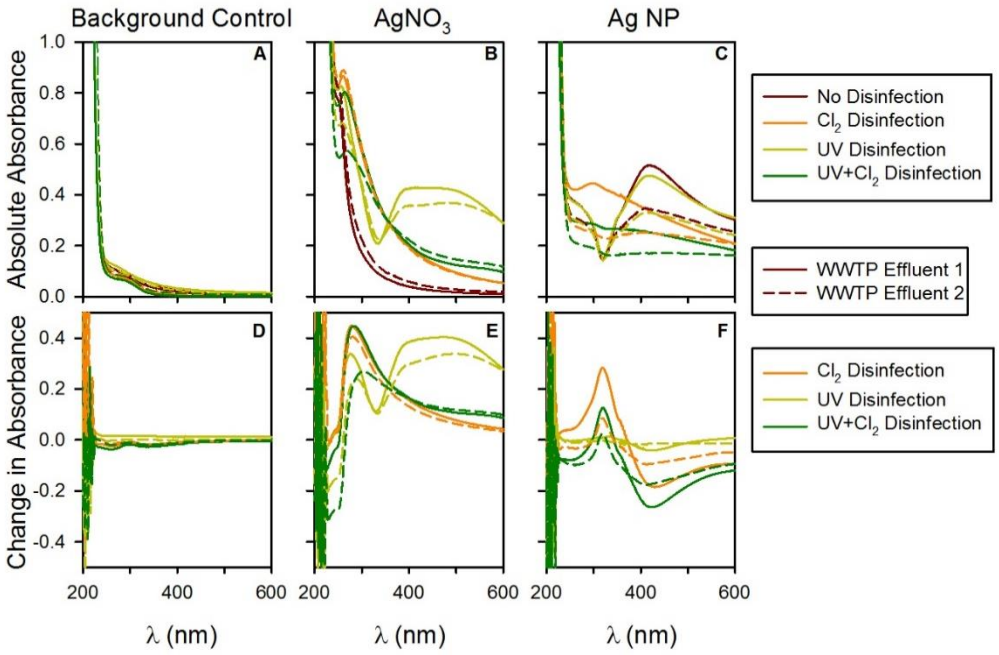

Figure 4. 4 A-C: UV-Vis absorbance spectra of effluents at each stage of disinfection (no disinfection, free chlorine, UV, and UV + free chlorine) for background and ion control and

AgNPs, at 20 mg/L. D-F: UV-Vis absorbance differential with respect to that condition with no disinfection, for background and ion controls and AgNPs, at 20 mg/L.

Yuan et al. (2013) investigated the chemical stability of polyvinyl alcohol (PVA) coated AgNPs during disinfection and observed that, at neutral pH, the AgNPs were stable following UV disinfection[41]. However, this stability was greatly reduced under more acidic or alkaline pH conditions. The effluents applied in the present study were near neutral in pH (Table C.2) and although the AgNP coating differed, they behaved similarly with respect to their stability during UV disinfection.

During chlorine disinfection; however, it was apparent that the AgNPs were not chemically stable, as indicated by the drastic reduction of the AgNP band at 400 nm. Previous studies investigating the stability of PVA[41] and PVP[37] coated AgNPs similarly concluded that AgNPs are not chemically stable during free chlorine disinfection and likely dissolve to produce other silver species. We believe the observed formation of UV-Vis peaks in the vicinity of ~300 nm following free chlorine disinfection is consistent with such a phenomenon as its temporal evolution is consistent with AgNP dissolution. The lack of chemical stability of the AgNPs during chlorine disinfection in conjunction with the increased formation of chloroform suggests that the AgNPs are transformed during the reaction and therefore should not be considered as catalysts that enhance the kinetics of chloroform formation. Interestingly, even though the AgNPs act as a sink for chlorine, there was still an increase in chloroform production. This result indicates the participation of AgNPs in the chloroform production, or at least in the alteration of NOM leading to the increased formation of chloroform.

Evaluation of the UV-Vis spectra also provides insight into why the AgNPs may have exhibited different patterns of DBP formation within the two WWTP effluent matrices. Differences in the spectra were most noticeable in the 10 and 20 mg/L conditions and were characterized by different shaped AgNP peaks for WWTP Effluents 1 and 2. The spectra suggest that the AgNPs were less stable in WWTP Effluent 2, without disinfection, as indicated by the smaller AgNP peak in WWTP Effluent 2 relative to WWTP Effluent 1. This could be related to the higher ionic strength of WWTP Effluent 2, as indicated above.

An unexpected discovery of this study occurred in the ionic silver controls. Spontaneous formation of AgNPs occurred when the $AgNO_3$ control was exposed to UV light, as indicated by the formation of a LSPR band at ~400 nm. The large breadth of this peak suggests that the particles formed via this mechanism were highly polydispersed. We note that various methods for generating AgNPs exist and that AgNPs have previously been synthesized using by UV_{254} irradiation of $AgNO_3$ in the presence of PVP[42]. It is therefore not surprising that UV treatment can reduce the silver ions to AgNPs in situ. Because these nanoparticles exhibit a LSPR band they must consist at least partially of AgNPs. Were they fully sulfidized (i.e., present as AgS_2 NPs) they would not be expected to exhibit a LSPR band[43,44]. It is interesting that such a reaction can occur unintentionally and that the organic matter in the effluents was able to stabilize the particles. Importantly, similar to the pre-synthesized citrate coated AgNPs, the spontaneously generated particles were chemically unstable during free chlorine disinfection (as evidenced by the decrease in the LSPR band), but they did not lead to increased chloroform production. This observation further supports the conclusion that the citrate coating plays a key role in the observed formation of chloroform.

4.5 CONCLUSIONS, ENVIRONMENTAL IMPLICATIONS

The present study determined that citrate coated AgNPs have the capacity to enhance chloroform formation in WWTP effluents at all concentrations of AgNPs investigated (1, 10, and 20 mg/L). It is hypothesized that the citrate coating plays a crucial role in the reactions enhancing chloroform formation, given that a similar study using PVP coated AgNPs observed no enhanced chloroform formation[37]. Citrate coatings are often used in studies investigating nanoparticle behavior as citrate often used to reduce metal salts to nanoparticles in industrial applications before the particles are coated with another substance. Based on the UV-Vis spectrum, AgNPs are not stable during free chlorine disinfection and are likely cycled from particulate to solvent forms. . This study demonstrates that it is possible that nanomaterials present in WWTP effluents could enhance the formation of disinfection by products. This enhancement of DBP formation could be of concern to receiving environments due to DBP toxicity to aquaculture as well a concern for downstream municipalities. As de facto wastewater

reuse now supplies downstream cities with a significant source of drinking water[45], increased DBPs in WWTP effluents will pose a challenge to water sustainability strategies. Such potential increases in DBP levels could also have implications in water reuse scenarios in which rigorous disinfection, including UV followed by free chlorine treatment, is commonly employed as an added safeguard[46]. This scenario may lead to violations in DBP regulations, or increased toxicity to persons exposed to reclaimed irrigation water vapors as inhalation has been identified as an important DBP exposure route[47].

While the presence of AgNP in WWTP effluent enhanced the formation of disinfection by-products, it was encouraging that three of the four nanoparticles tested did not increase THM formation. However, it is important to consider that the conclusions of this study are limited to the conditions that were tested and that different outcomes are possible with changes in water chemistry and nanoparticle characteristics, such as surface coating. Further, this study focused primarily on THM formation, whereas there are over 500 disinfection by-products that have been identified to date[17]. Therefore, increased levels of DBPs other than THMs could potentially be formed by these nanoparticles, which would not be revealed in the present study.

Collectively the experiments described in this work illustrate the liability of silver in wastewater systems. Although it was not the initial focus of this effort, the UV-Vis results indicate that UV exposure can convert Ag^+ into AgNPs and that free chlorine addition can reverse this process. The cycling of silver between its soluble form and nanoparticulate form during both wastewater and drinking water disinfection requires additional study.

REFERENCES

1. C. Marambio-Jones & E. M. V. Hoek, *J. Nanoparticle Res.*, 2010, **12,** 1531–1551.
2. F. Han, V. S. R. Kambala, M. Srinivasan, D. Rajarathnam, R. Naidu, *Appl. Catal. A Gen.,* 2009, **359,** 25–40 .
3. S. Eustis & M. el-Sayed, A. *Chem. Soc. Rev.,* 2006, **35,** 209–217.
4. A. Keller & A. Lazareva, *Environ. Sci. Technol.,* 2014, *Lett.* **1,** 65–70.
5. T. M. Benn & P. Westerhoff, *Environ. Sci. Technol.,* 2008, **42,** 4133–4139.

6. D. M. Mitrano, E. Rimmele, A. Wichser, M. Height, B. Nowack, *ACS Nano,* 2014, **8,** 7208–7219.
7. A. Weir, P. Westerhoff, L. Fabricius, K. Hristovski & N. von Goetz, *Environ. Sci. Technol.,* 2012, **46,** 2242–2250.
8. L. Wang, K. Zhang, Z. Song, S. Feng, *Applied Surface Science,* 2007, **253,** 4951-4954.
9. J. Lahaye, S. Boehm, PH. Chambrion, P. Ehrburger, *Cumbustion and Flame,* 1996, **104,** 199-207.
10. F. Fu, D. D. Dionysiou, H. Liu, *Journal of Hazardous Materials,* 2014, **267,** 194-205.
11. Y. Ma, J. W. Metch, E. P. Vejerano, I. J. Miller, E. C. Leon, L. C. Marr, P. J. Vikesland, A. Pruden, *Water Res.,* 2015, **68,** 87–97.
12. Y. Yang, J. Quensen, J. Mathieu, Q. Wang, J. Wang, M. Li, J. M. Tiedje, P. J. J. Alvarez, *Water Res.,* 2014, **48,** 317–325.
13. X. Zheng, Y. Chen & R. Wu, *Environ. Sci. Technol,* 2011, **45,** 7284–7290.
14. K. Hemalatha. G. Madhumitha, A. Kajbafvala, N. Anupama, R. Sompalle, S. M. Roopan, *J. Nanomater.,* 2013, **2013,** 1–23.
15. E. P. Vejerano, A. L. Holder & L. C. Marr, *Environ. Sci. Technol.,* 2013, **47,** 4866-4874.
16. S. W. Krasner, P. Westerhoff, B. Chen, B. E. Rittmann & G. Amy, *Environ. Sci. Technol.,* 2009, **43,** 8320–8325.
17. S. Richardson, *TrAC Trends Anal. Chem.,* 2003, **22,** 666–684.
18. M. L. Magnuson, C. A. Kelty, C. M. Sharpless, K. G. Linden, W. Fromme, D. H. Metz, R. Kashinkunti, *Environ. Sci. Technol.,* 2002, **36,** 5252–5260.
19. S. D. Richardson, M. J. Plewa, E. D. Wagner, R. Schoeny & D. M. Demarini, *Mutat. Res.,* 2007, **636,** 178–242.
20. A. J. Kennedy, M. S. Hull, A. J. Bednar, J. D. Goss, J. C. Gunter, J. L. Bouldin, P. J. Vikesland, J. A. Steevens, *Environ. Sci. Technol.,* 2010, **44,** 9571–9577.
21. E. P. Vejerano, E. C. Leon, A. L. Holder & L. C. Marr, *Environ. Sci. Nano,* 2014, **1,** 133–143.
22. C. W. McKinney & A. Pruden, *Environ. Sci. Technol.,* 2012, **46,** 13393–13400.

23. C. W. Li, M. M. Benjamin & G. V. Korshin, *Environ. Sci. Technol.*, 2000, **34,** 2570–2575.
24. I. Montesinos, M. Gallego, *Anal. Bioanal. Chem.*, 2012, **402,** 2315-2323.
25. Americnan Public Health Association (APHA). *Standard Methods for the Examination of Water and Wastewater*. (American Water Works Association and Water Environment Federation, 1998).
26. D. Baytak, A. Sofuoglu, F. Inal, S. C. Sofuoglu. *Science of the Total Environment,* 2008, **407,** 286-296.
27. H. Foster, I. B. Ditta, S. Varghese, A. Steele, *Appl. Microbiol. Biotechnol.,* 2011, **90,** 1847–1868.
28. M. D. Hernández-Alonso, A. B. Hungría, A. Martínez-Arias, M. Fernández-García, J. M. Coronado, J. C. Conesa, J. Soria, *Appl. Catal. B Environ.*, 2004, **50,** 167–175.
29. P. Ji, J. Zhang, F. Chen & M. Anpo, *Appl. Catal. B Environ.*, 2009, **85,** 148–154.
30. P. J. Vikesland & R. L. Valentine, *Environ. Sci. Technol.,* 2002, **36,** 662–668.
31. K. Awazu, M. Fujimaki, C. Rockstuhl, J. A. Tominaga, *J. Am. Chem. Soc.,* 2008, **130,** 1676–1680.
32. U.S. EPA. National Recommended Water Quality Criteria; Office of Water, Office of Science and Technology: Washington, DC, 2006.
33. G. R. Aiken, H. Hsu-kim, J. N. Ryan, *Environ. Sci. Technol.*,2011, **46,** 3196–3201.
34. D. P. Stankus, S. E. Lohse, J. E. Hutchison, J. A. Nasan, *Environ. Sci. Technol.*, 2010, **45,** 3238-3244.
35. M. Delay, T. Dolt, A. Woellhaf, R. Sembritzki, F. H. Frimmel, *Journal of Chromatorgraphy A,* 2011, **1218,** 4206-4212.
36. K. L. Garner, A. J. Keller, *Nanoparticle Res.*, 2014, **16,** 2503.
37. A-M. Tugulea, D. Bérubé, M. Giddings, F. Lemieux, J. Hnatiw, J. Priem, M-L. Avramescu, *Environ. Sci. Pollut. Res. Int.*, 2014, **21,** 11823–11831.
38. C. H. Munro, W. E. Smith, M. Garner, J. Clarkson & P. C. White, *Langmuir,* 1995, **11,** 3712–3720.
39. M. Y. Chan & P. J. Vikesland, *Environ. Sci. Technol.*, 2014, **48,** 1532–1540.
40. H. Wei, S. M. Hossein Abtahi & P. J. Vikesland, *Environ. Sci. Nano,* 2015, **2,** 120–135.

41. Z. Yuan, Y. Chen, T. Li & C. P. Yu, *Chemosphere*, 2013, **93,** 619–625.
42. H. H. Huang, X. P. Ni, G. L. Loy, C. H. Chew, K. L. Tan, F. C. Loh, J. F. Deng, *Langmuir*, 1996, **12,** 909–912.
43. J. Yang, J. Ying, *Chemical Communications*, 2009, **1**, 3187.
44. R. Chen, N. T. Nuhfer, L. Moussa, H. R. Morris, P. M. Whitmore, *Nanotechnology*, 2008, **19,** 455604.
45. J. Rice, A. Wutich & P. Westerhoff, *Environ. Sci. Technol.*, 2013, **47,** 11099-11105.
46. U.S. Envrionmental Protection Agency (EPA), *Guidelines for Water Reuse (EPA/600/R-12/618)*, 2012.
47. C. C. Wang, Z. G. Niu & Y. Zhang, *J. Hazard. Mater*, 2013, **262,** 179–188.

APPENDIX C: SUPPORTING INFORMATION FOR CHAPTER 4

C.1 SUPPORTING TABLES

Table C. 1 WWTP Effluent Total Organic Carbon (TOC)

Effluent 1		**Effluent 2**	
Date	**TOC (mg/L)**	**Date**	**TOC (mg/L)**
9-2-2013	8.33	9-11-2013	8.25
9-17-2013	8.45	9-24-2014	5.67
1-22-2013	12.18	2-10-2014	8.95
4-15-2014	5.2	2-15-2014	8.95
10-10-2014	6.2	4-15-2014	4.21
		10-23-2014	5.73
Average	8.07	**Average**	7.31
Standard Deviation	2.68	**Standard Deviation**	2.54

Table C. 2 WWTP Effluent pH

Effluent 1		**Effluent 2**	
Date	**pH**	**Date**	**pH**
1-22-2014	7.18	2-16-2014	7.15
5-22-2014	7.57	4-14-2014	7.67
4-14-2014	7.64	5-8-2014	7.56
Average	7.46	**Average**	7.46
Standard Deviation	0.25	**Standard Deviation**	0.27

Table C. 3 Trihalomethane and Chloropicrin formation in Presence of AgNPs (with citrate controls)

			DBP formation (ppb)				
WWTP Effluent	Disinfection	Condition	TCM	BDCM	TCNM	DBCM	TBM
1	Cl_2	BC	95.51	7.82	BD	BD	ND
		B/I	85.58	4.16	BD	BD	ND
		NP	166.44	6.94	BD	BD	ND
		Cit + E	88.08	8.09	BD	BD	ND
		Cit + NW	35.34	BD	BD	BD	ND
		NP + NW	341.20	BD	2.60	BD	ND
	UV then Cl_2	BC	115.72	8.75	BD	BD	ND
		B/I	98.04	3.97	3.16	BD	ND

		NP	674.70	5.52	BD	BD	ND
		Cit + E	101.24	8.86	BD	BD	ND
		Cit + NW	45.85	BD	BD	BD	ND
		NP + NW	361.25	BD	BD	BD	ND
2	Cl_2	BC	83.31	41.04	BD	15.28	BD
		B/I	97.19	22.68	BD	8.54	BD
		NP	138.11	40.38	BD	10.62	BD
		Cit + E	82.69	44.75	BD	15.65	2.20
		Cit + NW	35.34	BD	BD	BD	ND
		NP + NW	341.20	BD	2.60	BD	ND
	UV then Cl_2	BC	81.52	41.10	BD	25.16	BD
		B/I	93.03	32.04	BD	9.23	BD
		NP	495.08	55.35	BD	10.68	BD
		Cit + E	88.29	46.90	BD	25.48	2.07
		Cit + NW	45.85	BD	BD	BD	ND
		NP + NW	361.25	BD	BD	BD	ND
BC: Background Control, B/I: Bulk/Ion Control, NP: Nanoparticle, Cit + E: Citrate and effluent, Cit + NW: Citrate and Nanopure Water, NP + NW: AgNPs and Nanopure Water							
TCM: trichloromethane, BDCM: bromodichloromethane, TCNM: trichloronitromethane (chloropicrin), DBCM: dibromochloromethane, TBM: tribromomethane							

Table C. 4 Trihalomethane and Chloropicrin formation in Presence of TiO_2

			DBP formation (ppb)				
WWTP Effluent	Disinfection	Condition	TCM	BDCM	TCNM	DBCM	TBM
1	Cl_2	BC	127.62	10.01	BD	BD	ND
		B/I	128.73	9.62	BD	BD	ND
		NP	123.80	9.83	BD	BD	ND
	UV then Cl_2	BC	121.55	11.44	BD	1.67	ND
		B/I	114.79	11.50	BD	1.61	ND

		NP	119.29	11.51	BD	1.65	ND
2	Cl_2	BC	126.93	21.09	BD	7.42	BD
		B/I	121.73	20.18	BD	7.28	BD
		NP	129.94	21.01	BD	7.31	BD
	UV then Cl_2	BC	182.93	29.22	BD	12.33	BD
		B/I	177.82	29.04	BD	12.34	BD
		NP	204.70	28.82	BD	12.31	BD
TCM: trichloromethane, BDCM: bromodichloromethane, TCNM: trichloronitromethane (chloropicrin), DBCM: dibromochloromethane, TBM: tribromomethane							

Table C. 5 Trihalomethane and Chloropicrin formation in Presence of NZVI

			DBP formation (ppb)				
WWTP Effluent	Disinfection	Condition	TCM	BDCM	TCNM	DBCM	TBM
1	Cl_2	BC	164.58	14.96	BD	BD	ND
		B/I	13.68	1.44	BD	BD	ND
		NP	161.02	14.00	BD	BD	ND
	UV then Cl_2	BC	175.14	16.51	BD	BD	ND
		B/I	131.93	14.99	BD	BD	ND
		NP	182.18	17.16	BD	BD	ND
2	Cl_2	BC	452.02	26.51	BD	7.03	BD
		B/I	10.92	7.95	BD	3.07	BD
		NP	470.60	25.52	BD	6.68	BD
	UV then Cl_2	BC	540.70	14.83	BD	11.06	BD
		B/I	476.50	14.64	1.63	9.02	BD
		NP	544.42	30.03	BD	21.87	BD
TCM: trichloromethane, BDCM: bromodichloromethane, TCNM: trichloronitromethane (chloropicrin), DBCM: dibromochloromethane, TBM: tribromomethane							

Table C. 6 Trihalomethane and Chloropicrin formation in Presence of CeO_2

			DBP formation (ppb)				
WWTP Effluent	Disinfection	Condition	TCM	BDCM	TCNM	DBCM	TBM

1	Cl_2	BC	426.67	4.88	BD	BD	ND
		B/I	406.09	6.90	BD	BD	ND
		NP	384.15	7.00	BD	BD	ND
	UV then Cl_2	BC	486.05	5.69	BD	BD	ND
		B/I	484.11	8.42	BD	BD	ND
		NP	529.57	8.55	BD	BD	ND
2	Cl_2	BC	449.26	20.37	BD	6.87	BD
		B/I	292.36	17.60	BD	6.56	BD
		NP	386.26	19.59	BD	6.67	BD
	UV then Cl_2	BC	503.52	20.77	BD	9.03	BD
		B/I	494.69	20.65	BD	8.64	BD
		NP	490.64	39.87	BD	17.45	BD
TCM: trichloromethane, BDCM: bromodichloromethane, TCNM: trichloronitromethane (chloropicrin), DBCM: dibromochloromethane, TBM: tribromomethane							

Table C. 7 Trihalomethane and Chloropicrin formation in Presence of 1 mg/L AgNPs

			DBP formation (ppb)				
WWTP Effluent	Disinfection	Condition	TCM	BDCM	TCNM	DBCM	TBM
1	Cl_2	BC	286.51	24.53	4.03	BD	ND
		B/I	310.69	24.02	3.92	BD	ND
		NP	496.70	22.64	3.80	BD	ND
	UV then Cl_2	BC	332.90	34.81	4.14	BD	ND
		B/I	292.62	32.70	4.98	BD	ND
		NP	552.37	40.82	6.01	BD	ND
2	Cl_2	BC	245.79	65.49	1.36	35.10666	1.94424
		B/I	226.74	62.64	1.32	29.76284	1.438108
		NP	368.44	75.41	1.58	28.81848	1.276649
	UV then Cl_2	BC	221.52	80.30	1.55	43.13988	2.74107
		B/I	182.65	79.47	1.62	29.82173	1.765468
		NP	405.65	106.08	1.86	31.15115	2.120305
TCM: trichloromethane, BDCM: bromodichloromethane, TCNM: trichloronitromethane (chloropicrin), DBCM: dibromochloromethane, TBM: tribromomethane							

Table C. 8 Trihalomethane and Chloropicrin formation in Presence of 10 mg/L AgNPs

			DBP formation (ppb)				
WWTP Effluent	Disinfection	Condition	TCM	BDCM	TCNM	DBCM	TBM
1	Cl_2	BC	382.78	28.80	BD	BD	ND
		B/I	365.18	24.49	BD	BD	ND
		NP	720.28	22.21	BD	BD	ND
	UV then Cl_2	BC	553.70	38.26	BD	BD	ND
		B/I	589.45	27.11	BD	BD	ND
		NP	1257.87	21.83	BD	BD	ND
2	Cl_2	BC	386.79	70.28	BD	BD	ND
		B/I	387.66	65.44	BD	BD	ND
		NP	556.19	59.00	BD	BD	ND
	UV then Cl_2	BC	461.00	68.67	BD	11.56	ND
		B/I	523.27	46.94	BD	BD	ND
		NP	798.77	58.20	BD	BD	ND
TCM: trichloromethane, BDCM: bromodichloromethane, TCNM: trichloronitromethane (chloropicrin), DBCM: dibromochloromethane, TBM: tribromomethane							

Table C. 9 Trihalomethane and Chloropicrin formation in Presence of 20 mg/L AgNPs

			DBP formation (ppb)				
WWTP Effluent	Disinfection	Condition	TCM	BDCM	TCNM	DBCM	TBM
1	Cl_2	BC	343.91	27.96	BD	BD	ND
		B/I	354.12	17.87	BD	BD	ND
		NP	630.80	17.58	BD	BD	ND
	UV then Cl_2	BC	336.54	26.38	BD	BD	ND
		B/I	363.66	14.63	BD	BD	ND
		NP	1081.91	8.38	BD	BD	ND
2	Cl_2	BC	397.28	39.53	BD	BD	ND
		B/I	384.30	30.21	BD	BD	ND
		NP	759.54	24.77	BD	BD	ND

	UV then Cl_2	BC	325.22	37.33	BD	BD	ND
		B/I	296.87	17.57	BD	BD	ND
		NP	945.95	22.91	BD	BD	ND
TCM: trichloromethane, BDCM: bromodichloromethane, TCNM: trichloronitromethane (chloropicrin), DBCM: dibromochloromethane, TBM: tribromomethane							

Table C. 10 Chloroform Formation in the Presence of Citrate Coated Gold Nanoparticles in WWTP 1 Effluent

	Chloroform Formation (µg/L)	
Condition	Cl	UV + Cl
BC	27.76	42.37
B/I	20.30	33.42
NP	63.10	113.31
Chloroform quantified using EPA Method 551; B/I: Gold Chloride; NP: Gold nanoparticles synthesized by citrate reduction method		

C.2 SUPPORTING FIGURES

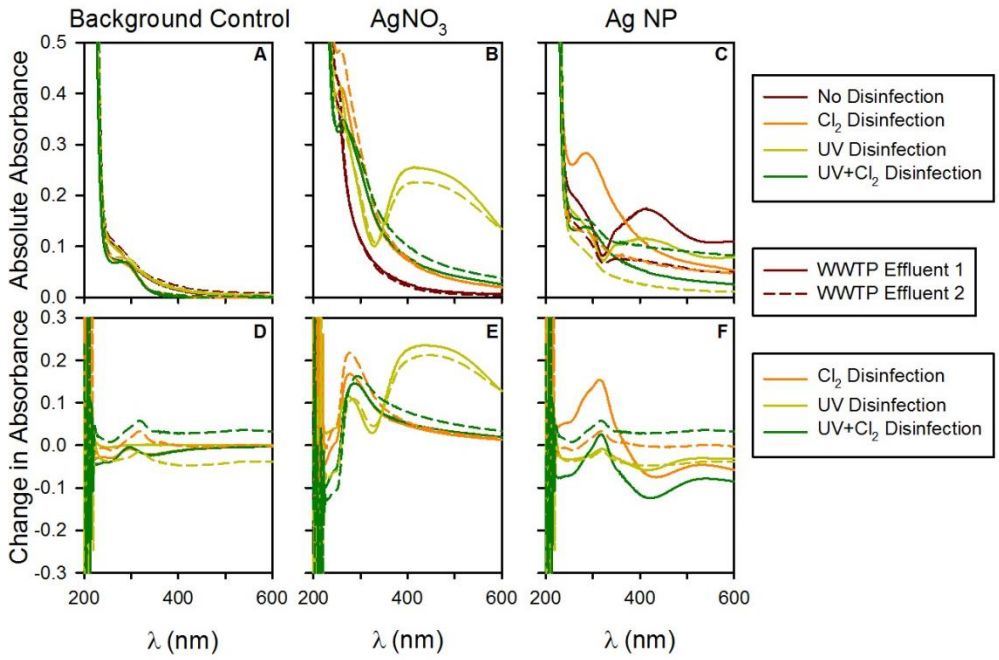

Figure C. 1 A-C: UV-Vis absorbance spectra of effluents at each stage of disinfection (no disinfection, free chlorine, UV, and UV + free chlorine) for background and ion control and AgNPs, at 10 mg/L. D-F: UV-Vis absorbance differential with respect to that condition with no disinfection, for background and ion controls and AgNPs, at 10 mg/L.

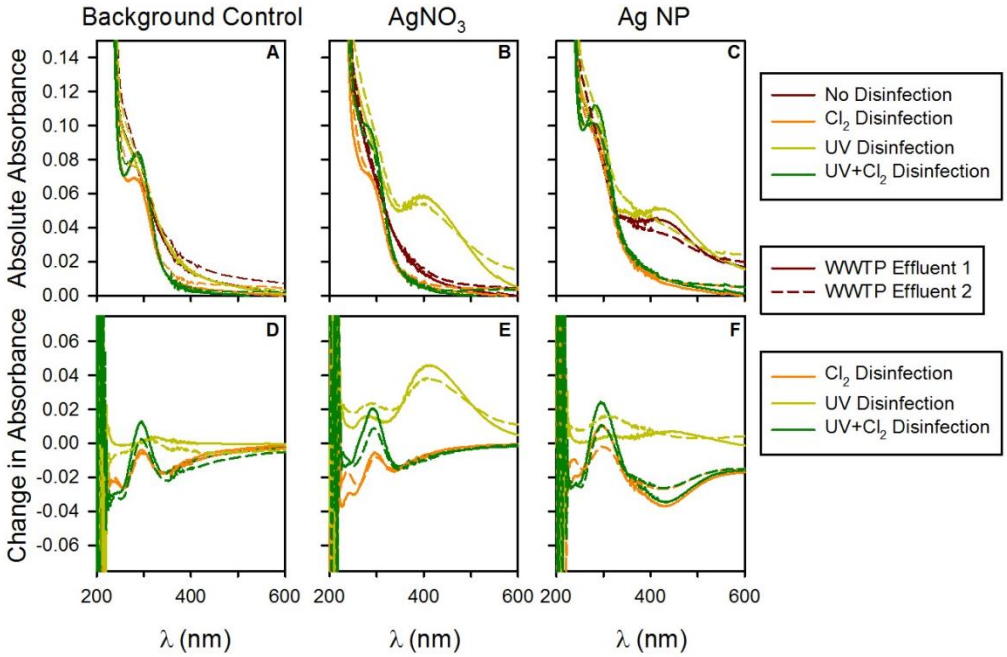

Figure C. 2 A-C: UV-Vis absorbance spectra of effluents at each stage of disinfection (no disinfection, free chlorine, UV, and UV + free chlorine) for background and ion control and AgNPs, at 1 mg/L. D-F: UV-Vis absorbance differential with respect to that condition with no disinfection, for background and ion controls and AgNPs, at 1 mg/L.

CHAPTER 5: CONCLUSION

In order for the continued reclamation and reuse of high quality WWTP effluents that both protect public health and the environment, research must keep pace with developing challenges. These challenges include increasingly stringent discharge regulations on nutrients and continued discovery of pollutants of concern that enter wastewater streams. This work sought to characterize microbial community dynamics during starvation of nitrifying microorganisms and to assess how variations in nanoparticle characteristics impact activated sludge microbial communities, resistance gene profiles and disinfection by-product formations in WWTPs.

Research presented in the second chapter demonstrated how traditional concepts of nitrification in activated sludge may be oversimplified. Illumina 16S rRNA amplicon sequencing on nitrifying decay reactors at various temperatures revealed that *Nitrospira* was the dominant nitrifying microorganism in all trials and had stable relative abundance throughout decay. This observation indicates the possibility of comammox bacterium in activated sludge and highlights the complexity of the nitrifying microbial community in WWTPs.

In the third chapter we discovered that nanoparticle morphology influenced activated sludge microbial communities more than surface coating. Here metagenomic analysis on gold nanoparticle dosed sequencing batch reactors indicated that gold nanospheres impart a selective pressure that was distinct from that of gold nanorods and controls. This result could be used in future nanoparticle design to limit the impact nanoparticles have on engineered and natural microbial communities. It was also found that gold nanoparticle surface coating impacted fate in activated sludge more than particle morphology. This indicates that it may be possible to tailor particle coatings to direct nanoparticle fate in WWTPs and the environment.

In Chapter 4, the discovery of enhanced disinfection by-product formation in the presence of citrate-coated silver nanoparticles was attributed to the citrate coating of the nanoparticles. Enhanced disinfection by-product formation due to nanoparticles in wastewater has the potential to degrade the safety of WWTP effluent and could negatively affect those who are turning to wastewater as an alternative water source. This

study demonstrates the need for a better understanding of the consequences of increased nanoparticle use in consumer products with respect to chemical reactions in WWTPs.

Overall, the research presented here demonstrates that we are understanding of the complexities of the microbial communities involved in wastewater treatment is improving, along with the influences of emerging pollutants on effluent quality. In order to further develop WWTP technologies and maintain the effectiveness of processes already in use, continuation of the research presented here is needed.

Nitrifying microbial communities in wastewater activated sludge need further exploration in order to: maximize utilization of these microorganisms, improve WWTP energy efficiency, limit reactor upsets and advance nutrient removal technologies. A more robust survey of how nitrifying microorganisms are impacted by environmental conditions in activated sludge systems would be useful in furthering our understanding of this important microbial system. Although studies have characterized nitrifying communities in wastewater treatment plants and have explored environmental effects on these communities, few if any have compared environmental impacts on different starting nitrifying microbial communities. Such comparative studies could allow us to determine an optimal nitrifying microbial community for certain WWTP applications. For example, based on the research presented in Chapter 1, the presence of *Nitrospira* in activated sludge may not be ideal for WWTPs attempting to employ shortcut nitrification-denitrification due to the possibility of comammox microorganisms that can independently oxidize ammonia to nitrate. Identifying ideal microbial community compositions for various WWTP processes and increased understanding of community dynamics would allow additional accuracy in predictive models and more informed management of these communities so reactor function is not disrupted with environmental changes.

Further research is also needed in assessing the impacts of emerging contaminants on activated sludge microbial communities and effluent quality. Chapter 2 demonstrated that nanoparticle properties play an important role in determining the affects nanoparticles have on WWTPs and ultimately public health and the environment. Here only two morphologies and two surface coatings were examined. While this is a good demonstration of nanoparticle property importance, the methodology should be used

going forward to examine other properties of nanoparticles such as size, surface functionalization, hydrophobicity, various compositions, and other particle morphologies. Activated sludge sequencing batch reactors coupled with metagenomic analysis could also be used to assess impacts of other emerging contaminants, such as various pharmaceuticals and personal care products. The discovery of enhanced disinfection by-product formation in the presence of nanoparticles, detailed in Chapter 3, demonstrates the ability for nanoparticles to also affect disinfection in WWTPs. Therefore, this study should be followed up with an investigation into the mechanisms responsible for this phenomenon, and whether nanoparticles interfere with disinfection effectiveness. The enhancement of disinfection by-products without significant change in chlorine demand may mean that there was a shift of chlorine utilized for pathogen inactivation to chlorine forming disinfection by-products, thereby limiting effectiveness of disinfection. Overall, although nanoparticles at relevant concentrations in WWTPs have not been found to interfere with traditional pollutant removal (organics, nutrients, etc.), this research shows that characterizing the impacts nanoparticles have on other important pollutants (antibiotic resistance, disinfection by-products, etc.) needs to continue in order to inform accurate risk assessment and applications going forward.